Politechnika Krakowska
im. Tadeusza Kościuszki

Izabela Czekaj
Natalia Sobuś

NANO-DESIGN OF ZEOLITE-BASED CATALYSTS FOR SELECTIVE CONVERSION OF BIOMASS INTO CHEMICALS

Kraków 2018

NANO-DESIGN OF ZEOLITE-BASED CATALYSTS FOR SELECTIVE CONVERSION OF BIOMASS INTO CHEMICALS

Politechnika Krakowska
im. Tadeusza Kościuszki

Izabela Czekaj
Natalia Sobuś

NANO-DESIGN OF ZEOLITE-BASED CATALYSTS FOR SELECTIVE CONVERSION OF BIOMASS INTO CHEMICALS

Kraków 2018

ISBN 978-83-7242-785-4

This book is the effect of the realization of the project "**Nano-design of zeolite-based catalysts for selective conversion of biomass into chemicals**" sponsored by the National Science Centre, Poland under Polonez-1 grant no. 2015/19/P/ST4/02482.

This project has received funding from the European Union's Horizon 2020 research and innovation programme under the Marie Skłodowska-Curie grant agreement No. 665778.

Wydawnictwo PK, ul. Skarżyńskiego 1, 31-866 Kraków; tel.:12 628 37 25, fax: 12 628 37 60
e-mail: wydawnictwo@pk.edu.pl www.wydawnictwo.pk.edu.pl

Adres do korespondencji: ul. Warszawska 24, 31-155 Kraków
Druk i oprawę wykonano w Dziale Poligrafii Politechniki Krakowskiej.
Obj. 8,0 ark. wyd.
Zam. 173/2018 Nakład 120 egz. Cena zł 26,25 z VAT

I dedicate this book to my father, Józef Czekaj, who passed away just a few days before we finished writing this book. He taught me the principles of engineering and always encouraged me to discover science and the world

Izabela Czekaj

CONTENTS

PREFACE

This book is intended to provide a comprehensive introduction to the basic information about biomass transformation into valuable chemicals and catalytic processes using zeolites that will be important in future modern industrial practice. It is necessary to know such basic information in order to work with biomass and zeolite catalysts in the laboratory and in pilot and commercial plants.

1. INTRODUCTION

Nowadays crude oil and natural gas are the main sources of the production of fuels and feedstock chemicals. These resources are limited and the application of (renewable) alternatives will be needed in future to sustain the progress of mankind.

A major challenge is to create fuels and chemical intermediates from available and renewable materials that do not compete with food crops for water or fertilizer, such as wood biomass or agricultural waste [1]. The urgent need for more sustainable production of chemicals from renewable feedstock like biomass has induced intensive research efforts.

2. BIOMASS

Biomass is an exceptional sustainable source of chemicals and fuels [2]. The U.S. Department of Energy predicts that 25% of chemicals and 20% of transportation fuels will be prepared from biomass in the next two decades [3].

According to Polish and European legislation, biomass can be defined as follows:

Biomass is a biodegradable portion of products, waste or residues of biological origin from agriculture (including vegetal and animal substances), forestry and related industries, including fisheries and aquaculture, as well as the biodegradable fraction of industrial and municipal waste (Directive of the European Parliament and Council 2009/28/EC).

Solid biomass includes organic, non-fossil substances of biological origin that can be used as a fuel to produce thermal energy or for the production of electricity, including wood, crops, biodegradable solid waste and others (Regulation of European Parliament and Council EC No. 1099/2008).

Biomass is biodegradable solid or liquid substances of vegetable or animal origin derived from products, waste and residues from agricultural and forestry production, as well as other types of biodegradable waste, in particular raw agricultural materials (Act of 25 August 2006 on biofuels and liquid biocomponents, Journal of Laws 2006 No. 169 item 1199).

Biomass – waste that undergoes aerobic and anaerobic decomposition with the participation of microorganisms (Act of April 27, 2001 on waste, Journal of Laws from 2007 No. 39, item 251).

According to the Regulation of the Minister of Economy of August 14, 2008 (Journal of Laws of August 28, 2008 No. 156, item 969, as amended), biomass is biodegradable solid or liquid substances of vegetable or animal origin that are derived from products, waste, residues and industrial processing in the agricultural and forestry sectors. They might also be other types of biodegradable waste and cereal grains that do not meet the quality requirements of cereals in the intervention purchase (referred to in Article 4 of Commission Regulation (EC) No. 687/2008 of 18 July 2008, which establishes procedures for the seizure of cereals by agencies and methods of analysis for the determination of cereal quality (Official Journal EU L 192 of 19.07.2008, page 20)), and cereal grains which are not subject to intervention [4–12].

The main objective of the European Union and other countries is to make every effort to reduce the global warming caused by the processing of fossil fuels. All attempts to protect the environment from the negative effects of economic development are included

in the EU climate and energy framework, which describes the reduction of greenhouse gas emissions and the development and implementation of efficient and modern technologies [13, 14]. In addition, quantitative targets have been introduced in EU countries which involve the reduction by 2030 of greenhouse gases and energy consumption by 40% and 27%, respectively, compared to 1990 [15]. Recently, technologies using organic waste as a raw material have developed rapidly; this is also true of the use of biomass for energy production, which constitutes 67% of primary energy, of which 48.1% is lignocellulosic biomass [16]. As a result of research into creating products from biomass, a new branch of industry has been established: biorefineries [13, 14, 17, 18]. From this perspective, heterogeneous catalysis processes have tremendous potential to overcome scientific and engineering barriers, thus making economic bio-based conversion routes feasible [19].

The technologies used in the production of valuable products from oil (chemicals, fuel etc.) cannot be used simply if biomass is a substrate. The abundant presence of oxygen makes biomass-derived molecules soluble in water, of low volatility, highly reactive, and prone to decomposition at high temperature. In the literature, numerous pathways (dehydrations, oxidations, hydrogenations, hydrogenolysis, isomerizations) are proposed for the production of a large number of molecules [20, 21]. Nevertheless, transforming these theoretical conversion routes into industrial reality is not straight forward. The production of chemicals from biomass is a very challenging process due to its diverse chemical composition; also, it is an additional route to energy production via the methanation process (Figure 1a).

Biomass from woody plant materials (e.g. corn and wood waste, grass etc.) is a promising biorenewable feedstock [1]. The general scheme (Figure 1a) illustrates the processes of fuel, chemical and energy production from biomass. The most crucial for the environment are the first three steps (Figure 1, dark blue color):

1) lignocellulose conversion (e.g. via dissolution by ionic liquids or hydrothermal gasification by Ru-catalysts),
2) methanation by Ni-catalysts,
3) selective conversion into chemicals (via isomerization, dehydration, oxidation etc. by zeolites).

Lignocellulose is built from cellulose crystals embedded in hemicellulose sugars and lignin polyphenols [21]. Figure 1b shows the main compounds derived from cellulose, hemicellulose and lignin. Cellulose is the most abundant and important constituent in plant cell walls. Its crystal structure and complex network with other carbohydrate polymers are key factors that determine the mechanical strength and degradability of plant cell walls [22, 23]. Another constituent is lignin, which is removed from wood meal by the paper industry.

The cell walls of plants are built of the three main biopolymers: lignin, cellulose and hemicellulose. Lignin consists of aryl ethers that are irregularly connected by a variety of linkages [25]; it is used as a base material to manufacture biopolymers by conventional

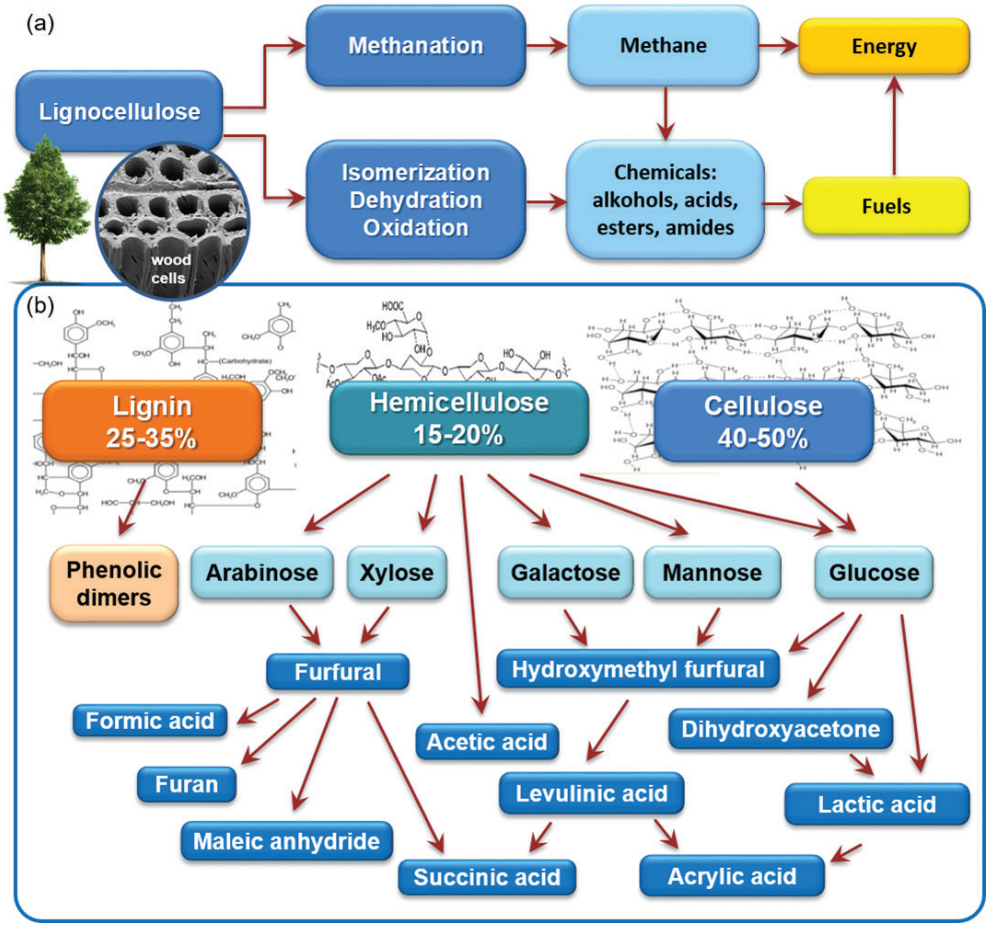

Figure 1. Scheme illustrating the processes of lignocellulosic biomass conversion: (a) different routes of biomass conversion, (b) the main compounds derived from lignocellulose (cellulose, hemicellulose and lignin) [24]

polymer techniques. A further application field is agriculture: lignin products can be the basis of delayed-action fertilizers which release nutrients slowly or serve as support for the production of humus in the soil. In view of its chemical composition, lignin is a rich raw material for aromatic (phenolic) compounds with high added value. In 2004, the pulp and paper industry alone produced 50 million tons of extracted lignin, but only approximately 2% of the lignin available is used commercially, with the remainder used as a low-value fuel [26]. Extraction of lignin from wood is especially difficult for various reasons [27]:

1) the strong covalent bonds between lignin and carbohydrates,
2) lignin has a high molecular weight and possibly forms a three-dimensional network [21],

3) hydrogen bonds and physical phenomena such as solid phase may be involved in the retention of lignin in wood-fiber walls.

There have been several electronic structure investigations of lignin and lignocellulose that tried to explain the role of these building blocks in the treatment of lignocellulose [28–30]. However, most of these investigations are still at a very basic level and do not explain the complexity of lignocellulose. Cellulose builds up the structural substance of unlignified cell walls and consists of fibrous macromolecules based on anhydroused *d*-glucose units. Single polysaccharide chains are hydrogen bonded and build microfibrils which are resistant to hydrolysis. A high degree of polymerization causes the orientation, elasticity and the high tensile strength of this carbohydrate. Hemicellulose is also a polysaccharide and consists of various monomers, such as arabinose, glucose, galactose, mannose and xylose, all of which build a random, amorphous structure. Arabinose is aldopentose, which is a component of mainly hemicelluloses and pectins [31–33].

2.1. Processing of lignocellulosic biomass

Lignocellulosic biomass is a waste from various industries (food and paper) which barely decomposes. In order to be able to use it as a raw material in conversion processes to obtain biofuels and various chemical substances, this material undergoes appropriate physical, chemical or enzymatic treatment to separate it into individual fractions such as cellulose, hemicellulose and lignin. In the following subsections, possible processes of lignocellulose decomposition into various products will be discussed.

2.1.1. Physical methods of biomass processing

Physical methods include grinding, shredding, irradiation and extrusion. These methods are used to reduce the size of particles (from 10–30 mm to 0.2–2 mm), and to facilitate and increase the efficiency of hydrolysis.

Extrusion is a physical and chemical method whereby the material is mixed, heated and sheared, resulting in changes in both chemical and physical properties. Another method is heating with the use of microwave radiation, which allows partial removal of lignin and hemicellulose fractions from lignocellulose, as well as increased carbohydrate hydrolysis [7, 8, 34, 35].

2.1.2. Conversion of lignocellulose with ionic liquids

Pretreatment of lignocellulose requires extreme conditions (e.g. temperature, pressure, and toxic reagents). However, recent reports have shown that some room-temperature ionic liquids (IL) can be used to dissolve both cellulose [36] and lignocellulose [37]. Ionic liquids

are organic salts whose anion and cation can be optimized for particular applications [38]. Studies of cellulose and lignocellulose dissolution in IL have recently been reviewed [39]. There are several electronic structure investigations of ionic liquids [40, 41], and theoretical work on lignin and lignocellulose in IL [42].

2.1.3. Physico-chemical methods of biomass processing

Physico-chemical methods are a combination of chemical and physical methods. Several treatment processes can be distinguished based on the action of ammonia, water vapor, carbon dioxide and hot water [4–7, 34, 35].

The AFEX method (ammonia fiber explosion) is based on the action of liquid ammonia on biomass. The process is carried out at a temperature of 60–120°C at a pressure of 1.73–2.08 MPa for 5–30 minutes, followed by a rapid drop in pressure [43].

Another method is the decomposition of biomass using steam. There are two processes: the first is so-called steam explosion, while the second is steam pretreatment. In the first process, there is an explosion of water vapor in the vessel in which the biomass is placed. The process takes place at a temperature of 160–260°C under a pressure of 0.69–4.83 MPa. Lignocellulose biomass remains in contact with steam for several seconds to several minutes, after which time a rapid decompression occurs to atmospheric pressure [44]. The difference between the steam explosion method and biomass processing using steam results from the different decompression time and the cooling of samples [4]. In the case of the action of water vapor on lignocellulose material, part of the hemicellulose fraction is hydrolyzed to acids, which may be used as catalysts that allow further hydrolysis of this fraction. The use of this method increases the efficiency of obtaining biogas from waste, e.g. municipal waste [45].

Another similar method is the use of carbon dioxide for the decomposition of biomass. Carbon dioxide molecules penetrate into the pores of lignocellulose in a process that takes place in a lower temperature range than in the case of processing with water vapor. This process also results in an explosion which causes the decomposition of biomass into smaller fractions. The advantage of this process is the lack of formation of fermentation inhibitors, and the obtained product is non-flammable [7].

The last method, which has also found application in biomass processing and is used in the paper industry, is the action of hot water (LHW – liquid hot water). The process consists in maintaining the lignocellulosic material at 200–230°C under high pressure for 15 minutes, without the presence of chemicals or catalysts. This treatment allows digestion of up to 80% of cellulose and promotes saccharification; inhibitors do not form or form only in negligible amounts. This method is used especially for the processing of sugar cane or maize and wheat straw [45].

2.1.4. Thermochemical processing of biomass

Thermal biomass transformation processes are more effective methods due to the percentage of use of various biomass-degrading fractions, including lignin. These fractions constitute a raw material in biomass conversion processes, and energy is obtained in the form of heat, electricity, transport fuels and other chemical compounds [8].

The thermochemical processes for biomass processing include the following methods (Figure 2):

1. Gasification of biomass – transformation into carbon monoxide and hydrogen.
2. Pyrolysis – the heating of anaerobic biomass and the formation of various fuel products.
3. Combustion in the presence of air to convert chemical energy into thermal and mechanical energy [8].
4. Direct liquefaction of biomass in the process of pyrolysis under the influence of high temperature or pressure to obtain liquid products [9, 46].

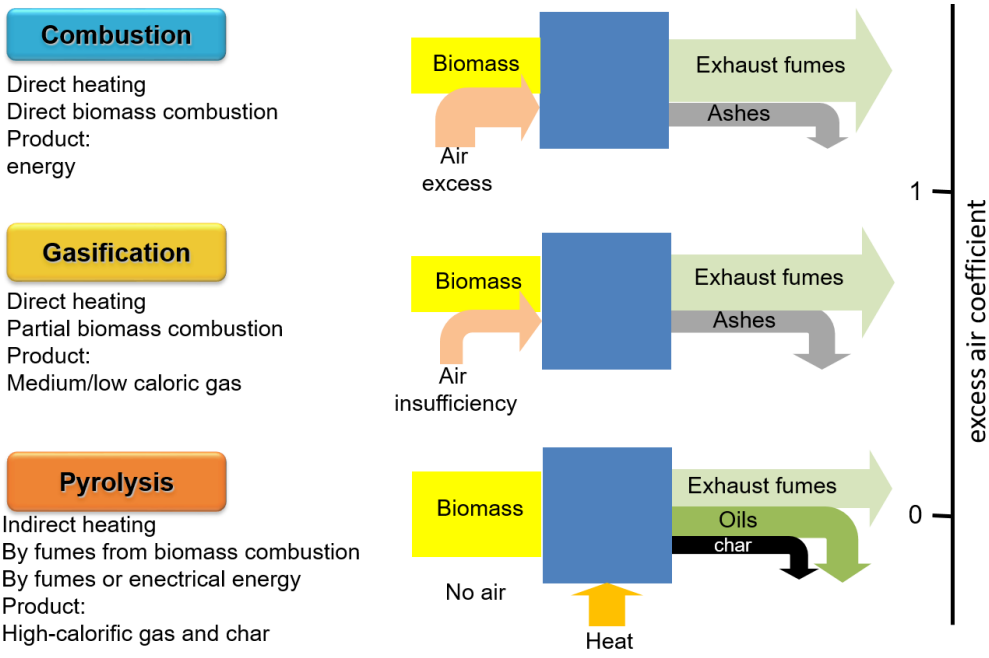

Figure 2. Comparison of thermochemical processing of biomass [8]

Hydrothermal gasification of biomass and the methanation process

The necessity of more extensive exploitation of renewable sources of energy has recently awakened interest in the production of methane from biomass-derived synthesis gas. Catalysts are essential for such biomass conversion processes because without them such processes would not be possible, or they would be not economical.

Gasification consists in transforming the carbon contained in biomass into gases (CO, CO_2) in the presence of a controlled amount of air at high temperatures (above 800°C). The CO_2 reacts with hydrogen and is directly converted into methane. Other chemical products may also be formed during this reaction in the presence of suitable catalysts [47].

The technological process of obtaining synthesis gas from biomass includes stages such as transport, storage, grinding to the required size of the raw material (this process is energy-intensive), drying (most biomass contains water – the drying process reduces the amount of pollutants and smoke produced during gasification), gasification, purification, gas conditioning, synthesis and ash removal. The synthesis gas produced as a result of this process may be used in Fischer-Tropsch synthesis for the production of liquid motor fuels [9, 46].

Fischer-Tropsch synthesis for the production of diesel oil

In 1923, Franz Fischer and Hans Tropsch attempted to convert syngas (CO, CO_2 and H_2) into a range of useful organic compounds. Among others, they pioneered the process of obtaining diesel oil by gasification of coal or biomass. In the Lurgi process, the coal and carbohydrates of various sizes in the biomass react with oxygen or water vapor, as a result of which hydrogen and carbon dioxide are obtained. The resulting synthesis gas mixture can be directly used in gas turbines for energy production. Alternatively, in the presence of various catalysts and under various process conditions, it can be converted to other compounds such as methane or methanol. The composition of the products depends on the process parameters, i.e. on the temperature, pressure, and residence time of the gas in the reaction space. One of the advantages of synthesis gas production and its use as a substrate is the wide range of intermediates, products or raw materials obtained for subsequent processes [47].

The synthesis gas obtained from biomass differs from that obtained from carbons. This gas contains sodium and potassium salts, as well as alkaline earth metals, which causes the formation of slag, coke and large amounts of tar during the process [9]. In turn, syngas obtained from raw fossil materials is sometimes contaminated with sulfur compounds (e.g. H_2S), nitrogen compounds (e.g. NH_3), halides (e.g. HCl) and tars (heavy organic compounds). Unpurified gas obtained as a result of gasification of either biomass or fossil raw materials may also contain benzene or toluene with xylene (this mixture is referred to as BTX). Any impurities may cause catalyst deactivation. Crude synthesis gas is often subjected to purification processes before conversion to biofuels. This is a complicated and expensive procedure [9, 11, 48].

Below is a generalized process for converting biomass into methane or other alkanes: Lurgi reaction:

$$C + H_2O_{(g)} \xrightarrow{\text{energy}} CO + H_2 \ (\text{syngas})$$

Fischer-Tropsch reactions:

$$CO + H_2 \xrightarrow{H_2, Pt} CO + H_2$$

or

$$CO + H_2 \xrightarrow{2H_2, Ni} CH_4 + H_2O$$

Obviously, the process of gasification of biomass for synthesis gas is still at the stage of laboratory tests due to limitations, production costs and the search for effective catalysts. Before commercial use can be made of this process, the gas purification stages and the development of technologies should be carried out on a production scale. Biomass is free of sulfur and nitrogen and contains very little or no aromatic compounds, thanks to which the obtained syngas is more environmentally friendly than production of diesel oil produced from raw fossil fuels [47].

Hydrothermal biomass gasification

In the case of hydrothermal biomass gasification in supercritical water, ruthenium catalysts are used. Carbon-supported ruthenium catalysts exhibit very good catalytic properties and are applied in the Haber-Bosch process [49] and Fischer–Tropsch synthesis [50] for hydrogenation reactions [51–53], the methanation of CO/CO_2 [54, 55], as well as for conversion of biomass to methane in supercritical water [56, 57]. This type of catalyst was originally developed by Tennison and co-workers [58] at British Petroleum (BP) for application in NH_3 synthesis and was later applied in the *Kellog Advanced Ammonia Process* (KAAP). To avoid self-gasification of the catalyst support via the *water-gas-shift reaction* (WGS), the carbon is stabilized by tempering at 1200–3000 K in an inert gas atmosphere. This converts the initial carbon material into *High Surface Area Graphite* (HSAG) and decreases the surface area [59, 60].

It is recognized that the aforementioned reactions are structure-sensitive, and in several reports [61–66] the observed reactivity is correlated with the existence of so-called B_5 sites. These were originally postulated by Van Hardeveld and Van Montfoort [67], who analyzed marble models of fcc crystals with cubo-octahedral morphology while investigating the adsorption and dissociation of nitrogen on Ni, Pd and Pd crystallites. The B_5 sites consist

of five metal atoms in a particular three-dimensional arrangement that exposes a three-fold hollow site (i.e. a kind of terrace) and a bridge site (i.e. a step edge) close together. Most such active sites were identified to be present at edges related to low-coordinated surface atoms, e.g. edge atoms on (110) and (113) planes and formed only on medium-sized clusters (diameters within the range 1.5–7.0 nm). However, it must be stated that the shape of catalytically active clusters on a support might be different.

While investigating catalytic ammonia synthesis over several different types of supported Ru catalysts, Jacobsen *et al.* [61] adapted the calculation of Van Hardeveld and Van Montfoort to the case of ruthenium, see Figure 3. They calculated the optimum Ru particle sizes which exhibit the maximum number of B_5 sites and found that for a given crystal morphology they should be in the range 1–3 nm in diameter; these ruthenium particles are considered to possess an irregular crystalline geometry that allows the formation of B_5 sites in the intersection between the crystallographic planes.

Jacobsen *et al.* also state that on very small crystals the likeliness of the formation of B_5 ensembles is very low, and that with increasing crystal size the decreasing fraction of B_5 sites is due to the rapid decrease in the fraction of edge atoms. García-García *et al.* [62] investigated ammonia decomposition over ruthenium supported on commercial activated carbon. They reported that the catalytic activity is influenced either by the degree of graphitization of the carbon support or by a promoter; they detected that sintering resulted in Ru particles with an average diameter in the order of 3–5 nm. These clusters exhibited remarkably increased catalytic activity compared to small single atom particles; this was related to the formation of B_5 sites, as depicted in Figure 4.

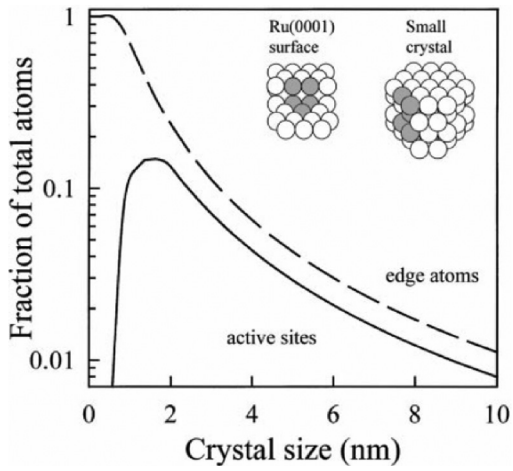

Figure 3. Fraction of edge atoms and active sites on small Ru crystals relative to the total number of atoms as a function of crystal size, as obtained by Jacobsen *et al.* [61]. The inserts show crystal models exposing the (001) and (100) hcp surface planes

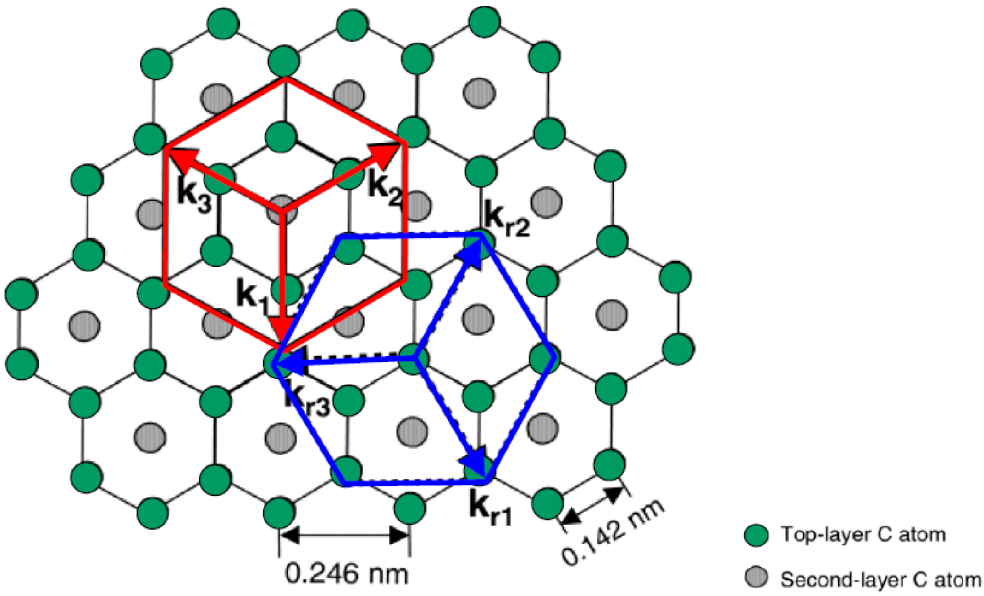

Figure 4. Possible ruthenium cluster arrangements as a function of size, as suggested by García-García *et al.* [62]. The location of B_5 sites is shown by grey spheres on the middle cluster

The activity of a catalyst is related not only to the dispersion of active nanoparticles, but also to interactions with the support [61]. It was recognized that both the dispersion and the interactions with the support control the size and morphology of the crystals. Additionally, there might be electronic effects of the support that depend on its status or pre-treatment (e.g. oxidation state, extent of graphitization). Therefore, knowledge about these effects is important in order to understand structure-sensitive catalytic reactions. Consequently, the growth of Ru on *highly-oriented pyrolytic graphite* (HOPG) was investigated by Nielsen *et al.* [68] and Song *et al.* [63]. Both groups found that, depending on the applied preparation method, different nanoparticle morphologies can be obtained which exhibit different catalytic behavior.

Song *et al.* [63] report that by controlling the texture of a HOPG surface (which should mimic an activated carbon support) and the Ru surface concentration, two cluster types were obtained: round and flat clusters, and layered Ru clusters. Both types grew epitaxially on the graphite. The authors discuss two possible epitaxial growth orientations which are rotated relatively by 30° (see Figure 5).

Nielsen *et al.* [68] deposited ruthenium on HOPG by applying two different techniques; they report that the pre-treatment of the graphite surface and the method of deposition influences the size, shape and dispersion of the nanoparticles. Soft-landed, pre-formed mass-selected Ru nanoparticles resulted in round particles, with evidence of

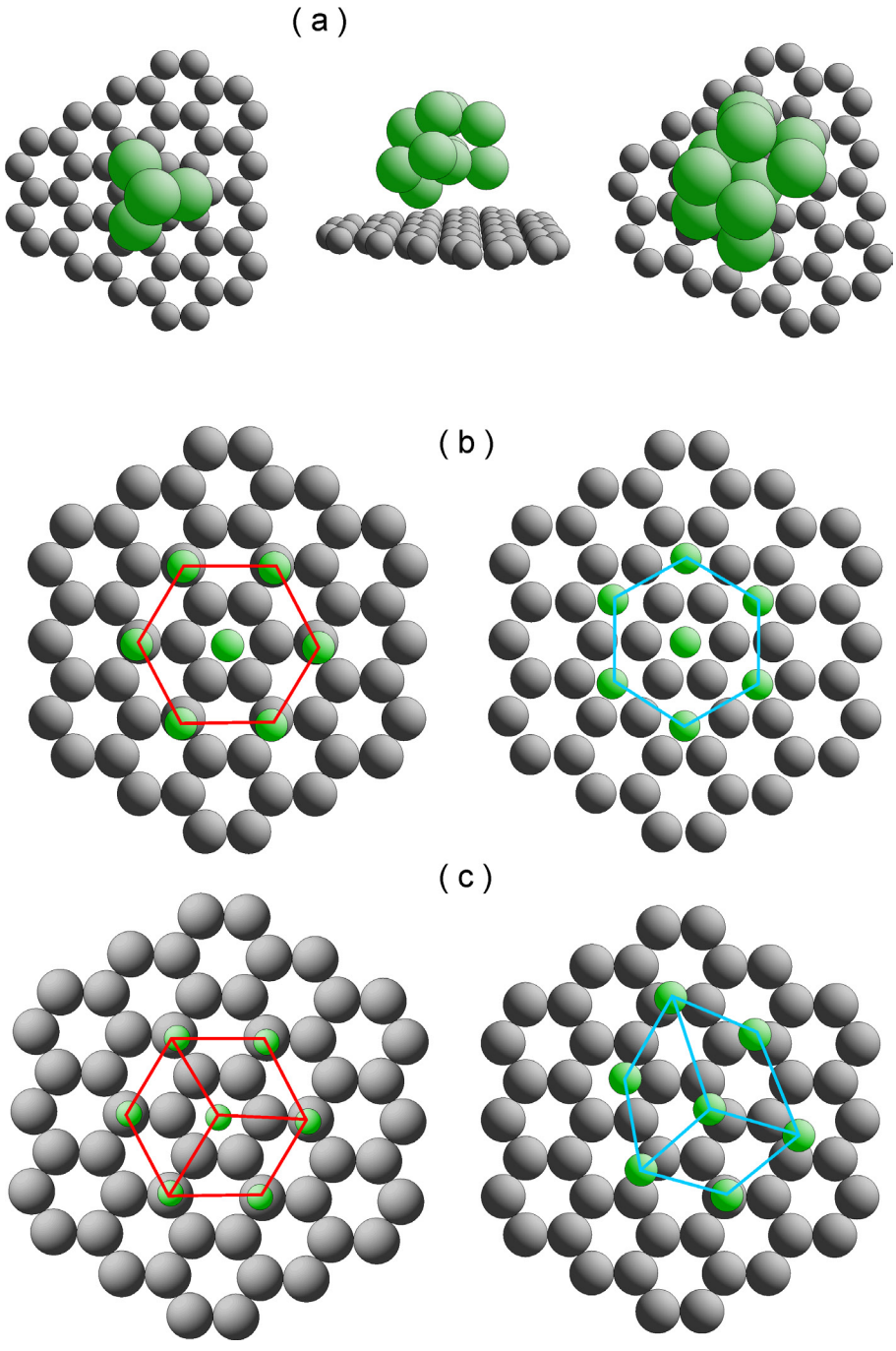

Figure 5. Two possible epitaxial growth orientations of the Ru lattice on graphite suggested by Song *et al.* [63]: a) blue = "30°" with k_{ri} = 0.246 nm (lattice mismatch = +9.2%), b) red = "0°" with k_i = 0.284 nm (lattice mismatch = -4.8%)

facets on the larger particles. Annealing these nanoparticles showed them to be stable against sintering when deposited onto sputtered HOPG surfaces. The size and shape of thermally deposited nanoparticles depended on the state of the graphite support and the deposition temperature. On non-sputtered HOPG, bimodal growth with large flat particles on the substrate terraces and smaller diameter particles aligned along the substrate steps were found, whereas on sputtered HOPG the formation of 2 nm round particles with a narrow size distribution was recorded.

There are several theoretical investigations of Ru catalysts, mainly based on periodic calculations [69–72]. Peterson *et al.* [73] describe how methane and water decomposition take place on a stepped metallic ruthenium surface. We investigated the interaction between the Ru nanoparticles and the graphitic support, their influence on the location of the Ru clusters, their structure, and the possible number of active sites [74]. It was found that the type of support influences the shape and electronic properties of the cluster and the active B_5 sites. Additionally, the number of active sites depends on the size of the ruthenium nanoparticles. Among the large group of nanoparticles with various structures and sizes that was examined, only those compatible with the structure of the carbon support stabilized on the surface. Based on the stable configuration, a three-dimensional model of ruthenium nanoparticles with three centers of B_5 type was created (Figure 6). The model of stable nanoparticles with exposed B_5 centers offers the possibility of further studies on the adsorption of molecules and the mechanism of catalytic reaction. In addition to the detailed definition of the topology of ruthenium nanoparticles, an innovative achievement of the work was the use of geometric structures obtained from the DFT method to simulate the NEXAFS spectra and the valence states of XPS spectra. The close agreement between the simulations and the experiment revealed that the DFT calculations yield an extremely sharp image of the catalyst

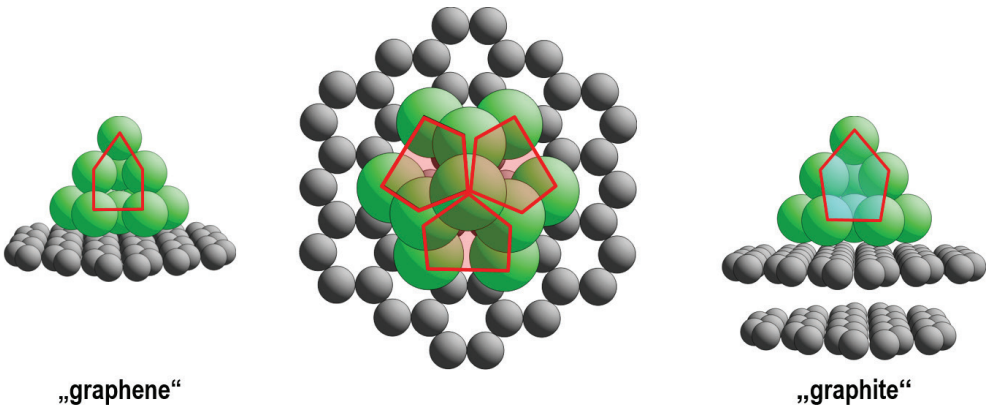

Figure 6. Stable ruthenium cluster at a carbon support: graphene and graphite type. Red pentagons show the position of active B_5 sites [74]

and determine which support is present in the majority of real catalysts. From the analysis of the combined theoretical and experimental results, we assumed that ruthenium nanoparticles over graphene are present in the majority of real industrial catalysts.

Methanation of biomass

Another type of lignocellulosic biomass usage is methanation of biomass [75]. This is a catalytic process with nickel-based catalysts, which are often used in industrial processes such as the hydrogenation, hydrotreating and hydrogenolysis of hydrocarbons, the stream reforming of hydrocarbons, and methanation [76–78]. Different supports have been used for dispersing nickel particles in surface science studies: γ-Al_2O_3, TiO_2, Pt, zeolites or SiO_2 [79–82]. The activity and selectivity of the supported metal catalysts are strongly influenced by the amount of metal employed, the size of the dispersed metal particles, the metal–support interactions, and the composition of the support. We focused our attention on the effect of the degree of dispersion (i.e. the crystallite size) on the electronic properties and reactivity observed in various systems. The biomass-derived synthesis gas does not only require the design of a dedicated methanation process, but also exposes the catalyst to extremely demanding conditions which lead to carbon deposition, sulfur adsorption at the surface, and therefore to catalyst deactivation. The industrial process of obtaining methane gas from biomass takes into account not only the methanation catalyst, which is nickel on Al_2O_3 support, but also desulfurization catalysts such as ZnO (Figure 7A). So far, publications on the methanation reaction over supported Ni highlighted the general formation of carbon whiskers and the early steps of detaching Ni clusters from the support [83–84].

Identification of certain nickel carbide compounds such as Ni_3C that are formed only after extended exposure times is important because the initiation of the detachment mechanism of the nickel clusters from alumina support could be closely related to the appearance and existence of Ni_3C. In the literature only 'general' NiC_x and nickel carbide formation is described in the case of pure metallic nickel [85–87].

Understanding the detailed mechanism of the methanation and the accompanying processes requires detailed research in many areas of the process. Therefore, research has been conducted at all levels from industrial installations, through the microscopic analysis of the catalysts, up to the detailed analysis of the surface and theoretical modeling at the atomistic level (Figure 7B). Some research included a detailed spectroscopic analysis of the surface and theoretical modeling of the possible reaction mechanisms.

Wambach's team performed methanation reaction experiments in a high-pressure cell (HPC) integrated in the XPS system and under fixed-bed conditions [75]. The interactions of the different reformer biomass-derived synthesis gas on the surface properties of the catalyst and on its activity under methanation conditions were studied on a nanoscopic

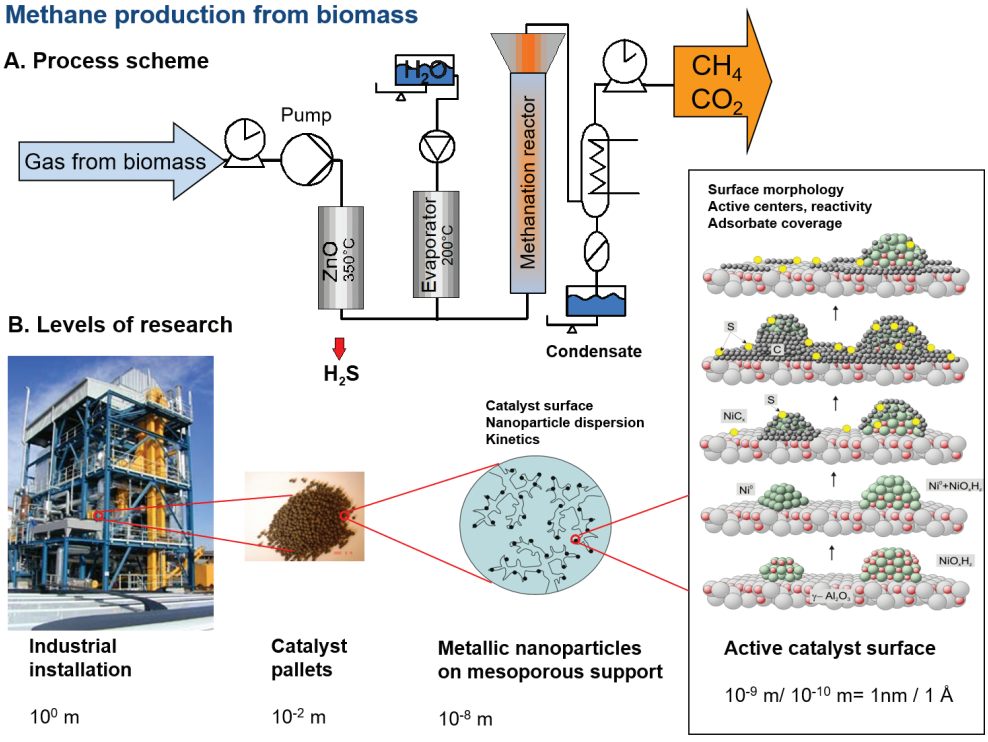

Figure 7. Scheme of methane production from biomass [75]

level. A detailed description of the changes in metal particle morphology and carbon deposit was presented. The mechanism of C-whiskers formation during long exposure to methanation conditions is described (Figure 8). The role of additional components in the gas mixture, such as CO_2, H_2O, CH_4, C_2H_4, C_2H_2, C_3H_6 and C_2H_6, were studied in detail. Furthermore, the roles of different nickel compounds such as oxides, hydroxides, carbides and carbonates were discussed.

A notable scientific achievement was the development of novel method for the analysis of industrial catalysts by a combination of theoretical modeling and surface analysis in in-situ conditions to obtain surface changes and a complete description of the catalyst deactivation mechanism in industrial conditions [88, 89]. The proposed mechanism of surface processes that occur during the methanation of biomass using Ni/Al_2O_3 catalyst is shown in Figure 8 (middle part). The 'as delivered' catalyst surface consists of Ni particles with a diameter of 2–4 nm, in both oxidized and hydratized form (Fig. 8a). This surface is not active in the methanation reaction. Activation under H_2 leads to a partial reduction of the surface Ni^{2+} species-forming Ni^0 (reduced catalyst, Fig. 8b). Besides the Ni^0, the reactive surface also contains mixed Ni^0 + hydratized/oxidized NiO_xH_z particles, e.g. NiO and $Ni(OH)_2$.

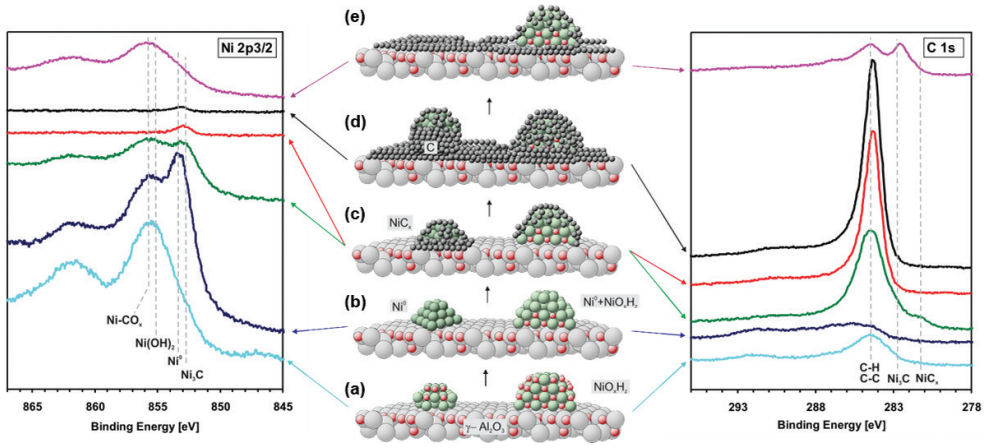

Figure 8. Analysis of the industrial process simulated in laboratory conditions: in situ XPS – Ni $2p_{3/2}$ (left) and C 1s (right) region [75]

Mixed nickel compounds (e.g. nickel oxides and hydroxides) may be present in relatively large particles. Metallic Ni can be located at the exterior surface, and NiO_xH_z or $NiAl_2O_4$ compounds exist in a sub-surface region near the nanoparticle-support interface. During the methanation process and in the presence of hydrocarbons, the surface becomes decorated with carbon species (working catalyst, phase 1, Fig. 8c). This picture is typical of results after a 5-hour methanation run. Longer methanation under fixed-bed conditions results in severe carbon deposition and formation of C-whiskers, followed by a detachment of Ni-particles from the support (working catalyst, phase 2, Fig. 8d). This picture is typical for long methanation runs (19–137 hours). After all methanation runs, it was possible to remove the deposited carbon easily, resulting in partial loss of the Ni particles (C-removal, Fig. 8e).

The proposed mechanism of catalyst deactivation has been confirmed by theoretical studies. For this purpose, an innovative research program was created which includes combined experimental studies of the model catalyst and the theoretical modeling of the surface of the nanoparticles deposited on a support. The model catalyst was produced.

In our investigation, Ni deposition and cluster growth on model catalyst samples (10 nm thick, polycrystalline γ-Al_2O_3 on Si(100)) were investigated by XPS. Changes in Ni $2p_{3/2}$ binding energy during Ni deposition indicate differences in nanoparticle growth. We investigated the molecular structure of the catalyst using Density Functional Theory calculations (StoBe) with a cluster model and a non-local functional (RPBE) approach. An $Al_{15}O_{40}H_{35}$ cluster was selected to represent the γ-Al_2O_3(100) surface. Ni clusters of different sizes were cut from an Ni(100) surface and deposited on the $Al_{15}O_{40}H_{35}$ cluster in order to validate the deposition model determined by XPS.

The DFT data suggest that nickel is stabilized on the γ-Al_2O_3 surface, thus influencing the electronic properties of the newly formed surface. On the basis of the results of structure optimization and analysis of experimental results, we were able to determine very precisely that in the case of nickel deposition, growth that follows a modified Stranski-Krastanov model is observed [89]. At low coverages ($\leq$ 0.2 ML), Ni was localized in AlO_4 tetrahedra between rows of AlO_5, and only after a certain time of deposition are three-dimensional clusters formed. The very good agreement of the experimental data with the theoretical model allows us to state that the procedure using theoretical modeling of nanoparticles on the support can be applied to other catalytic systems, such as zeolites.

Pyrolysis

Pyrolysis takes place through anaerobic thermal decomposition of biomass (at temperatures of 350–700°C) [46]. After the gaseous products are obtained at elevated temperature, they are then condensed after cooling to form a liquid mixture of over 350 compounds such as acids, alcohols, aldehydes, sugars, esters, ketones and aromatics, which are referred to as 'bio-oils' [9, 46, 90, 91]. Short residence times (in the order of seconds) are necessary for the production of liquid bio-oils. At longer reaction times the main product of pyrolysis is solid coke, which can be used to generate energy in combustion processes [46].

Biomass pyrolysis processes can be divided into three categories: slow (so-called carbonization), fast and rapid pyrolysis [47, 90]. Figure 9 shows a comparison of different pyrolysis processes.

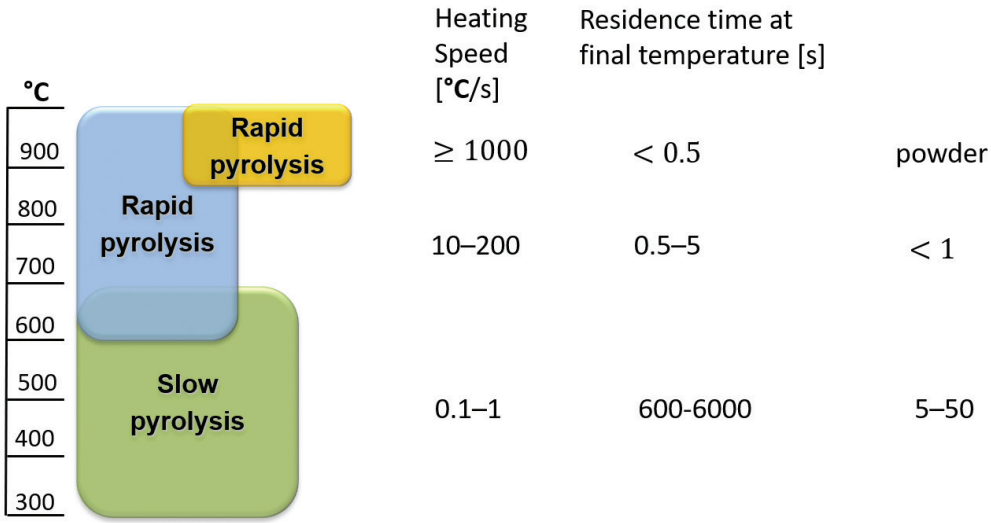

Figure 9. Comparison of process conditions for different types of pyrolysis [47, 90]

Slow pyrolysis is a conventional method that is based on a slow heating rate of 0.1–1°C s^{-1}. The main product of this process is coal and, to a small extent, so-called pyrolysis oils. Slow pyrolysis requires low temperatures and a very long time (5–30 minutes) in the biomass reaction space [46]. In fast pyrolysis, the biomass decomposes very quickly, generating mainly steam, aerosols and residual solid phase. Vapors and aerosols, after cooling and condensation, form a dark brown liquid that has a calorific value of about half that of conventional fuel oil. These are the most important features of fast pyrolysis:

- short reaction time,
- fast cooling of vapors and high yields of liquid products,
- the right choice of parameters, i.e. temperature [90].

This rapid pyrolysis is characterized by the following conditions:

- fast heating (10–200°C s^{-1}),
- process temperature 500–700°C,
- short process time,
- quick cooling of volatile products into bio-oils with a 75% yield [90].

The rapid pyrolysis of biomass usually takes place in a temperature range of 500–700°C and requires a very fast heating time, e.g. 300°C per minute. For this process, raw materials with very small particle sizes (105–250 μm) are required. Gas products of rapid pyrolysis require rapid cooling or quenching to reduce the formation of active radicals that give intermediate products.

In general, fast and rapid pyrolysis are promising techniques for obtaining biofuels from biomass. Products obtained from these techniques could be a renewable alternative to fossil fuels and become precursors for various chemical compounds [90, 92].

A pyrolysis method was developed that produces aromatic compounds directly from a lignocellulosic mass with a yield of 20–30% [9]. It has been reported that pyrolysis takes place in the presence of a ZSM-5 catalyst. Pyrolysis has received considerable attention as a cheap option for processing whole biomass and can also be used to process lignin after extraction of carbohydrates from lignocellulose. However, a pure pyrolysis product is not suitable for use as a fuel. Its main limitations are high acidity (which can cause corrosion of engines), high content of oxygen compounds, as well as low density.

Liquefaction of biomass

Liquefaction is the thermochemical conversion of biomass to liquid fuels. It is otherwise known as the biomass to liquid (BTL) process. Liquefaction consists in biomass treatment at low temperatures (300–350°C) and high pressure (5–20 atm) for about 30 minutes, often using a basic catalyst like sodium carbonate in the presence of hydrogen (in this case, the process is called catalytic liquefaction). However, non-catalytic liquefaction of biomass is also possible.

This process is also known as direct condensation. Under these conditions, the water remains in a liquid state, and liquefied biomass is directly converted into products without drying. This is very important due to the high energy consumption of the drying process. Liquefaction processes and pyrolysis are often confused, but there are a few differences between them. For example, pyrolysis requires pre-drying and usually occurs at higher temperatures but at lower pressures. However, in the case of the liquefaction of biomass, the product obtained contains less oxygen (12–14%) than bio-oils produced as a result of pyrolysis. The products of liquefaction have been successfully tested in engines with minor modifications. The only problem that occurs after obtaining a product from the liquefaction of biomass is its inability to tolerate long-term storage [46, 93, 94].

Biomass combustion

Direct combustion of biomass (i.e. biomass burning in the air) is another way of transforming chemical energy into heat and electricity. Globally, it is the most commonly used and economical biomass conversion process: about 97% of biomass-derived energy is produced in this way in furnaces and boilers. Burning occurs at a temperature of 800–1400°C, or more. The generated heat is immediately transformed into energy or used directly for heating houses. There are several factors that affect the combustion process, such as moisture content, ash in the raw material and the concentration of inorganic components. These factors depend on the origin of the biomass and the method of its production. In some cases, biomass must be pre-dried to reduce the moisture content to below 50% [95].

Combustion can be done on a small scale (e.g. heating a home), on an medium scale (in hospitals, offices, etc.) and on a large scale for industrial purposes. An example of this is the use of biomass burning in the United States, where rice hulls are burnt on a large scale [96]. In addition to biomass combustion, there is also so-called co-combustion, in which biomass and coal are combusted together, either directly or indirectly. This process can increase the profitability of technologies and the use of biomass for energy production, while reducing greenhouse gas emissions [7]. Three technological variants of co-combustion can be distinguished which depend on the combination of biomass and coal:

- direct co-combustion, combustion occurs when a stream of biomass or coal is fed separately or as a mixture,
- indirect co-combustion occurs in two cases:
  - ✓ biomass combustion takes place in a so-called the pre-furnace, while the thermal energy of the generated exhaust gases is used in the main combustion chamber,
  - ✓ biomass is gasified in a gasifier, then the produced gas is transported to the combustion chamber, where it is combusted in gas burners [97].

2.1.5. Chemical processing of biomass

In addition to thermochemical methods, there are also chemical methods that allow the conversion of biomass to biofuels or specific chemical compounds; the most popular methods are hydrolysis of biomass in an acidic or alkaline environment, and ozonolysis.

Acid hydrolysis

The acid hydrolysis of biomass is most often carried out using sulfuric, hydrochloric, orthophosphoric and nitric acids. The process is based on biomass treatment with diluted or concentrated acids (usually the weight ratio of acid to substrate is 0.2:2.5%), at a temperature of 130–210°C for a few minutes or even several hours. The selection of appropriate parameters of the hydrolysis process is very important. Increasing the temperature may contribute to the formation of inhibitors (furfural, hydroxymethylfurfural) that prevent the subsequent fermentation process. Of the aforementioned acids, sulfuric acid is most commonly used, and its dilute solutions improve the hydrolysis process. The disadvantage of this method is the high costs compared to other physical and chemical methods [98, 99].

Basic hydrolysis

In alkaline treatment, sodium, potassium, calcium and ammonium hydroxides are most often used. The process takes place at room temperature or at an elevated temperature of 100–150°C, at atmospheric pressure and for a period of time from a few seconds up to several days. The advantage of this method is reduced degradation of sugars and easier methane fermentation thanks to the possibility of lignin degradation and hemicellulose decomposition [100].

Ozonolysis

The ozonolysis process is carried out at room or elevated temperature (185°C) in organic solvents such as methanol, ethanol or acetone. During the pre-treatment of lignocellulosic biomass using ozone, the lignin is degraded to lower molecular weight compounds (e.g. formic or acetic acid) and the decomposition of hemicellulose without infraction of the cellulose. The advantages of this process are low energy demands and the absence of toxic products and inhibitors. Unfortunately, this process is unprofitable due to the high costs and significant ozone gas requirements, which limit its use on an industrial scale [8, 35].

2.1.6. Biological biomass processing

Biological treatment consists in the decomposition of lignocellulosic biomass using enzymes produced by microorganisms. Lignin is degraded due to the presence of fungi (such as *Phanerochaete, Pycnoporus sanguineus* or *Chrysoporthe cubensis)* and actinomyces

(*Nocardia*), all of which allow the decomposition of hemicellulose. The cellulose is decomposed by so-called brown rot fungi [8, 101, 102]. In addition to those mentioned above, other enzymes are also used such as manganese peroxidase, lignin peroxidase, laccase, endo-xylanases, β-mannosidases, α-galactosidases, endoglucanases, β-glucosidases [101]. The biological biomass treatment process is a less energy-consuming method and does not require expensive equipment, and the products obtained are not toxic. The only disadvantage of this method is its long duration [101, 102].

2.1.7. Catalytic conversion of biomass

The processes of catalytic conversion of biomass to obtain various chemical products have been a continuous subject of intense research over the last decade. A number of articles have been published that describe reactions using various types of biomass, and many types of reactions have been carried out. The main interest is in the following reactions: oxidation, hydrogenation/hydrogenolysis, or isomerization using as substrate carbohydrate, triglyceride, 5-hydroxyfurfural, cellulose, hemicellulose, or lignin [103]. Some of the most interesting processes of catalytic conversion of biomass will be described in chapter 2.3.

2.1.8. Depolymerization of polysaccharides with the participation of catalysts

Cellulose is a polysaccharide consisting of glucose monomers and, in turn, glucose is a chemical compound that can be transformed into various chemicals by fermentation or by chemical processes. Therefore, the hydrolysis of cellulose to glucose is a key process for the efficient use of biomass. However, due to the crystalline structure and the presence of strong β-1,4-glycosidic linkages, cellulose biomass hydrolysis is difficult [104]. A lot of research has been done recently, focusing on the hydrolysis of biomass using enzymes, acids and catalysts. Enzymatic hydrolysis is a promising cellulose hydrolysis technology. However, the currently obtained product is achieved with low efficiency, and the use of enzymes is associated with high costs. When using acid hydrolysis, only dilute acids may be used, as concentrated and organic acids are not recyclable, are corrosive, and may pose a threat to the environment. On the other hand, solid acid catalysts have attracted considerable attention in the conversion of biomass due to their properties and the fact that they can be separated from the product. An example of a catalyst that enables the biomass hydrolysis reaction is ZrO_2/WO_3 and H-ZSM-5 [105].

2.1.9. Catalytic conversion of biomass fermentation products

Fermentation processes are one of the main methods of obtaining compounds in biotechnology. The obtained products can be used in medicine, or in cosmetics, food and other branches of the chemical industry. The advantage of this technology is its high selectivity, its mild reaction conditions, and the conversion of biomass into desirable products. This method obviously has

limitations related to the costs of the apparatus; moreover, it generates serious environmental pollution, which makes it difficult to apply on a large production scale. There is a continuous search for solutions that enable the biomass conversion processes; various research teams have confirmed the possibility of the biological production of, for example, succinic or lactic acid. The selective conversion of biomass that contains a carboxylic functional group in its structure is becoming an attractive method for the preparation of various chemical compounds in biorefineries. In order for the fermentation process to be more cost-effective, studies are in progress to combine this method with the chemical conversion method using catalysts. At the present moment, this concept is in the laboratory phase, although it is a promising biomass conversion process [105, 106].

2.2. Bio-refinery concept

A biorefinery is a technological system that combines biomass conversion processes that result in products that can be further processed into biofuels and chemical compounds. This technology is the equivalent of plants that process crude oil. The bio-refining of raw biomass materials is more environmentally friendly [7, 107]. Biorefineries are a new branch of industry which uses renewable energy sources as raw materials, thanks to which they can compensate for non-renewable energy sources such as oil and natural gas [9].

Biomass conversion technology, known as biorefineries, has no specific concept. Leja *et al.* selected the elements that characterize this new branch of industry and created a definition of a biorefinery [107], according to which a "biorefinery is an integrated bio-industry that uses various technologies to obtain products (such as chemicals, biofuels, food, feed ingredients, biomaterials as well as heat and energy), focusing on maximizing added value while taking into account the three sustainable pillars of "the environment, the economy and society". In this bio-chemical industry, various renewable raw materials are used such as corn and cereal grains, oilseeds, waste from the agri-food industry, wood and organic waste (such as municipal waste) [9, 107].

Of course, this technology is at the stage of continuous development and improvement. However, the raw materials and products do not pose a threat to the environment. According to the Joint European Biorefinery Vision for 2030, a significant part of the EU-wide demand for chemicals and energy will be covered by products from biomass conversion processes. It was estimated that by 2030:

- 30% of the total production of biomass-based chemical compounds (chemicals, polymers) is expected, this value may be as high as 50%,
- 25% of energy demands in transport will be covered by biofuels,
- 30% of electricity and heat in Europe will come from biomass [7].

Unfortunately, most processes are still in the research phase. Due to recent technological advances, four biorefinery systems can now be distinguished in the pre-production phase:

- biorefineries with input from the whole plant,
- biorefineries with input from inedible parts of plants,
- biorefineries with lignocellulose input,
- two-platform biorefineries.

2.2.1. Biorefineries with input from the whole plant

Agro-refineries use whole-crop plants as raw materials. However, due to the fact that these plants, especially grains, are a raw material in the agri-food industry for food production, using them as a raw material in the biorefineries is considered unethical. Therefore, other solutions were sought, and second-generation fuels were created [7, 107] using non-food raw materials. This is a significant advantage due to the reuse of waste from the agri-food industry in the new goal of energy production. The biorefinery concept of using whole plants assumes the division of cultivated plants into edible and non-edible parts. From the edible part, starch derivatives and flour can be obtained, which are either the final product or further for fuels, chemical compounds or other materials. Heat, energy and waste are also produced in these processes. In the case of inedible parts, the plant is processed into lignocellulose, from which the biorefinery process produces energy.

2.2.2. Biorefineries with input from inedible parts of plants

This is called a 'green' biorefinery, in which specific parts of plants are used as raw material: wet biomass, grass, clovers and unripe cereals. In this type of biorefinery, plants that are redundant or useless for breeding are also considered. In this case, biomass is converted by extrusion methods into liquid and solid substances; the former are subjected to various biotechnological, biochemical or physical processes, as a result of which proteins or sugars are obtained. From the remaining solids, cellulose and lignocellulose are obtained as a result of enzymatic and thermal processes. The products obtained from solid and liquid substances are processed into chemical substances and biofuels [108].

2.2.3. Biorefineries with lignocellulose input

In this case, plants rich in lignocellulose are used as the batch substrate. This biomass is widely available and cheap. The sources of biomass for this particular process are:

- reeds, grasses, and coniferous and deciduous trees,
- quickly growing trees, e.g. willows and poplars,
- wood waste such as straw, hay or stalks,
- post-process lignocellulose: wood waste from the pulp and paper industry, corn cobs, municipal waste [9].

Loads of lignocellulosic material are first subjected to physical, chemical or enzymatic treatment in order to separate them into lignin, cellulose and hemicellulose. Lignin is transformed by chemical methods into raw lignin material, whereas sugars from cellulose are obtained using biotechnological or chemical processes. From lignin, cellulose and hemicellulose fractions, fuels and chemical substances are obtained [9, 108].

2.2.4. Two-platform biorefineries

The concept of this type of biorefinery is the simultaneous production of synthesis gas and sugars in two technological platforms: biofuel production by thermo-chemical methods, and the obtaining of raw chemical materials as a result of chemical transformation of raw sugar. The raw material used is biomass from various industries, including agriculture, forestry and shipping, or municipal waste [108].

2.3. Selective conversion into chemicals

Modern technologies for obtaining valuable biomass-derived chemicals such as furfural, levulinic acid, adipic acid, dihydroxyacetone, lactic acid and acrylic acid are essential for future research. In this chapter we are trying to show the current status of such technologies.

2.3.1. Production of polyols and other chemical compounds from lignocellulosic biomass

Polyhydroxyl compounds, including sugars, alcohols and glycerol, can be converted into various products by catalytic conversion. However, in contrast to crude oil, the structure of biomass contains high oxygen content and the carbon skeleton structure is more complicated. In order to achieve high product yields, the key is selective oxygen removal from the lignocellulosic biomass structure. In the following chapters, examples of compounds that can be subjected to catalytic hydrogenolysis will be presented [105, 109].

2.3.2. Hydrogenation and hydrogenolysis of cellulose biomass

The main source of cellulosic biomass is agricultural and forestry waste. Cellulosic biomass is used in various processes (almost 40 billion tons per year). Cellulose differs from starch in that it is not digested by the human digestive system. Therefore, instead of starch, cellulose has become one of the largest renewable raw materials that can be converted into energy, heat and chemical compounds. Many studies have been successfully carried out on the conversion of cellulose biomass into useful products involving heterogeneous catalysts in hydrogenation and hydrogenolysis processes [110].

As Xian described [105], the first research into the process of hydrogenation of cellulose was described in 2006 by Fukuoka, who, among others, tested Pt and Ru catalysts, which showed the highest activity in cellulose conversion at 463 K under 5 MPa pressure in a hydrogen stream. Noble metals also catalyze the process of glucose hydrogenation. In order to reduce the crystallinity and particle size of cellulose, which causes a reduction in the efficiency of the conversion process, ball milling of the substrate is used to accelerate the degradation. Xian also referred to Liu's work from 2008, in which the process of glucose hydrogenation was carried out with the participation of an Ru/C catalyst. After 30 minutes, the yield of hexitol was 39.3% at a conversion of 85.5%, reacted at 518 K under 6 MPa in a hydrogen stream. Wang and others developed a method for hydrogenation of cellulose with tungsten carbide [110]. The usage of WC catalyst under the same reaction conditions as in the above work produces a higher yield of ethylene glycol than with the use of platinum or ruthenium catalyst [105]. Wang also considered the possibility of using other catalysts [111]. One of the tested catalysts was nickel, which is generally considered to be effective in hydrogenation and hydrogenolysis reactions. However, this catalyst shows weak activity in the production of polyols. Mu and others conducted a series of studies on the conversion of glucose with a nickel catalyst. After trials and modifications, they showed that a 20% Ni/ZnO catalyst can produce glycol products with a process efficiency of 70.4%. However, the disadvantage of this catalyst is its lack of hydrothermal stability, resulting in a decrease in catalytic activity after repeated series of reactions.

2.3.3. Hydrogenolysis of sugars and sugar alcohols

Sorbitol is obtained directly from starch or by hydrogenating glucose. In combining the hydrolysis reaction with the hydrogenation process, it is possible to obtain a cheap raw material in further conversion to obtain polyols. The nickel and ruthenium catalysts used in the hydrogenolysis reaction are able to prepare C_2–C_3 products, such as ethylene glycol, 1,2-propanediol and glycerol [109]. 40% selectivity was obtained at 50 wt.% Ni catalyst on a diatomaceous earth support from $Ca(OH)_2$. Hydrogenolysis of sorbitol with the participation of 6 wt% Ni-NaY catalyst gives a yield of 62% 1,2-propanediol and 14% ethylene glycol. The main product was glycerol on the Pt-NaY catalyst. Another promising raw material for the preparation of polyols is xylitol, which is obtained as a result of the combined hydrogenation or hydrogenolysis of hemicellulose. 10 wt% of xylitol solution was heated at 200°C under 4 MPa in the presence of 4% by weight Ru/C catalysts in the presence of a $Ca(OH)_2$ promoter in a hydrogen stream. As a result of this process, products with the appropriate selectivity of 32.4% ethylene glycol, 24.9% 1,2-propanediol and 9.6% glycerol at 20% conversion were obtained.

Hydrogenation of glucose to sorbitol is carried out using a Cu-Ni-Al catalyst in ethanol [112]. In the case of reactions under the same conditions but in a 1,4-butanediol

solvent, sorbitol can also be obtained in 67% yield. This catalyst may also be used in the hydrogenation of fructose, mannose, xylose and arabinose to the corresponding polyols (with a yield of 65%).

Hydrogenation of fructose leads to sorbitol and mannitol. The challenge was to maximize the selectivity of the mannitol process. Many processes were carried out using various catalysts. The possible processes [105] are presented in Table 1 below.

Hydrogenolysis of 20% by weight aqueous solution of erythritol in an acidic medium was carried out at 200°C, under a pressure of 8 MPa in a stream of hydrogen, on an Ir-ReO_x/SiO_2 (Re/Ir = 1) catalyst to yield butanediols [113]. The maximum selectivity of 1,4- and 1,3-butanediol was obtained at 33% and 12% at 74% conversion and was maintained for four repeatable tests.

Table 1. Hydrogenation of fructose to mannitol [105, 109]

Catalyst	Reaction conditions	Selectivity [%]
20% wt Cu/SiO_2	30 g fructose; 250 ml H_2O; 0.5 g cat.; 60°C; 2 MPa	67 (85 borate)
2.5% wt Pt/C 2.5% wt Pt/C, 1% wt ZnO	1 g fructose; 80 ml H_2O; 0.05 g cat.; 100°C; 10 MPa	47 63
61% wt CuO, 39% wt ZnO	30 wt% fructose; 110°C; 5 MPa	68
20 wt% Cu/SiO_2	110°C; 5 MPa	63
70 wt% CuO, 25 wt% ZnO, 5 wt% Al_2O_3	----------	66

2.3.4. Hydrogenolysis of glycerol

Glycerin is a chemical substance from which many useful intermediate or final products can be obtained, especially from catalytic reactions, e.g. oxidation, dehydration, esterification, etherification or hydrogenolysis. Glycerin is obtained as an intermediate in the transesterification reaction of triglycerides to fatty acid esters used as a propellant, or as a by-product in the production of ethanol and the fermentation of sugars [114].

A number of studies have been carried out in which glycerin was subjected to catalytic dehydroxylation to 1,2-propanediol and 1,3-propanediol [105, 109].

2.3.5. Conversion of glycerol to 1,2-propanediol and 1,3-propanediol

Depending on its purity, 1,2-propanediol (1,2-PDO) can be used as a hydraulic fluid (antifreeze) or in cosmetic and food applications. The dehydroxylation reaction mechanism passes through the dehydration step to acetol, followed by the hydrogenation of acetol to

1,2-PDO. This process takes place in an acidic environment, but the initial stage takes place in an alkaline environment [105].

One catalyst that allows conversion of glycerol to 1,2-propanediol with an efficiency of 80% is $Cu/ZnO/Ga_2O_3$. The hydrogenation process of glycerol occurring in the liquid phase on CuO-ZnO (60:40) as a catalyst occurs at a temperature of 200°C under a pressure of 5 MPa in a hydrogen stream. This reaction proceeded with a conversion of 52% and a selectivity of 98%. However, achieving a selectivity of 98% at 80% conversion is possible due to the presence of a $Cu_{0.4}/Mg_{5.6}Al_2O_{8.6}$ catalyst. It is also possible to convert glycerol to 1,2-PDO with catalysts such as Cu/Al_2O_3, $CuO/ZnO/Al_2O_3$ [109].

Many studies have been carried out on the use of ruthenium as a catalyst [109, 115]. Due to the high activity of Ru catalyst, the selectivity of conversion to 1,2-PDO is lower than, e.g., for copper catalyst. In most studies, the maximum efficiency with which 1,2-propanediol was obtained was lower than 40%, therefore various additives are used to increase this. An example is a reaction on a Ru/TiO_2 catalyst that yields 1,2-propandiol with 48% selectivity at 66% conversion. The process takes place at 170°C at 3 MPa in a hydrogen stream for 12 hours. Another modification is an Ru catalyst on a ZrO_2 and SiO_2 support. These catalysts also show high selectivity to 1,2-PDO (61%), but with lower conversion of glycerine (41% and 21% respectively).

1,3-propanediol (1,3-PDO) is used for the production of polytrimethylene terephthalate by copolymerization from terephthalic acid, which is currently synthesized from ethylene oxide or by fermentation of carbohydrates. Samples were tested to produce 1,3-PDO by hydrogenolysis from glycerol. It was confirmed that the selectivity was significantly lower than in the case of 1,2-PDO. Conversion tests were carried out with various catalysts as well as with variable conversions. An example of use is $Pt/WO_3/ZrO_2$ catalyst with a different mass fraction (2 wt%, 3 wt% and 1 wt%), yielding a 1,3-PDO product with yields of 24%, 32% and 32%. Another process was also carried out under similar conditions with various catalysts. The reaction was carried out in an aqueous environment at a temperature of 180°C, under pressure of 5 and 3 MPa for 10–12h. In this case, 2% by weight was used.

2.3.6. Fructose: aldo-keto isomerization of glucose

Due to the low raw material costs, acquiring fructose from biomass is an interesting pathway for obtaining a variety of useful monomers. One method of fructose production is isomerization of biomass-derived glucose. Another essential process is fructose transformation into glyceraldehyde (GLA) and dihydroxyacetone (DHA) via retro-aldol reactions. Figure 10 shows the reaction pathways of glucose and fructose [110].

Fructose may be an intermediate in subsequent transformations to HMF or lactic acid. One way of performing fructose reactions is to obtain a catalyst with Lewis active centers. For this purpose, a Sn-Beta zeolite was designed which has the ability to convert

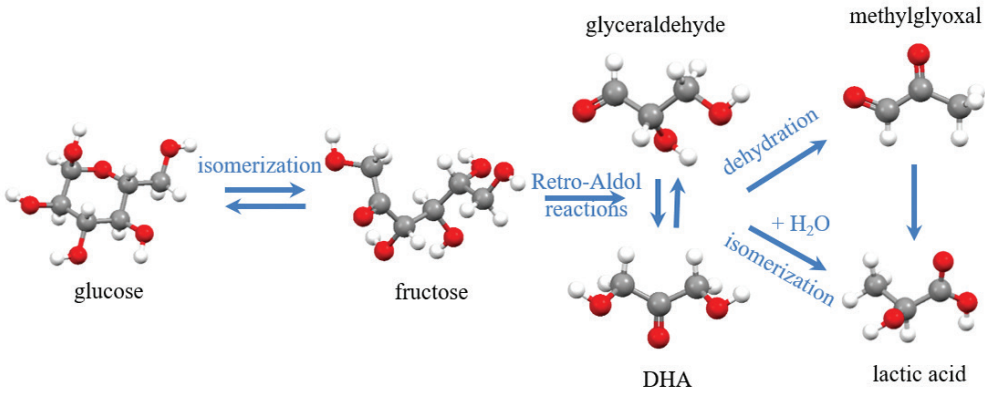

Figure 10. Scheme of reaction pathways of glucose and fructose [110]

glucose to fructose. The presence of additional sodium cations in the structure enables the transformation of glucose into mannose [110, 111]. In order to confirm the effectiveness of this catalyst, theoretical studies were carried out using the DFT method. Reaction barriers for partially hydrolyzed and fully coordinated tin at specific locations using energy distribution analysis were tested. In addition, Sn was replaced with other metals such as Ti, Zr, V, Nb, Si and Ge. It was found that Sn and Zr are metals that have the lowest energy barrier for glucose isomerization. The energy barrier also depends on the physical properties of the metals used and the basicity of the centers of active oxygen atoms associated with the metal atoms [113]. Another example of zeolite usage in a glucose isomerization reaction is Y, H-beta and H-USY zeolite. This reaction occurs in two stages in various solvents. The first step is the reaction of the isomerization of glucose in methanol to produce methyl-fructoside, followed by hydrolysis to fructose after the addition of water. The reaction takes place at 120°C for 1h with the aforementioned catalysts. As a result of this process, a product was obtained with the highest yield of 55% using H-USY. Conducting this process at higher temperatures leads to a product such as methyl levulinate [114].

The process of glucose isomerization to fructose was also carried out on NaY zeolite with magnesium cations incorporated into zeolite (0–15 wt%). It was observed that the increase in magnesium content in the structure (10 and 15% by weight) significantly improved the degree of glucose conversion (6–49%). However, the yield of fructose was only about 32% [115]. Tests were also carried out with A, X, Y zeolites, and hydrotalcites. Alkaline cations Na^+, K^+, Cs^+, Ca^{2+}, Ba^{2+} were introduced into the structure of these materials on the basis of ion exchange. The process was carried out in an aqueous environment at 95°C at 8 bar. The best of the tested zeolites were NaX and KX, with 90% selectivity into fructose and 10–20% conversion of glucose [116].

2.3.7. 5-hydroksymethylfurfural and furfural

The production of 5-hydroksymethylfurfural (HMF) and furfural should be essential for industry since both compounds are used as substrates in several syntheses. HMF is formed by the dehydration process of different aldoses from the hydrolysis of biomass [117]. HMF can be converted to a range of derivatives that have potential applications in the biofuel, polymer, and solvent industries. There are several promising studies concerning catalytic processes of HMF production from biomass using a variety of catalysts (from hydroxyapatite-supported chromium chloride, metal chlorides up to ZSM-5) [118–120].

Examples of reactions catalyzed with the corresponding zeolites are given in Figure 11. One zeolite used in the production of HMF is dealuminated BEA zeolite, which is formed by calcination of the NH_4^+BEA form at a temperature above 700°C or the treatment of this material with steam at 500°C. The Si-O-Al bonds inside the zeolite structure are broken, resulting in an increase of Lewis active centers. Calcinated BEA zeolite was used in the reaction of conversion of glucose to HMF with selectivity of 55% at 78% conversion [121]. Another possibility is to conduct the HMF production process from glucose in a 1-butyl-3-methylimidazolium chloride solvent with BEA zeolite (Si/Al = 25) as a catalyst. This catalyst has the highest activity, resulting in HMF with 50.3% yield at 80.6% glucose conversion at 150°C for 50 minutes [122]. The HMF production process is also possible in 1-butyl-bromide-3-methylimidazolium ionic liquid solvent in MOR zeolite [123]. Also, the conversion of glucose to HMF takes place with the participation of catalysts such as SAPO-34 [124], H-, Fe, Cu-ZSM-5 [125] or over hierarchical Zr-Al-BEA [126].

The catalytic reaction of hydrogenation of HMF to DMF is possible with precious metal catalysts such as Pd, Pt, Ru, and Rh in a neutral environment. In the case of acidic pH, the products of this process lead to diols of C_6 and triols. 2,5-dimethylfuran was obtained with

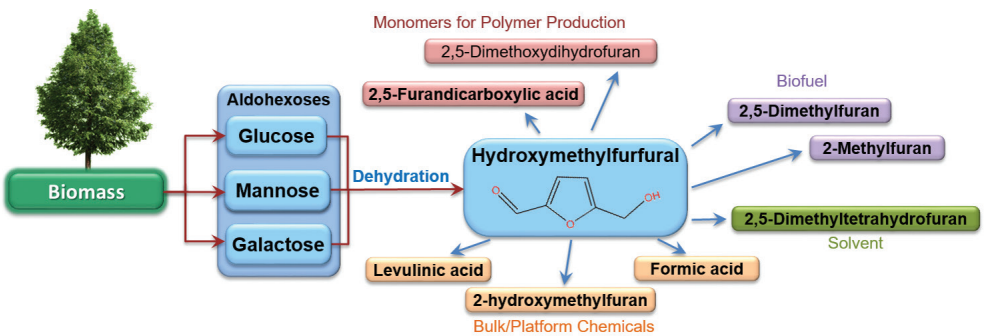

Figure 11. Scheme illustrating the targeted product (HMF) from biomass-derived feedstocks and its usage as substrate in further synthesis into valuable chemicals [44]

a 79% yield through hydrogenolysis in the gas phase with 10% wt. HMF in 1-butanol. The process was carried out in a flow reactor containing a Cu-Ru/C catalyst (Cu: Ru = 3:2). A DMF yield of 95% is possible as a result of heating HMF to boiling point in the presence of formic acid, sulfuric acid (VI) and Pd/C catalyst [105,109].

When a Ni-Pd (Ni/Pd = 7) catalyst is used on a silica support, a yield of 96% DHMTHF is obtained, and the use of 1 wt%. Ru/CeO_2 gives the same compound with a yield of 91%, and C_6 polyols are formed as by-products. In turn, an increase in the proportion of by-products is possible in the case of reactions in which the substrate is DHMTHF. The reaction takes place in an acidic medium with 6.5% by weight Rh and 6 wt% Re/SiO_2 on sulfonated carbon. 1,6-hexanediol (1,6-HDO) was obtained as the product with 86% yield and 15% yield of 1,5-hexanediol. Another DHMTHF hydrogenolysis reaction takes place in an aqueous environment at 120°C under a pressure of 8 MPa in the presence of 4% by weight $Rh\text{-}Re/SiO_2$ (Re/Rh = 0.5); 1,2,6-hexanetriol was obtained with a selectivity of 84% at 32% conversion after 4h of the process [109, 120].

It is also possible to obtain two products with comparable performance to HMF: DMF (60.3% efficiency) and MF (61.9% efficiency). Furfural and HMF mixture (in a ratio of 1: 1) occurs in 1-butanol at 260°C for 1.5 hours, with Ru/C catalyst [121].

As well as the conversion of biomass to HMF, it is also important to obtain furfural, which is a valuable strategic industrial intermediate [127]. It is converted into furfuryl alcohol, methylfuran and furan via metal-catalyzed hydrogenation, reduction and decarbonylation, respectively (see Figure 12). Also, various valuable products are produced from furfural: α-furfuryl alcohol, tetrahydrofurfuryl alcohol, methylfurfuryl alcohol, 5-dimethylaminomethylfurfuryl alcohol, furoic acid, furfurylamine, methylfuran, 2-acetylfuran and 2,5-dimethoxydihydrofuran.

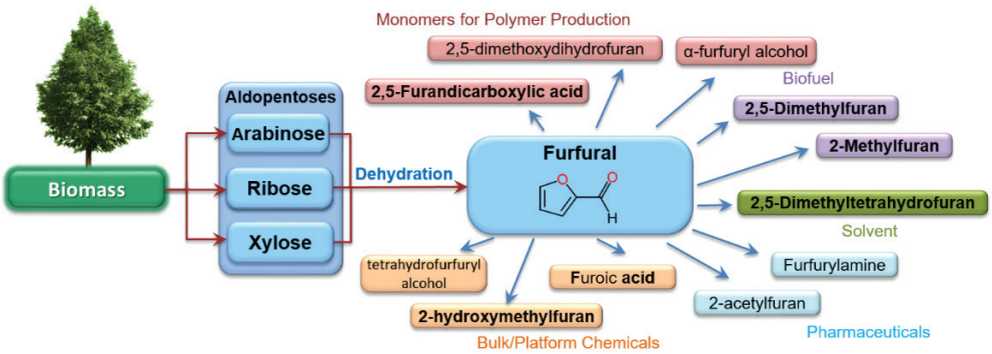

Figure 12. Scheme illustrating the targeted product (furfural) from biomass-derived feedstocks and its usage as a substrate in further synthesis into valuable chemicals [116]

Millions of tons of furfural (FAL) are produced annually around the world as a result of hemicellulose hydrolysis followed by the dehydration of an intermediate xylose. Due to the availability and cost effectiveness of the process, scientists are eager to develop and improve methods for converting biomass to furfural. By its hydrogenation, it can be transformed into furfuryl alcohol (FA), 2-methylfuran (MF) and tetrahydrofurfuryl (THF) alcohol [116].

FAL is currently produced on an industrial scale as a result of combined hydrolysis methods and dehydration or by cyclization of xylose with acid catalysts. Depending on the type of catalyst and the process conditions, various products can be obtained. The majority of the research aims to increase the selectivity of furfural hydrogenation, primarily to tetrahydrofurfuryl alcohol, which is currently used for the production of foundry resins and adhesives [109, 117]. This process takes place in the gas phase using a copper-chromate catalyst.

Research is continuing to find more efficient and environmentally friendly catalysts. Examples of catalyzed FA to FAL, MF and THF reactions are presented in Tables 2 and 3 [109], which also show the types of catalysts, reaction conditions and possible products of furfural hydrogenation.

The reaction of C_5 monosaccharides (xylose, arabiose, ribose derived from corn fiber) to furfural using H-beta zeolites, sulfuric acid (VI) and H-mordenite has been carried out [127]. Furfural has been obtained with yields of 62%, 55% and 44% using H-beta, H-mordenite and sulfuric acid, respectively. H-beta zeolite has been found to be the most active due to the presence of Brönsted and Lewis centers (respectively at a ratio of 1.66). H-beta catalyst gives a bifunctional effect: isomerization (due to the presence of the Lewis center) and dehydration (presence of the Brönsted center) of monosaccharides into HMF. Dumesic *et al.* developed a reaction to obtain HMF from xylose, fructose and glucose using various catalysts [46]. Their process was carried out in γ-valerolactone at 175°C. The catalysts used were γ-Al_2O_3, Sn-beta, Sn-SBA-15, H-ZSM-5, zirconium sulfate, 0.02M sulfuric acid (VI), Nafion-SAC-13, sulfonated carbon, H-beta, Amberlyst 70, and SBA-15 with propylsulfonic acid. From all tested catalysts, H-mordenite has the highest activity: in the case of glucose conversion (97%), HMF was obtained with a yield of 32% and 36% for fructose at 100% conversion rate [128].

A process of hydrolytic hydrogenation of arabinogalactan from hemicellulose into 5-hydroxymethylfurfural and furfural in the presence of a modified Ru-USY zeolite (Si/Al = 15 and 30, 1–5% ruthenium) has been also developed [129]. Another example is the usage of H-ZSM-5 zeolite in the dehydration of xylose to furfural. The process was carried out at a temperature range of 140–220°C. The highest selectivity was obtained at 200°C [130]. Other zeolites, such as SAPO-34 zeolites [131] and K-BEA [132], have the ability to carry out this reaction. Zhang *et al.* conducted a process of glucose conversion

on BEA zeolites (ion exchange Fe-BEA, Sn-BEA, Zr-BEA) [121], obtaining furfural and HMF as by-products. Sn-Beta zeolite showed the highest activity, producing a yield of 69.2% [133].

Table 2. Hydrogenation of FA to FAL [105, 109, 116]

Catalyst	Reaction conditions	Selectivity [%], (Efficiency [%])
0.6 wt% Pt/SiO_2	solvent: 2-propanol; 10 MPa; 100°C	98.7 (36)
0.6 wt% $Pt\text{-}Sn_{0.3}/SiO_2$	----------	96.2
2 wt% Ir/TiO_2 (473°C)	solvent: heptane/ethanol; 0.6 MPa; 90°C	21 (30)
2 wt% Ir/TiO_2 (773°C)	----------	100 (30)
$Ir\text{-}ReO_x/SiO_2$	solvent: water; 0.8 MPa; 30°C; 6h	> 99 (>99)
MoNiB/γ-Al_2O_3 (Mo:Ni = 1:7)	10 g FAL; 40 ml ethanol; 2 g cat.; 5 MPa; 80°C; 3h	91 (99)
$Cu_{11,2}Ni_{4.7}$/MgAlO	30 ml FAL; 90 ml ethanol; 1 g cat.; 1 MPa; 200°C; 2h	89 (93)

Table 3. Hydrogenation of FAL to MF, FU and THF [105, 109, 116]

Catalyst	Reaction conditions	Selectivity [%], (Efficiency [%])
Cu:Zn:Al:Ca:Na = 59:33:6:1:1	Gas phase; H_2:FAL = 25, 250°C	87 MF (99.7)
Cu-Fe/SiO_2 (Cu:Fe = 50:50)	Gas phase; 0,6 ml FAL in toluene; H_2:FAL = 5; 252°C	98 MF (99)
5% wt Pd/C	1 ml/min CO_2; 0.05 ml/min FAL; 15 MPa; 250°C; 0.5 g cat.	98 FU
stabilized colloidal particles Pd/C	2 mmol FAL; 1.5 ml formic acid; 1.5 ml water; 0.1 g cat.; 100°C; 30 min; microwave radiation	15 FU, 80 THF (90)

2.3.8. Levulinic acid and γ-valerolactone

Levulinic acid has been identified as a promising bio-compound derived from biomass. It is a platform molecule that is used as a precursor for pharmaceuticals, plasticizers, and various other additives (Figure 13). It arises as a result of depolymerization and dehydration of the cellulose fraction [124]. It can be obtained through hydrolysis/dehydration of aldohexoses such as glucose and fructose, or hexose-containing polymers like starch and cellulose.

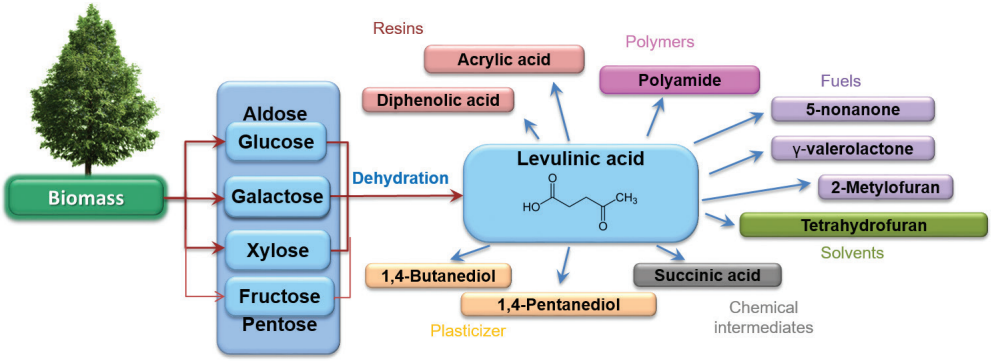

Figure 13. Scheme illustrating the targeted product (levulinic acid) from biomass derived feedstocks and its usage as substrate in further synthesis into valuable chemicals [124]

Biofine Renewables LCC CO developed a process in which to obtain HMF, agricultural residues undergo hydrolysis and dehydration in a H_2SO_4 solution in the first reactor. This relationship is recovered and transformed in a second reactor to LA at 60% yield in relation to the monomers contained in the starting substrate, which is cellulosic biomass [109, 125].

Levulinic acid was obtained as a result of glucose, starch and cellulose conversion in a hydrothermal process using Ga-MOR zeolite [134]. The process lasted for 6 hours at 175°C with a yield of 59.9%. Amin *et al.* developed a hybrid catalyst containing chromium chloride and a HY zeolite. As a result of the reaction at 145.2°C for 146.7 minutes they obtained a product with a yield of 55.2% [135]. Another example is dehydration of glucose using MFI zeolite with a different silicon module (Si/Al = 25, 30, 80, 120, 260). This process was carried out at 180°C for 8 hours. MFI zeolite with Si/Al=30 has been found to be the most active; the product obtained in this case had a yield of 35.8% [136]. They also developed a number of Fe-HY catalysts with various percentages of iron (5%, 10%, 15%). Of these catalysts, 10% Fe-HY catalyst showed the highest catalytic efficiency of around 62% [137,138]. Levulinic acid (LEA) has also been obtained by conversion of xylose in the presence of hot steam using alkaline zeolite catalysts. Zeolite Y was treated with a sodium base with various molar concentrations (0.05 M and 0.25 M). Dealuminated Y zeolite, 0.25 M NaOH, proved to be the most effective catalyst. The product was obtained with a yield of 30.4% and a conversion of 84.3%. The process was carried out for 3 hours at 170°C [139]. Zeolite LZY has also found application in the catalytic dehydration of fructose. The process was carried out in a batch reactor at 140°C for 15 hours. 0.432 g of levulinic acid was obtained from 1 g of fructose [140].

γ-valerolactone (GVL) is a potential fuel and green solvent; it can be obtained from furfural by hydrogenation at 120°C in 2-butanol solution on Zr-BEA and Al-MFI catalysts [111, 141–143]. GVL is also produced via hydrogenation reaction from levulinic acid.

Other important chemicals like 1,4-pentanediol or 2-methyltetrahydrofuran can be obtained by chemoselective hydrogenolysis of GVL.

Selective and effective hydrogenation of levulinic acid to γ-valerolactone (GVL) is possible with a complex catalyst consisting of dipyridylamine as the core and ruthenium and iridium ligands. The reaction has been carried out in formic acid and triethylamine, using 0.05 mol% of ruthenium [124]. Reaction attempts have also carried out using Au/Al_2O_3, Au/CeO_2 and Au/TiO_2 catalysts. It has been confirmed that in the gas phase the efficiency of the LEA to GVL reaction is 100%. These results were achieved in stoichiometric conditions, H_2/LEA = 1 [126]. Other examples of the LEA reaction with specific catalysts are summarized in Table 4.

Table 4. Hydrogenation of levulinic acid to GVL [109]

Catalyst	Reaction conditions	Selectivity [%], (Efficiency [%])
1 wt% Ru/C	Gas phase; 10 wt% LEA in dioxane; 0.1 MPa; 265°C; WHSV= 0.514 h^{-1}	98.6 (100)
5 wt% Cu/SiO_2, 8 wt% Ni, 27wt% Cu/SiO_2	Gas phase; LEA in dioxane; 1 g cat. WHSV = 0.513 h^{-1}; 265 °C; 1 MPa (a); 2.5 MPa (b)	99.0 (100) 90 MTHF (100)
5 wt% Ru/C	50 wt% LEA in dioxane; 0.36 MPa; 150°C; 4 h	97 (100)
5 wt% Ru/C	50 wt% LEA in H_2O; 0.35 MPa; WHSV= 4.8 h^{-1}	96 (100)
1 wt% Pt/TiO_2	200 °C; 4 MPa; (molar ratio) H_2/LEA 5:1; WHSV= 9 h^{-1}	> 95 (95)
0.64 wt% Ru/TiO_2	LEA w H_2O; 0.4 mol% Ru; 150°C; 3.5 MPa	93 (100)
Cu/ZrO_2	5% wt LEA in 95 ml H_2O or MeOH; 0.5 g cat.; 200°C; 0.35 MPa; 5 h	100 (100) in H_2O 90 (100) in MeOH
5 wt% Ru/C	5 g LEA (43.1 mmol); 250 mg Ru (0.12 mmol); 1.3 MPa; 25°C; 50 h	97.5 (100
Ru-Sn/C (Ru:Sn = 3.6:1)	2 M LEA in 2-sec-butylfenol; 220°C; 3.5 MPa; WHSV = 2.2 h^{-1}	95.8 (98)
Ru particles with $Ru_3(CO)_{12}$	8.6 mmol LEA in H_2O; 3 mg Ru (0.005 mmol z $Ru_3(CO)_{12}$; 130°C; 2.5 MPa; 24 h	99(100)

2.3.9. Adipic acid

Adipic acid is used in the production of nylon, PVC and polyurethanes; production is about 2.5 MTon/year. Adipic acid is produced from a mixture of cyclohexanol and cyclohexanone, oxidative cleavage of cyclohexene using hydrogen peroxide, or by the hydrocarboxylation

of butadiene [144]. It has traditionally been produced from various petroleum-based feedstocks (e.g., phenol, benzene, and cyclohexane), but shifts in the hydrocarbon market have resulted in the virtual elimination of phenol as a feedstock. In recent years, cyclohexane-based processes have accounted for about 93% of global production capacity. Two steps are involved in ADA production: 1) oxidation of cyclohexane to produce KA oil (cyclohexanone and cyclohexanol) and 2) nitric acid oxidation of KA oil to produce adipic acid.

Recently, start-up companies such as Rennovia, Verdezyne, BioAmber, Celexion, and Genomatica have developed bio-based routes to produce adipic acid. Rennovia's patented two-step process for the production of bio-based adipic acid from glucose involves:

(i) selective catalytic oxidation of glucose to glucaric acid
(ii) selective catalytic hydrodeoxygenation of glucaric acid to adipic acid (see Figure 14).

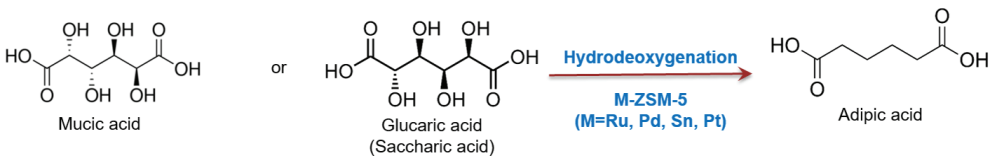

Figure 14. Scheme illustrating the targeted product (adipic acid) from biomass-derived feedstocks (glucaric acid) [148]

Two basic motivations for considering alternative biomass feedstock sources for production of ADA are: 1) in the long term they could be less expensive to produce than conventional methods using crude oil derivative cyclohexane; 2) societal demands for the production of industrial chemicals via 'sustainable' methods; 3) technology-specific market demands that require production of ADA from bio-chemical resources. Potential catalysts for hydrodeoxygenation are metal (Ru, Pd, Sn, Pt) on ZSM-5.

2.3.10. Hydrogenation of succinic acid

Succinic acid has been obtained as a result of anaerobic digestion from glucose, with bacteria such as *Anaerobiospirillum succiniciproducens*, *Actinobacillus succinogenes*, and *Mannheimia succiniciproducens* [123]. The obtained product can be used as a precursor of many industrially important chemicals for the production of food or medicines. After assessing the costs of raw materials and estimating the potential size of the market, the results indicated that the current process of producing succinic acid from petroleum-based compounds may be replaced in the future by biomass fermentation. The hydrogenation reaction of succinic acid is presented below. With suitable catalysts and reaction conditions, it is possible to obtain 1,4 - butanediol (1,4-BDO), γ-butyllactone (GBL) or tetrahydrofuran (THF) [105]. The results are shown in Table 5.

Table 5. Catalytic reactions of succinic acid [105,109]

Catalyst	Reaction conditions	Select. GBL [%]	Select. BDO [%]	Select. THF [%]
1 wt% Au/TiO_2	12 mmol succinic anhydride; 50 ml dioxane; 0.2 g cat.; 240°C; 5 MPa;	97		
5 wt% Pd/Starbon*	10 mmol SUC*; 30 mmol EtOH; 50 mmol H_2O; 0.1 g cat.; 1 MPa; 100°C; 24h	30 (75) 15 (78)	70 (75) 85 (78)	60 (90)
5 wt% Pt/Starbon*		10 (60)	90 (60)	
5 wt% Rh/Starbon*		30 (90)	10 (90)	
5 wt% Ru/Starbon*				
5 wt% Pd/AX (aluminum gel)	0.2 g SUC* in dioxane; 240°C; 6 MPa; 4h	71 (76)		
5 wt% Re/MC (mesoporous carbon)	0.5 g SUC* in 50 ml dioxane; 0.2 g cat.; 240°C; 8 MPa; 8h	26.8 (100)	4.5 (100)	38.3 (100)
Re- 2 wt% Pd/C	15 g SUC* in H_2O; 1g cat.; 160°C; 15 MPa		66 (100)	
Re- 2 wt% Ru/C			40 (100)	
3.6 wt% Re – 2 wt% Pd/TiO_2	5 wt% SUC* in H_2O; 1 g cat.; 160°C; 15 MPa		83 (100)	

SUC * – succinic acid, Starbon * – mesoporous carbon

2.3.11. Hydrogenation of itaconic acid

Itaconic acid is an organic acid that is used as a raw chemical material in the production of various chemical substances such as poly(itaconic acid), resins and biocomponents. This compound and its derivatives are widely used in the textile, chemical and pharmaceutical industries. Due to growing consumer needs and the depletion of fossil fuels, interest in biotechnology processes is growing; for example, the development of a method for the preparation of itaconic acid based on glucose fermentation, or the conversion of lignocellulosic biomass. The possible catalyzed reactions of itaconic acid are presented below [127]. 80% IA undergoes a hydrogenation reaction to 2-methylbutanediol (MeBDO) and methyl-γ-butyrolactone (MeGBL) with the participation of a 1 wt% catalyst. Pd, 4 wt% Re on a TiO_2 support. This process was patented by DuPont. Additionally, BASF developed a hydrogenation process in 2001, in which 100 wt. IA yielded 45.2 wt%. MeBDO and 47.9 wt.% MeGBL in the presence of Pt and Re. In order to extend the life of the catalyst, itaconic acid esters undergo hydrogenation reactions. Therefore, the first

step was esterification, after which the researchers carried out a process of catalytic activity involving Cu-Cr-Mn-Ba and CuO-ZnO on a fixed bed. This process was carried out with 100% efficiency [105]. Another example is the decarboxylation reaction of itaconic acid with the participation of Pd/Al_2O_3, Pt/Al_2O_3, Pd/C and Ru/C catalysts. As a result of the reactions, methacrylic acid was obtained at 50% yield with a high selectivity of 84% [128].

2.3.12. Dihydroxyacetone

A new chemocatalytic technology for the continuous oxidation of glycerol (GLY) to dihydroxyacetone (DHA) in the gas phase has been developed [145]. This process takes place over the Fe-MFI catalyst in the presence of molecular oxygen. The reaction was carried out in a fixed bed reactor. Activation of the steam generator at 600°C showed dispersed iron in the form of cations and FeOx clusters, which guarantee a product efficiency of 50%. A method for converting dihyroxyacetone to C_1–C_4 alkyl lactate has also been developed [146]. The process was carried out using MFI, MOR, FER, BEA zeolites with gallium particles. Ga-FAU proved to be the most active, giving products such as n-propyl, n-butyl lactate and ethyl lactate. Another possibility is the reaction of dihydroxyacetone into ethyl lactate on a Ga-USY catalyst [147].

2.3.13. Lactic acid/alkyl lactates

Developing efficient catalysts for the conversion of bio-renewable feedstocks to selected key chemicals such as lactic and acrylic acid esters (see Figure 15), which would be an alternative to the currently used techniques of obtaining them from non-renewable resources, is the main issue for scientists working in the field of catalysis.

Lactic acid is used in the food industry and for the production of other chemicals and polymers; its production is about 2.7 Mton/year. Lactic acid has three available atoms for adsorption: the oxygen atom of the alcohol group and the two oxygen atoms of the carboxyl group. Based on the literature [145], lactic acid adsorption over metallic cations gives several

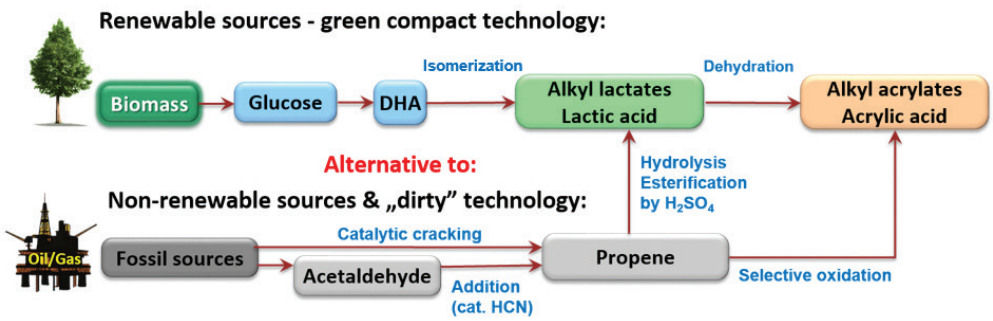

Figure 15. Scheme illustrating lactic acid, acrylic acid, and their esters [44]. (DHA=dihydroxyacetone)

possible binding modes at zirconia surfaces: monodentate, bidentate bridging and bidentate chelating, for which a dissociative bidentate bridging mode is preferred. The classical pathway through a carbocation proceeds with a very high activation energy; therefore, another mechanism through a carbanion and with acrylic acid formation was suggested.

From the family of biomass-derived compounds, lactic acid is the most promising and can generate multiple final and intermediate chemicals such as acrylic acid, pyruvic acid, 1,2-propanediol, 2,3-pentanedione or acetaldehyde (see Figure 16) [21, 101]. This compound can also be polymerized into biodegradable plastic, i.e. polylactide (PLA), or solvents.

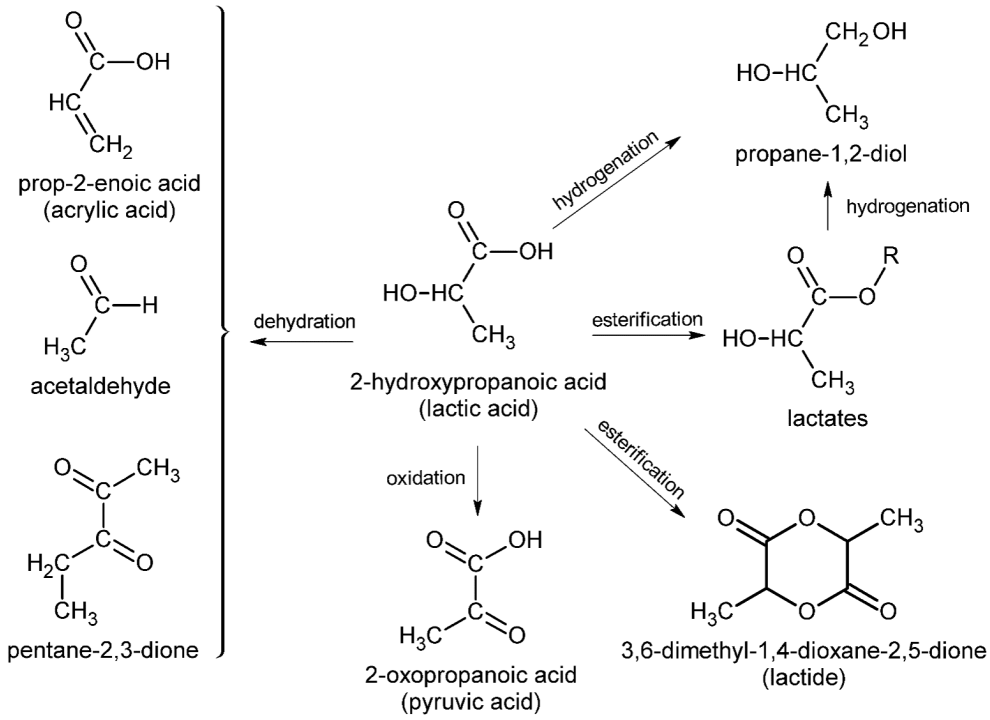

Figure 16. Scheme illustrating lactic acid reactions [9]

Dehydration of lactic acid provides the most promising and environmentally friendly way to produce, for example, acrylic acid. However, dehydration of lactic acid may be accompanied by other competing reactions such as hydrogenation, condensation, decarboxylation and esterification, where decarboxylation to acetaldehyde is a major side reaction and has a significant effect on the low production of acrylic acid. To inhibit the formation of acetaldehyde and improve the selectivity of the desired acrylic acid, the effects of many different catalysts have been tested by various researchers [9].

2.3.14. Acrylic acid and alkyl acrylates

Acrylic acid is important for the synthesis of organic compounds. It is widely used for the preparation of a variety of materials such as water-absorbent polymers, adhesives and textile treating agents (see Figure 17).

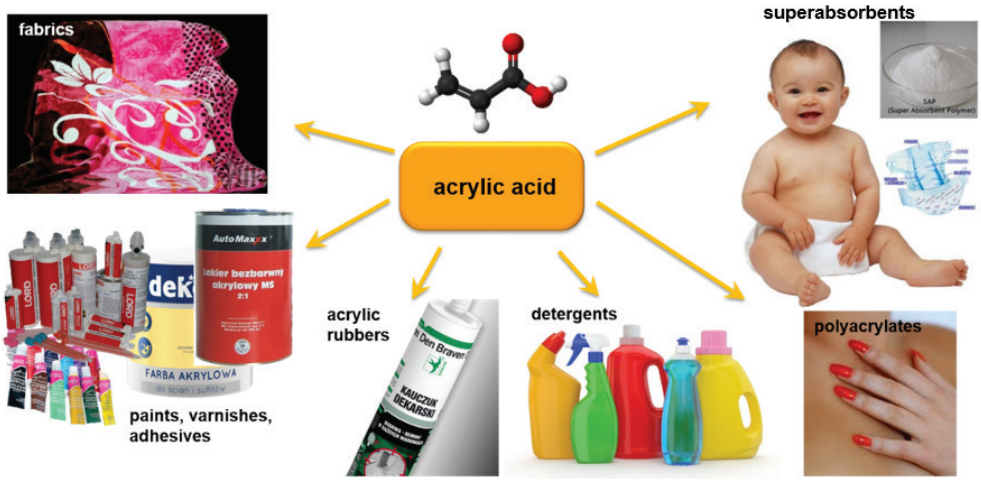

Figure 17. Scheme illustrating the main types of acrylic acid processing [149]

The most common industrial process for preparing acrylic acid is the selective oxidation of propylene; this is the basic method of obtaining the product in the fossil industry. Due to the high demand for fossil fuels and the relatively low stocks of crude oil, the price of propylene and its by-products is rising, which leads to increased pressure on the production of acrylic acid from sources other than propylene.

Acrylic acid is a platform molecule that is used as a building block to produce acrylate polymers and plastics [150]. Its production increased at a rate of 4% a year between 2006 and 2011, reaching 4.2 Mton in 2011; it is predicted to increase by about 5% per year between 2012 and 2017, and recently its production has been about 4.7 Mton/year. [151]. Acrylic acid is currently produced by catalytic oxidation of propylene using a two-step process (Figure 2). The acrylic acid market in 2013 was worth $11 billion, and the forecast until 2020 is around $18.8 billion per year [150]. In the next 5 years, the global demand for acrylic acid will be around 8.169 billion tons a year.

An alternative route to producing acrylic acid is therefore required, especially in the context of commitment to environmentally friendly catalytic processes; for example, the single-step dehydration of lactic acid. Catalytic dehydration of lactic acid to acrylic acid has received increasing attention in the last two decades, but high selectivity has proven elusive.

Metal-exchanged zeolites are promising catalysts for further development for LA to AA dehydration. However, acrylic acid is rarely obtained selectively from lactic acid because of the easy decarbonylation/decarboxylation of lactic acid, which leads to acetaldehyde and CO_x. High yields of acrylic acid have been obtained using modified zeolites, but they suffered from coking and hydrothermal instability.

As described by Zhang [140] in 1958, Holmen was the first to show that acrylic acid could be obtained by the dehydration of lactic acid using a mixture of sodium sulfate and calcium sulfate as a catalyst.

One method of acrylic acid production could be the dehydration of lactic acid over hydroxyapatite (Ca-HAP) catalysts with different mole ratios of Ca/P and the calcination temperatures, as described by Bo Yan *et al.* [152]. Hydroxyapatites (HAP) are known to be important acid–base catalysts. According to the study of Bo Yan *et al.*, the HAP sample (with Ca/P = 1.62 and calcination temperature of 360°C) was identified as the most effective for the selective formation of acrylic acid from lactic acid, showing an acrylic acid selectivity within the range 71–74% and an acrylic acid yield of 50–62%. The gas-phase dehydration of lactic acid was conducted under atmospheric pressure in a vertical fixed-bed quartz reactor. The reaction feed includes an aqueous solution containing 35.7 wt% or 10 mol% lactic acid served with a space velocity of 2.1 h^{-1} at 360°C.

Huang *et al.* [153–156] performed a lactic acid dehydration process on NaY zeolites modified by rare earth metals (lanthanum, cerium, samarium and europium), of which La-NaY had the best selectivity. The catalysts were obtained by ion exchange of the corresponding cations (lanthanum, cerium, male and europium) in an aqueous nitrate solution. The modified zeolite was marked with the silicon module Si/Al = 4.5. Subsequent scientists have developed a catalyst by modifying NaY zeolite with potassium. The addition of potassium to NaY significantly improved its lifetime [157].

The other method obtaining acrylic acid that was described by Xianghui Zhang *et. al.* [158] involves ZSM-5 zeolite as a catalyst. It is well known that ZSM-5 has strong acidic sites on the surface of H-ZSM-5, which gives very low selectivity for acrylic acid. Fortunately, the surface acidity of H-ZSM-5 zeolite can be regulated over a wide range by alkaline treatment. Firstly, the H-ZSM-5 zeolite was treated with NaOH aqueous solution. The dehydration reaction of lactic acid was then carried out in a vertical fixed-bed steel reactor. Studies using 30 wt% lactic acid have shown that for differently modified ZSM-5 catalysts, lactic acid conversion changes little: it only changes in the small range of 95.8–97.3% in the temperature range 335–380°C; however, the selectivity for acrylic acid exhibits a volcano-type dependence on NaOH concentrations. The best acrylic acid selectivity of over 65% can be achieved when the concentration of NaOH is 0.3–0.5 mol/L. Increasing the NaOH concentration causes decreased acrylic acid selectivity and the appearance of unknown products. The best catalytic performance (96.9% lactic acid conversion and

77.9% selectivity for acrylic acid) was obtained over the resulting ZSM-5 catalyst, treated with 0.5 mol/L NaOH and 0.5 mol/L Na_2HPO_4 under the optimized reaction condition (350°C, LHSV = 4 h^{-1}). One of the main problems is the stability of catalysts for the dehydration reaction of lactic acid. Conversion of lactic acid in a reaction time of 52 hours is still 88% at a selectivity as high as 65% acrylic acid. The slight decrease in conversion and selectivity may be due to the inevitable deposition of coke, which is typical of acid-base catalysts.

Another way to modify ZSM-5 zeolites is by using an ion exchange with alkali metals [159]. ZSM-5 zeolite (Si/Al molar ratio = 75) was preheated at 550°C for 6 h and treated with an aqueous solution of MNO_3 (1 mol/L; M = NH_4, Li, Na, K, Rb, or Cs; 14 g of ZSM-5 zeolite in 140 mL of MNO_3) at 80°C for 6 h to obtain ion-exchanged ZSM-5. The modified zeolites gave improved catalyst performance in dehydration of lactic acid to acrylic acid. Conversion of lactic acid decreases in the following order: H> Li> Na> K> Rb> Cs-modified ZSM-5. The highest selectivity of acrylic acid was prepared using a KZSM-5 catalyst ($K_{0.84}Na_{0.16}$ZSM-5). These results indicate that the introduction of the alkali metal effectively inhibited the decarbonylation and decarboxylation of lactic acid to acetaldehyde. It was found that the introduction of alkali-metal cations decreases the total acid-base number, which improves acrylic acid selectivity.

Another article by Yan *et al.* discusses the dehydration of lactic acid carried by Rb^+- and Cs^+-exchanged Beta zeolite catalysts [160]. In this case, raw powders of as-synthesized Beta zeolite (SiO_2/Al_2O_3 = ca. 40) were used and the Rb^+- and Cs^+-ions were added by ion-exchange with aqueous solutions of $RbNO_3$ and $CsNO_3$, respectively. The gas-phase dehydration of lactic acid was carried out under atmospheric pressure at 360°C in a vertical down-flow fixed-bed tubular quartz reactor. This study shows that Rb^+- and Cs^+-exchanged Na zeolites with suitable exchange degrees could be highly efficient for catalyzing the gas-phase dehydration of bio-derivative LA for sustainable AA production. $Rb_{0.95}Na_{0.05}$ and $Cs_{0.81–0.90}Na_{0.19–0.10}$ samples were identified as the best-performing catalysts for AA production by optimizing the exchange degrees for Rb^+ and Cs^+, respectively, to uncover the suitable acidity–basicity balance; this offers acrylic acid selectivity as high as 69–70% and yields more than 65 mol%.

Alkyl lactates are more promising for acrylic acid and its ester production. Alkyl lactates are easier to vaporize and less polymerizable than lactic acid. Their ester functions, which are less reactive, limit decarbonylation/decarboxylation reactions. The standard industrial reaction for producing, for example, methyl acrylate, is esterification with methanol under acid catalysis (sulfuric acid, p-toluene sulfonic acid, acidic ion exchangers [149]). Ethyl acrylate is produced by acid-catalyzed esterification of acrylic acid, which in turn is produced by oxidation of propylene. It may also be prepared from acetylene, carbon monoxide and ethanol by a Reppe reaction. Biomass as a renewable resource for alkyl acrylate seems a more ecologically friendly.

Interest in the use of alkyl lactate instead of lactic acid as a reactant to reach higher acrylic acid selectivity has previously been illustrated for a $Ca_3(PO_4)_2$–$Ca_2(P_2O_7)$ (50/50 wt%) mixture [161]. The highest acrylic acid molar selectivity was found for ethyl lactate (79%), followed by methyl lactate (75%) and lactic acid (54%). Moreover, the use of alkyl lactates could simplify the separation and purification process and reduce production costs [162], even if it implies the recycling of co-produced alcohols. In that regard, additional molecules of alkyl lactates could be produced. Alkyl lactates (AL) have been shown to be effective starting materials for the production of acetaldehyde, 2,3-pentanedione, lactide (a biopolymer starting material), and alkyl acrylates (AA) [163]. Growth in demand for acrylic acid is forecast at 4.5% per year in 2016-2021, driven by the production growth of acrylate esters at about 4% per year. After butyl acrylate and ethyl acrylate, methyl acrylate is the third most important acrylic ester, with a worldwide production of about 200,000 tons per year [164]. Alkaline earth phosphates were prepared and evaluated in gas phase dehydration of ethyl lactate to acrylic acid and ethyl acrylate [165]; however, zeolites are much more promising materials for biomass conversion into lactates and acrylates.

3. ZEOLITES

Zeolites and microporous or crystalline aluminosilicates are effective catalysts in many applications [166]. Due to their ability to catalyze many types of hydrocarbon reactions, they are ideal candidates for the production of chemicals from biomass [24, 25]. Effective zeolite-based catalysts integrate three main functions and length scales: active sites located in micropores, access and transport provided by the introduced mesopores, and the macroscopic shape of the catalyst body.

3.1. Zeolite structure

The various zeolitic materials are characterized by a variety of micropore structures featuring specific sizes, shapes, and connectivity (Figure 18), as well as the possibility of tuning the acid/base properties. Zeolites are effective three-dimensional supports for active nanoparticles. However, the industrial performance and selectivity of microporous zeolites in the production of the desired chemicals on an industrial scale is far from being

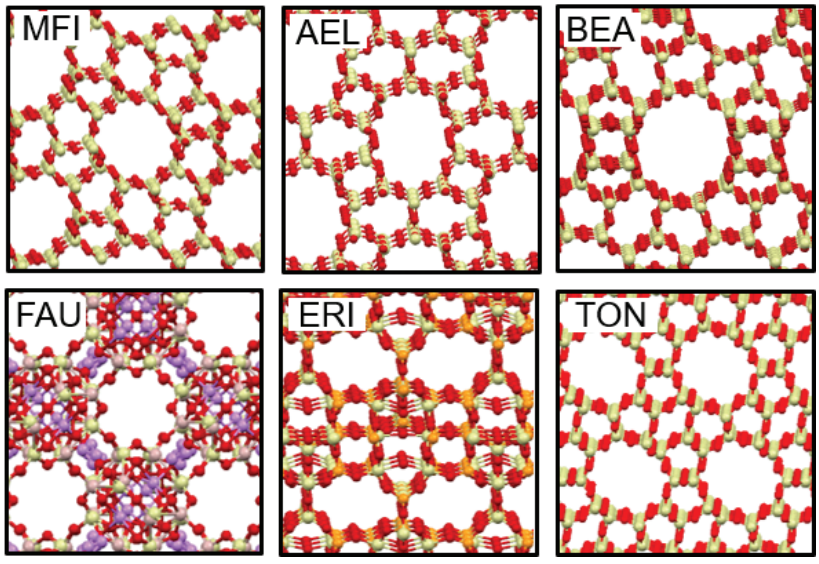

Figure 18. Differences in natural micropores in various zeolite structures [157]

optimal due to limited access to micropores with active basic/acid sites or nanoparticles and diffusion limitations. On the other hand, ordered microporous metallosilicates containing auxiliary mesoporosity have shown improved performance compared to purely microporous zeolites in a wide range of catalyzed reactions.

We selected zeolites with 3D (ZSM-5 and faujasite) and 1D (ZSM-22) pore topologies for the detailed description of the crystal structure below.

ZSM-5

The ZSM-5 framework has a three-dimensional pore structure and consists of straight and zig-zag internal channels along the x- and y-axis, (see Figure 19a and b). The ZSM-5 structure along the z-axis consists of chains (Figure 19c) separated from each other by an open zig-zag channel. The crystal structure along the z-axis also has an interesting structure

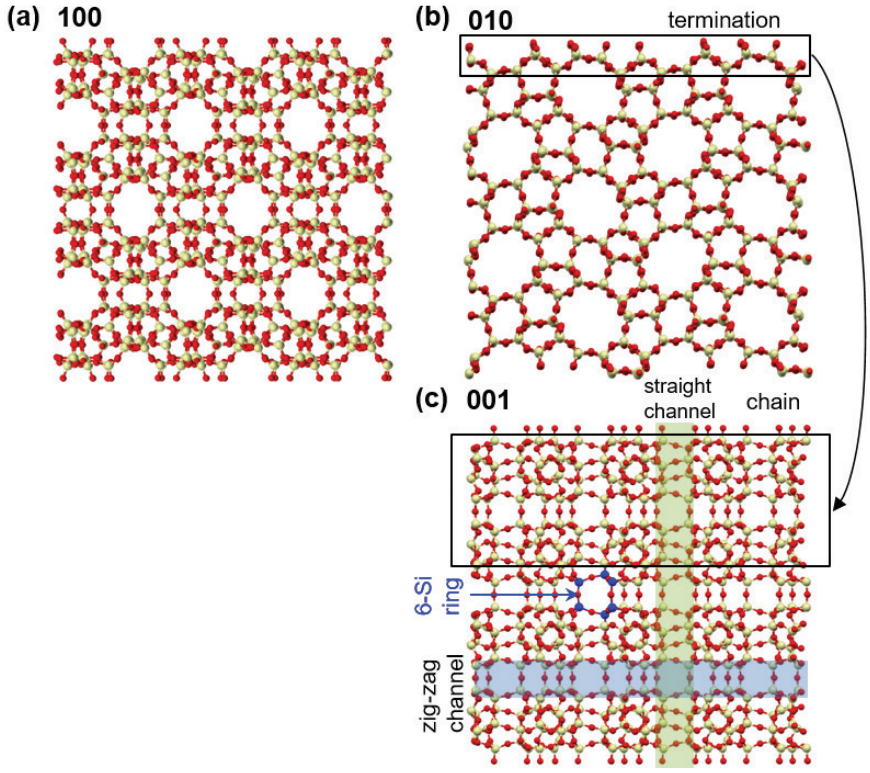

Figure 19. ZSM-5 structure: orientations along the Cartesian axis: (a) x-axis – zig-zag channels, (b) y-axis – straight channels, (c) z-axis – cross-section of zig-zag and straight channels are shown. Between the zig-zag and the straight channel, the 6-ring is shown in blue. The black box at (010) surface refers to the chosen termination of the (001) surface (own work)

and can take part in demetalation. The termination of (001) surface is shown in Figure 19b (black box) and corresponds to that shown by Diaz *et al.* [167, 168] in HRTEM.

The (001) surface is terminated by full SiO_4 tetrahedra just above the straight channel and contains the chains shown in Figure 19c. The 6-Si ring is located between the chains and the cross-section between the straight and zig-zag channels (blue, Figure 19c).

BEA

The crystal structure of BEA was chosen from Database of Zeolite Structure [152]. The tetragonal phase of BEA framework type is described by the space group P 41 2 2 (no. 91) with lattice constants a = b = 12.6320 Å and c = 26.1860 Å. The crystal unit cell contains 192 atoms.

The BEA framework (purely siliceous silicalite-1 and aluminum-containing BEA) has a three-dimensional channel system consisting of straight channels along the *a* and *b* axes and a tortuous channel along the *c*-axis [169]. The pore-limiting diameter of the largest pore is 6.9 Å (Figure 20) [170]. The maximum sphere diameter that can diffuse along BEA pores is 5.95 Å [152].

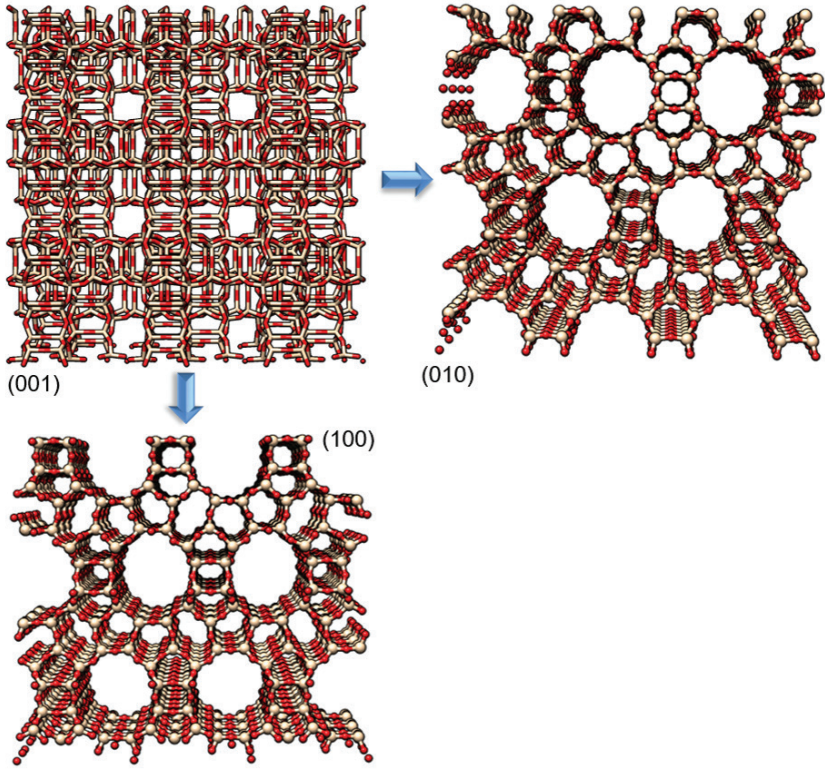

Figure 20. BEA structure (own work)

FAU

The cubic phase of framework type FAU (Figure 21) is described by the space group F d-3 m (# 227) with lattice constants a = b ==c= 24.3450 Å [152]. The crystal unit cell contains 706 atoms.

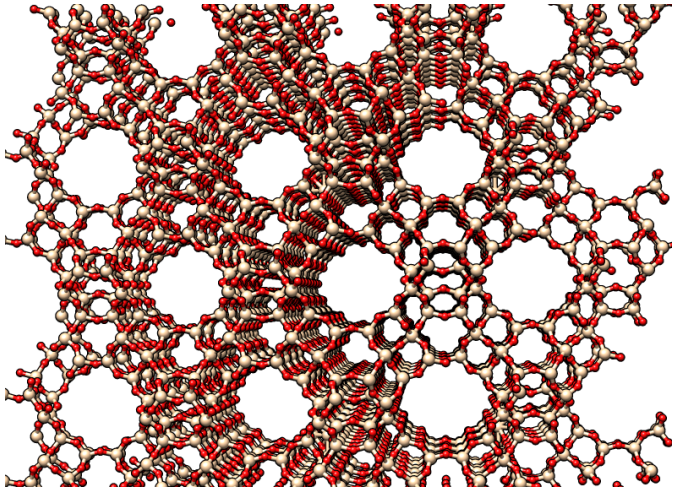

Figure 21. Structure of faujasite (own work)

The faujasite framework consists of sodalite cages (Figure 22) that are connected with hexagonal prisms. The pore, which is formed by a 12-membered ring, has a relatively large diameter of 7.4 Å. The inner cavity has a diameter of 12 Å and is surrounded by 10 sodalite cages.

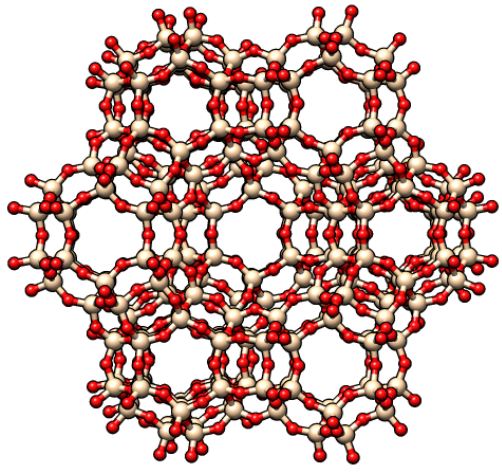

Figure 22. Single unit of faujasite (own work)

ZSM-22

The orthorhombic of framework type ZSM-22 is described by the space group C m c m (# 63) with lattice constants a = 14.1050 Å, b = 17.8420 Å and c= 24.3450 Å [152]. The crystal unit cell contains 72 atoms.

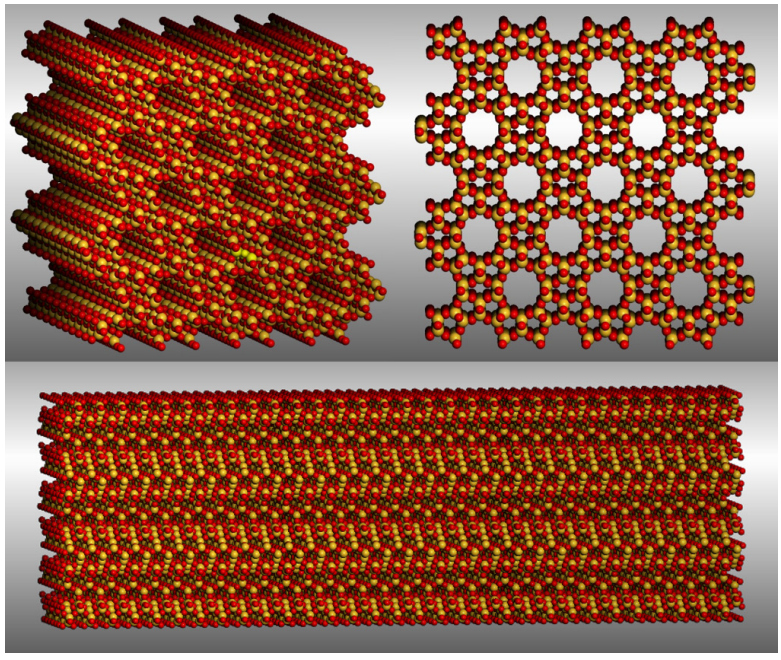

Figure 23. Structure of ZSM-22 (own work)

ZSM-22 crystals typically comprise needle-shaped agglomerates of individual nanorods (Figure 23) [171, 172]. ZSM-22 has 1D pore topologies. This particular morphology is intimately connected to the Al distribution in the crystals [172].

3.2. Synthesis

Obtaining zeolites

The hydrothermal synthesis of zeolites with silicate gel or aluminosilicate in an alkaline medium is given at high temperatures of 60–240°C with 0.1–2 MPA pressure [158]. The first attempts to obtain these materials were carried out by R. M. Barrera and R. Milton; in the 1940s, their research led to the synthesis of artificial zeolites such as P, Q, A and X. The next significant stage of receiving zeolites was the release of templates. Currently over

200 zeolites have been obtained as a result of this hydrothermal process in the presence of organic templates.

Organic templates play a very important role in the synthesis of zeolites. Thanks to these so-called templates, it is possible to obtain materials with a specific space and pore size. Unfortunately, most of these templates are toxic and removing them from the zeolite structure can cause high temperature processes and the formation of heat-treated gases such as NO_x and CO_2. Of course, it is possible to solve these problems, but this is associated with increased cost of the synthesis process. The new possible ways of synthesizing zeolites with the appropriate templates are presented below [159].

Synthesis of zeolites using organic templates

In 1961, for the first time, organic quaternary ammonium cations were used in the synthesis of zeolites by Barrera and Danny, who successfully synthesized clean high-silica zeolites [158]. Although the synthesis procedure for zeolite is rather simple, it is a complex process which is influenced by many factors: the type of obtained zeolite (e.g. shape or crystal size), morphology or composition. Another important factor is the use of an appropriate mineralizing agent, which is referred as a template. Usually amines, amides, pyrrolidine, organic quaternary ammonium cations and metal chelate complexes are used as templates [151, 158, 160, 161].

Synthesis of zeolites with the participation of low-toxicity templates

The organic templates which are used in the synthesis of zeolites are generally too expensive and toxic. Finding cheap substitutes and reducing the toxicity of the process is crucial to in order to reduce the negative impact on the environment. Zone and his co-workers obtained aluminosilicate zeolite SSZ-25 (MWW) by using low-priced isobutylamine with a small amount of aminoadamantane to eliminate the more expensive examethyleneimine. Another example is the use of a low-toxicity organic template for synthesis of zeolite by the Xiao team. Tetramethylguanidine, an animal metabolism product, was applied as a template to obtain AIPO-5 (AFI), SAPO- 5, MnAPO-5 and CoAPO-5 [162].

Synthesis of zeolites with low-cost templates

A new approach to the synthesis of zeolites, i.e. the use of a small part of the template to determine the nucleation of the product, was developed by Zones and co-workers [161]. The addition of amine in certain quantities is an essential step in maintaining the alkalinity of the product. Ammonia and methylamine were used as small-molecule amines which combined with imidazole to give zeolite SSZ-32. Of course, based on the application of small-molecule amines, it is possible to obtain many zeolites SSZ-13 (CHA),

SSZ-33(CON), SSZ-35(STF), SSZ-42(IFR) or SSZ-47. Conducting the process in such conditions allows reduction of the cost of using templates and waste treatment.

Cu-tetraethylenepentamine (Cu-TEPA) copper–amine complex was designed by Ren and others to be a novel template for synthesis of aluminosilicate zeolites CHA (SSZ-13) in view of (1) the good stability between Cu-TEPA and CHA, (2) strong interaction between the templated molecule and negatively charged silica, and (3) its high stability in strongly alkaline media [158].

Synthesis of zeolites with the use of renewable templates

Davis and his scientific collaborators have done pioneering work on extracting organic templates from micropores of zeolites [158]. They reported the possibility that TEA^+ cations can be easily extracted from CIT-6 zeolite by using acetic acid. This method can also be applied in the case of MFI. Furthermore, they showed that the ability to remove organic templates is dependent on their size and on the strength of interaction between the template and zeolite. Moreover, they used a cyclic ketal as an organic template which, under zeolite synthesis conditions (high pH), remained intact; thus, after its removal, the zeolite structure was not destroyed. The concept consists in the cleavage of an organic template into at least two compounds during the treatment of zeolite (in this case ZSM-5) by 1 M HCl for 20 h at 80°C, followed by a mixture of 0.01 M NaOH and 1 M NaCl for 72 h at 100°C. After removing the template from the aluminosilicate structures, it can certainly be recombined and reused [158]. Studies have also been carried out on the elimination of SDA from ZSM-5 and beta zeolite by extraction with methanol, acetic acid and dimethylformamide, followed by calcination of zeolite. This two-stage process does not produce many greenhouse gases. Processes of replacing high temperature calcination with microwave radiation, ultraviolet radiation and ozone operation have also been successfully developed [163].

Synthesis of zeolites without the use of organic templates

Zeolites were prepared without the use of organic templates; they were rich in aluminum and were synthesized with the use of basic metal cations [151, 164]. However, zeolites are commonly obtained using organic SDA due to the size of their metal cations and the hydrophobicity of zeolite (the silicon module increases, and the pore space becomes also hydrophobic). Recently, due to the cost of synthesis and a greater emphasis on environmental protection, research is being carried out on zeolite preparations with the elimination of the use of organic templates.

Synthesis of zeolites without the use of solvent

Traditionally, the synthesis of zeolite under hydrothermal sol-thermal conditions takes place in the presence of a solvent. The addition of solvent to the mixture is associated with

an increase in production costs and also generates waste that is difficult to clean. For this reason, new solutions for the synthesis of zeolites without the use of solvents are sought. Xio's team carried out the process of obtaining zeolite materials without the addition of a solvent. For this purpose, the dried raw materials were heated to a suitable temperature [162]. As a result of this method, MFI, SOD, MOR, BEA and FAU were obtained. Also, processes of incorporating heteroatoms (Al, Fe, B, Ga) were carried out, thanks to which the zeolite materials gained catalytic properties. It is interesting that a hierarchical Si-ZSM-5 material can be obtained by adding $CaCO_3$ nanoparticles (around 100 nm) as a template. Another example is the use of NH_4F in zeolite synthesis; NH_4F is added to milled anhydrous reactants and the mixture is heated at 140–240°C. Attempts to obtain MFI, BEA, EUO and TON zeolites have been successful with this method. The presence of F-ions causes the crystallization of zeolite grains from the amorphous phase. Compared with conventional hydrothermal synthesis, this method is not only simpler but also increases process efficiency. In the future, it could successfully replace the current synthesis method, which is carried out in a solvent [173]. Zhang's team developed a synthesis of nanoporous aluminophosphates (SF-APO) with incorporated cations (SF-MAPO, where M = Co, Fe, Cr) by grinding and material treatment, and heating at the right temperature without the use of solvent [174]. Another possibility is to use a fixed $NH_4H_2PO_4$ template during the synthesis of SAPO-34. The process is the same as in the previous method: grinding the substrates and heating them [175].

PREPARATION OF SELECTED SYNTHETIC ZEOLITES

ZSM-5 zeolite

The synthesis of MFI zeolite can be divided into six stages [176]. The first is the production of a silicate solution. For this purpose, TEOS, template-TPAOH and H_2O were mixed together. The content was placed in a polypropylene bottle and shaken on a shaker for 24 h at room temperature to hydrolyze the TEOS and to obtain a clear solution. The second step is to obtain the aluminate solution. After about 22 h, a mixture containing a solution of the aluminate source (aluminum oxide or sodium aluminate) NaOH, TPAOH and H_2O was prepared. The whole mixture was stirred for 2 h to obtain a clear solution. The third stage was a combination of the first two stages, in which two solutions were mixed with rapid stirring for about 10 minutes. The obtained content was placed in an autoclave equipped with a Teflon pad and a magnetic stirrer. The autoclave was sealed and placed in an oil bath at 150°C and kept for the right time. The fourth stage is hydrothermal treatment. The fifth stage is cleaning of the product. When the autoclave has cooled to room temperature, the mixture is removed and centrifuged to recover the product. This product was washed several

times and centrifuged. In the final, sixth stage, the freeze-dried crystals were calcined for 16 h at 500°C (heating rate – 5°C/min) to remove the templates.

Synthesis of Mesoporous ZSM-5 Zeolite Crystals by Conventional Hydrothermal Treatment

As was described in the literature [159, 160, 165, 166], researchers Grose and Flanigen prepared a zeolite with the use of Na_2O-SiO_2-Al_2O_3-H_2O without a template. In turn, Shiralkar and Clearfield stated that an appropriate Si/Al and Na/Al silicon ratio is the key to obtaining ZSM-5 zeolite without the presence of SDA. Another method is the synthesis at 180°C for 24h during high speed compounding of the composition with a suitable molar ratio of 12 Na_2O:100 SiO_2:2 Al_2O_3:2500 H_2O. It is also possible to synthesize ZSM-5 through the growth of nanocrystalline silicate layers in inorganic precursors (SiO_2, $Al_2(SO_4)_3$, NaOH and H_2O). It was also found that the formation and growth of grains of crystallite depends on a silicon ratio in the range 111–130. The synthesis time can also be reduced by conducting the process with microwave radiation instead of conventional heating.

Synthesis of Al-ZSM-5, which occurs in two stages with a molar ratio of 3.25 Na_2O:Al_2O_3:30 SiO_2:958 H_2O, was developed by Lechert and Kleinwort and verified by other researchers [177]. The first stage is the growth of crystal seeds. To this end, 710.3 g H_2O with 13.8 g NaOH and 117 g TPAOH (tetrapropylammonium hydroxide) were mixed well until the contents of the beaker dissolved. Then 158.9 g of SiO_2 and 0.5 H_2O were added in portions. The solution was stirred for one hour at ambient temperature and for another 16 hours at 100 °C. In the second stage, ~87 g of the product was obtained. 86.8 g H_2O with 8.8 g NaOH and 10.3 $NaAlO_2$ were placed in a beaker, stirred until dissolved, then 131.1 g of SiO_2: 0.5 H_2O was added in portions. This mixture was stirred for 1 hour and then the 50 g of crystal seeds formed in the first stage were added. The obtained gel was crystallized. The contents of the beaker were placed in an autoclave for 40 hours at 180°C. Finally, the product was cleaned by washing several times with distilled water and dried for 24 hours at 105°C.

Moussa Zaarour and Svetlana Mintova [178] synthesized a nanoparticle silicate with the participation of a tetrapropylhydroxy ammonium template (Nanosized TPA-silicalite-1). A solution (20 g TEOS, 35 g TPAOH and 5.26 g H_2O) was stirred and hydrolyzed for 24 h (180 rpm). It was then crystallized in a polypropylene beaker for 30 hours at 90°C, centrifuged (20,000 rpm, 1h), and washed with distilled water to pH = 8. It was then dried for 15 hours at 70°C and then calcined for 6 hours at 600°C. In total, 2.9 g of product was obtained.

Zeolites can also be obtained without the participation of templates, as was presented recently [151, 164]. An example is the developed ZSM-5 preparation with a molar ratio of 10 Na_2O:100 SiO_2:2 Al_2O_3:2250 H_2O. The zeolite synthesis consists in mixing 60 g

of colloidal silica (Ludox AS-40) with 21.4 g of 10% NaOH (1). The resulting mixture was added to 30 g H_2O and stirred on a magnetic stirrer for 3 h (200 rpm) (2). The next stage is placing 57 g H_2O in a second beaker with 1.8 g 10% NaOH and 2.2 g $NaAlO_2$. The beaker's contents were stirred on a stirrer for 3h (3). The content of the beaker was then added to 27 g H_2O (4). The final stage is the combination of stages (4) and (2), then mixing the contents of the combined solutions until a homogeneous mixture is obtained. The mixture was crystallized for 2 hours at 190°C and for 35 hours at 150°C, then mixed in a stainless-steel autoclave with a Teflon liner, equipped with a double agitator with cutting blades and a sampling port at 200 rpm. After the process, the resulting product was filtered and washed using a filtration membrane (Advantec MFS, Inc., 0.2 μm pore size) and dried at ambient temperature or at 100°C.

Another example is the synthesis of high-silicon MFI on α-Al_2O_3 substrates [179]. Colloidal silicalite-1 (75 nm) colloidal crystals were used to instill the substrate. For this purpose, as well as the substrate, 1M TPAOH was mixed with colloidal silica (CAB-OSILR M-5) and distilled water was added. The mixture was stirred for 2 hours and then hydrofluoric acid (40% HF) was added. The molar composition of the gel obtained is 3 TPAOH:25 SiO_2:1500 H_2O:3HF, pH was 6.7 ± 0.1. Molecular sieves of ZSM-5 were prepared on polycrystalline plates of α-Al_2O_3, which were washed in acetone and kept for 5 minutes in acidic 6H_2O:1H_2O:1HCl (30% H_2O_2 and 37% HCl). The cleaned media was inoculated with the obtained colloidal crystals from silicate-1. The substrates with crystallites were calcined for 6 hours at 500°C and then placed in a polypropylene reactor with the gel obtained earlier. The contents of the reactor were crystallized for 96 h under static conditions at 100°C under reflux in an oil bath. After this process, the sample was cooled and washed in distilled water [180].

Nishiyama and others developed a preparation of ZSM-5 using two templates [181]. The precursor solution was prepared using 95% wt. TEOS (tetraethylorthosilicate) with $Al(NO)_3 \cdot 9H_2O$, 10 wt. TPAOH and deionized water. The molar ratio is 2.0 SiO_2: 0.0125 Al_2O_3: 0.5 TPAOH: 170 H_2O. The mixture was stirred vigorously for 1h after which the second template, polyvinyl alcohol, was added (PVA, specific gravity: 13,000–23,000, 87–89%, content x% by weight, where x was from 1.5 to 4.5) and mixed for another hour. The contents were then placed in an autoclave lined with Teflon and heated for 24 hours at 180°C with rotation (5 revolutions per minute). The resulting powder was separated from the solution, washed, dried at 90°C, and calcined for 8 h at 550°C to remove the templates.

Tetrapropylammonium bromide can also be used as a template in the synthesis of MFI zeolite [182]. The process was carried out in Teflon bottles. The following molar compositions were obtained: 0.0035 moles of alumina, 0.03 tetrapropylammonium bromide, 0.06 moles H_2SO_4, 0.3 moles SiO_2 and 0.16 moles NaOH in 9 moles H_2O. The zeolite synthesis was carried out for 5 h at 95°C. After the process the samples were

centrifuged and separated. The obtained powder was washed several times in deionized water, dried in a vacuum oven at room temperature and calcined for 48–72 h at 550°C in an aerobic atmosphere.

Arai *et al.* carried out an experiment in which they obtained nanoscale ZSM-5 and reduced the size of the zeolite to 20 nm by adding alkyl alkoxysilane gel, specifically alkyl trioxysilane (ATES) during the synthesis [183]. To this end, ATES (A = propyl, methyl or orthyl) was mixed with TPAOH and $NaAlO_3$. The resulting solution was stirred for 15 minutes at 25°C to make it clear. Then TEOS was added and stirring was continued for another 6 hours. A molar composition of TEOS: ATES:Al_2O_3:Na_2O:TPAOH:H_2O gel was used with a ratio of 100-x: x: 2.5: 3.3: 25: 2500, respectively, (where x = 2.5–15). The mixture was placed in an autoclave lined with Teflon and heated hydrothermally for 3 days at 170°C. The final product was filtered, washed with deionized water, dried at 100 °C, and calcined for 4 h at 500°C to remove the organic template.

BEA zeolite

BEA zeolite was first synthesized using a tetraethylammonium cation as a template in 1967. For over 40 years, it was believed that this zeolite could be obtained only with the use of organic templates [159]. An example is the synthesis carried out by Joaquin Pérez-Pariente and Miguel Camblor. For this purpose, 59.4 g of H_2O, 89.6 g of TEAOH (40%), 0.53 g of NaOH were mixed together with 1.44 g KCl until dissolved (1). Next, 29.54 g of SiO_2 (Degussa Aerosil 200, 99 +% SiO_2) was added to the mixture and mixed for a further 10 minutes (2). A second solution of 20 g H_2O, 0.33 g NaOH and 1.79 $NaAlO_2$ was also prepared, which was mixed until dissolved (3). The final step was to combine steps (2) and (3) to obtain a gel for 10 minutes. The product obtained was crystallized in an autoclave at 60 rpm with a Teflon insert for 15–20 h at a temperature 135 ± 1°C. After the process, the product was recovered by washing several times until pH = 9 was reached; it was then dried [178].

Another example is the work of Choi *et al.,* whose received hierarchized mezo- microporous zeolite BEA as a result of a so-called cyclic diammonium template (3,10-diazoniabicyclo [10.2.2] hexadecane-12,14,15-triene and 3,3,10,10-tetramethyl dihydrochloride -CD). CDs were obtained in a one-step reaction by mixing α, α'-dichloro-p-xylene with N, N, N', N'-tetramethyl-1,6-hexanediamine in acetonitrile (Figure 24) [184]. In the BEA synthesis, about 90% of the silica source was supplied from diatomaceous earth and 10% from water (29% w/w SiO_2, Si/Na = 1.75). The gel was obtained by mixing 4.1 g of water glass, 3.2 g of NaOH, 0.7 g of CD, 0.29 g of $Al_2(SO_4)_3 \cdot 18H_2O$ and 190 g of H_2O; 10.8 g of diatomaceous earth were then added. The molar ratio of the composition was $30Na_2O$:2.5 Al_2O_3:$100SiO_2$:10CD:$15H_2SO_4$:$6000H_2O$. The obtained gel was subjected to a crystallization process in an autoclave lined with Teflon for 2 days at 170°C. The product was filtered, washed with distilled water, dried at 130°C and calcined to remove the template at 550°C.

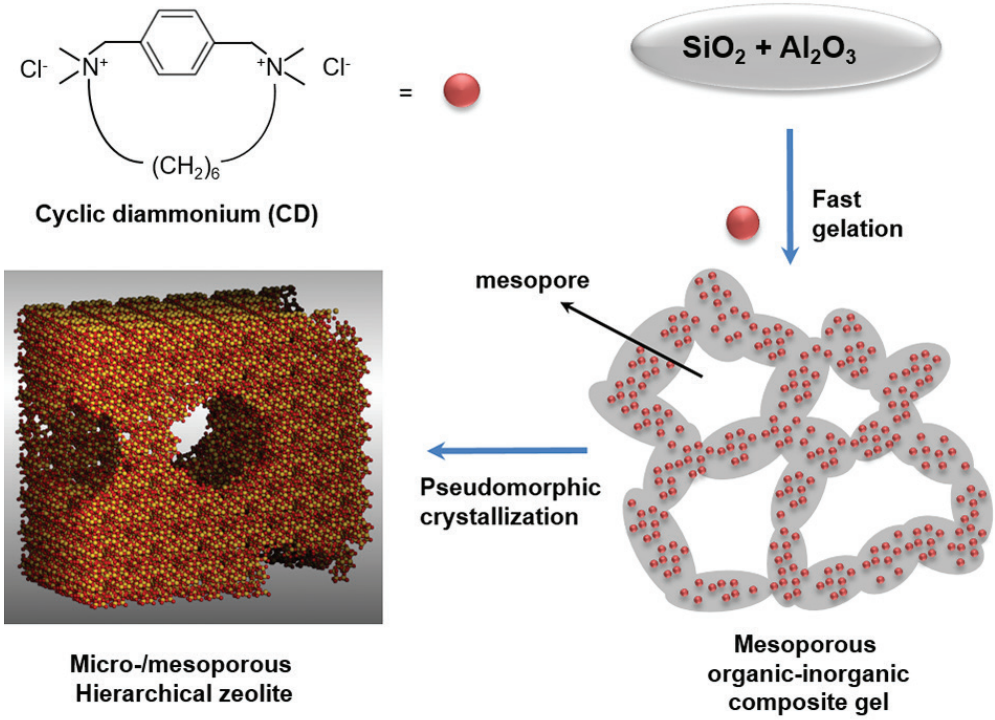

Figure 24. Schematic representation of the 'pseudomorphic crystallization' of a hierarchical BEA zeolite in the presence of cyclic diammonium (CD) as a structure-directing agent [184]

The Feng-Shou Xiao team synthesized BEA using as a template PDADMA (apolydiallyl dimethyl ammonium chloride or polydiallyl diethyl ammonium chloride). A zeolite with a silicon Si/Al = 9–12 module was obtained under hydrothermal conditions from aluminosilicate gels (Si/Al = 22–45). 0.08 g $NaAlO_2$ was combined with 0.3 g NaOH and dissolved in 12.1 ml H_2O followed by the addition of 2g PDADMA (1-2x105.20 wt% aqueous solution). It was stirred for 0.5h until a clear solution was obtained and 0.935 g of colloidal silica was added. This was then stirred for 12 hours and transferred to an autoclave, in which the obtained crystallization gel was subjected to 180°C for 96 hours. The obtained powder was filtered, washed, dried at 100°C, and calcined for 5 h at 550°C to remove organic templates [185].

In 2008, the Xie team announced the possibility of fast BEA synthesis in the absence of SDA by adding the calcined crystals of this zeolite to aluminosilicate gel. Later, Kamimura and others studied the influence of various parameters on the growth of crystallite grains in the presence of inorganic templates with appropriate i) substrate ratios of SiO_2/Al_2O_3, H_2O/SiO_2 and Na_2O/SiO_2, and ii) the impact of the Si/Al module. Zeolite can be successfully

synthesized using a wide range of aluminum silicate gel compositions (SiO_2/Al_2O_3 = 40–100, Na_2O/SiO_2 = 0.24–0.325 and H_2O/SiO_2 = 20–25) with the addition of calcined Beta grains with a Si/Al module = 7–12 [159, 186, 187].

FAU zeolite

The synthesis of FAU zeolite is carried out using aluminum oxide (e.g. sodium aluminate) and silica (e.g. sodium silicate) as a source. The synthesis is carried out in an alkaline medium (aqueous sodium hydroxide solution). After dissolution of the substrates and crystallization at 70–300°C (usually at 100°C), faujasite in the sodium form was obtained [188]. The next step is the ion exchange, during which the sodium cation is exchanged with the ammonium cation, which in turn is removed as a result of calcination. FAU zeolite occurs in two forms: X and Y. These forms depend on the Si/Al ratio. In zeolite X this ratio is in the range 2–3, and in Y from 3 or more.

Lechert *et al.* synthesized the synthesis of zeolite X with $NaAlO_2$: 4 SiO_2: 16 NaOH: 325 H_2O [178, 189]. To this end, 100 g of distilled water with 100 g of sodium hydroxide was mixed until dissolved. Then, 97.5 g of aluminum oxide was added to the solution. The whole was stirred at 100°C until dissolved, then cooled to 25°C, and 202.5 g of distilled water was added. Subsequently, 612 g of distilled water and 59.12 g of sodium hydroxide were added to 100 g of the obtained solution. A new second solution was also prepared: 219.7 g of sodium silicate solution, 612 g of distilled water and 59.12 g of sodium hydroxide. This was mixed until dissolved, after which the two solutions were mixed and continued for 30 minutes. The crystallization process was then carried out in polyethylene bottles at 90°C for 8 hours. The product was filtered and washed to pH 10, then dried at 100°C.

Wilhelm Schwieger's team received FAU zeolite (X). They mixed sodium silicate (mass% 26.5 SiO_2:8.3 Na_2O:65.2 H_2O), sodium hydroxide and distilled water, followed by the addition of sodium aluminate solution (wt% 19.1 Al_2O_3: 19.8 Na_2O: 61.1 H_2O). The mixture was stirred for 1 hour at 1300 rpm and 3-trimethoxysilyl propyl hexadecyl dimethylammonium chloride (TPHAC, 50 wt% methanol) was added. A gel was obtained with molar composition $1Al_2O_3$:$3.5Na_2O$:$3SiO_2$:$180H_2O$:0.06TPHAC. The gel was aged at room temperature for one day and crystallized in polypropylene bottles at 75°C for 4 days in a convection oven. The sample was filtered, washed with distilled water to pH = 8, dried at 75°C, and calcined to remove the organic template in a furnace at 650°C for 8 h [190].

Ginter developed the synthesis of Y zeolite ($Na_{56}[Al_{56}Si_{136}O_{384}]$:250 H_2O) [191]. In a 50 ml plastic bottle, 19.95 g of deionized water was mixed with 4.07 g of sodium hydroxide and 2.09 g of sodium aluminate until dissolved (1). Then, 22.72 g of a sodium silicate solution was added to (1). After stirring for 10 minutes, the bottle was sealed and left to stand at room temperature for 1 day (2). 130.97 g of deionized water, 0.14 g of sodium hydroxide and 13.09 g of sodium aluminate were placed in a 500 ml plastic beaker

and mixed until dissolved (3). Next, 142.43 g of sodium silicate solution was added to the solution (3) and stirred vigorously (4). 16.5 g of solution (2) was added to the beaker (4), which was then stirred for 20 minutes, placed in a polypropylene bottle (300 ml), crystallized, and incubated at room temperature for a day and then at 100°C. After about 5 h, the gel separated into a solid phase (containing NaY zeolite) and a supernatant. Heating was continued for another 2 h until a clear supernatant was obtained. The liquid phase was separated; the powder was washed with distilled water to pH = 9 and dried at 110°C.

The team of Christidis developed a synthesis of zeolite using natural raw materials: sintered glass and perlite glass [192]. For this purpose, sintered glass was dissolved at 95°C, which was reacted for 90 minutes in 5M NaOH in solid to liquid ratio of 1:10. The perlite was reacted for 2 h in 2M NaOH (ratio of solid, liquid 1: 5) for 2 h and then dissolved in an autoclave (Parr Instruments) at 120°C. After dissolution, it was filtered under vacuum; the precipitated SiO_2 was filtered, neutralized with HCl to pH 8, washed to remove the chloride (with $AgNO_3$) and dried at 105°C. In the next stage, a solution of sodium aluminate was prepared by dissolving the appropriate amount of $Al(OH)_3$ in NaOH at 250°C for 1 h. This amorphous SiO_2 was mixed with $NaAlO_2$ and a gel with molar SiO_2:Al_2O_3:Na_2O:H_2O (Na_2O:Al_2O_3 = 4.2:1 ratio, the SiO_2:Al_2O_3 ratio was changed from 7:1 to 15:1). A gel was also obtained whose molar ratio was SiO_2:Al_2O_3 = 10.5:1 and Na_2O:Al_2O_3 was in the range 3.2:1 to 5.2:1). Both gels were homogenized at room temperature for 24h with stirring at 150 rpm. Synthesis of zeolites was performed in an autoclave with a Teflon pad at 95°C for 3–120 h.

CHA zeolite

The synthesis of CHA zeolite was developed and presented in the patent of the Bourgogne team [193]. The starting raw material was USY (Y Zeolite). They described the following possible procedure for obtaining CHA. A Y-type zeolite-type sodium was used with a SiO_2/Al_2O_3 ratio of 4:1 and a crystal size in the range 3–5 μm. 50 g of zeolite was added to ammonium nitrate solution (M) at 80°C for 4 h. The solid was then filtered, washed with water and dried at 80°C for 4 h, after which the temperature was increased to 180°C and dried for a further 16 hours. This process was repeated three times. The separated and dried solid was then added to ammonia solution (M/2) at 80°C for 2h, after which it was filtered, washed and dried at 40°C. The ammonium form of Y zeolite was obtained, which was calcined at 550°C for 2 hours. The next step was to treat USY with 328 ml of potassium hydroxide (liquid to solid ratio of 1:10) at 100°C for 96 h. This was placed in a beaker in an autoclave with a Teflon pad. Finally, 43.7 g CHA was obtained.

Based on the preparation described above, Davis *et al.* developed synthesis of CHA zeolite during the hydrothermal conversion of zeolite Y [194]. To this end, 238 ml of deionized water was mixed with 32.2 ml of 40 wt%. KOH solution, and 30 g of commercial USY was

used (Zeolyst, CBV712, SiO_2/Al_2O_3 = 12). The mixture was placed in a polypropylene bottle which was heated at 100°C and shaken for 30 seconds and then heated at 100°C for 4 h. The solid product was recovered by centrifugation, washed with water and acetone, and then dried at 100°C overnight. The K-CHA form was obtained. The next step was the ion exchange; for this purpose, zeolite was treated with 1M ammonium nitrate solution at 90°C for 2 h (1 g of solid substance per 100 ml of liquid); this was repeated three times to give the NH_4-CHA form.

The preparation of the CHA zeolite ($K_{11}[Al_{11}Si_{25}O_{72}]$:40 H_2O) prepared by Thomas R. Gaffney is presented below [178]. A composition was obtained with a molar ratio of 0.17 Na_2O:2.0 K_2O:Al_2O_3:5.18 SiO_2:224 H_2O. 198.2 ml of demineralized water was mixed with 26.8 ml of KOH (45% solution) and 25 g of zeolite Y was added. The mixture was placed in a polypropylene bottle, shaken for 30 seconds and crystallized at 95°C for 96 h. It was then filtered to recover the solid, which was washed twice in water (500ml) and dried at room temperature. 26 g of product was received.

Another example of a zeolite with a CHA structure is a zeolite with the abbreviated name SSZ-13. The preparation was developed by L. T. Yuen and S. I. Zones [178]. A zeolite with the structure $[Al_{2.4}Si_{33.6}O_{72}]$: in H_2O (w = 1–7) was obtained; also, a gel was obtained with Na_2O composition: 2.5 Al_2O_3:100 SiO_2:4400 H_2O:20 RN-OH (N, N, N-trimethyl-1-adamantamic acid hydroxide). To this end, 2 g 2 M NaOH was mixed with 2.78 g 0.72 M RN-OH and 3.22 g deionized water. Then 0.05 g of aluminum hydroxide was added and stirred until dissolved, then 0.6 g of colloidal silica was added and mixed until a homogeneous solution was obtained. The mixture was transferred to a Teflon pad autoclave and crystallized at 160°C for 4 days. The solid was filter and separated, washed in approximately one liter of deionized water, and dried at room temperature [195]. In addition, the obtained product was calcined at 550°C (1°C/min and air flow of 200 cm^3/min).

SAPO-34 is a microporous zeolite of the aluminosilicate-phosphate family and has a structure similar to chabazite. The synthesis of this given compound was described by Marchese *et al.* [196]. SAPO-34 was prepared by mixing the appropriate amounts of $Al(OH)_3$, 85% H_3PO_4 and distilled water until a gel structure was obtained; then, SiO_2 and morpholine (MOR) were added as an organic template (SDA) and the mixture was placed in an autoclave with a Teflon lining in 195°C for 10 days. The solid was then filtered, washed several times and dried at room temperature.

The synthesis of SAPO-34 using triethylamine (TEA) and morpholine (1:1) as a template and polyethylene glycol (PEG-400) as a crystal growth inhibitor has been performed [197]. A gel with molar composition was obtained by vigorous stirring: 1 Al_2O_3: 0.85 P_2O_5: 1.0 SiO_2: 3 SDA: 0.2 PEG-400:60 H_2O. The mixture was transferred to an autoclave containing a Teflon cartridge and placed in a salt bath on a hot plate with a mixer for hydrothermal synthesis at 200°C for 30 h. After synthesis, the product was separated

by centrifugation, washed three times with deionized water, dried at 120°C in N_2 flow and calcined at 600°C for 5 h [198].

SAPO-34 zeolite was developed as a result of microwave heating of the reaction system [199]. Crystals with an average particle size of 300 nm were obtained as a result of this method by mixing $Al(O\text{-}i\text{-}Pr)_3$ (aluminum isopropoxide), TEAOH (tetraethylammonium hydroxide) and deionized water. The mixture was stirred for 2 hours until a homogeneous solution was obtained, then AS-40 colloidal silica was added, stirring continued for another 2 h, then H_3PO_4 (85%) was added and stirring continued for 3 h at room temperature. A gel was obtained with a molar ratio of 1.0 Al_2O_3 : 2.0 P_2O_5: 0.6 SiO_2: 4.0 TEAOH: 75 H_2O. The mixture was transferred to a Teflon-lined autoclave and heated in a microwave reactor (CEM Mars Microwave Reaction System with XP-1500) at 180°C for 10 minutes and the temperature was maintained for a further 7h. The reaction system was cooled to 70°C and the solid was separated by centrifugation (7000 rpm) for 30 minutes. The operation was repeated four times and the zeolite was dried at 50°C overnight.

In the work of the Xu team, molecular SAPO-34 sieves were obtained by the hydrothermal method. Pseudobemite (70 wt% Al_2O_3), phosphoric acid (85 wt%) and silica gel (30 wt%) were used as the source of aluminum. Organic triethylamine (TEA) was used as an organic template. The pseudobemite, phosphoric acid and water were mixed together and stirred for about one hour. TEA was then added, and stirring continued for another 30 minutes, after which silica gel precursor was added to the solution. A gel with a composition of 1 Al_2O_3:1 P_2O_5: 0.6 SiO_2: 60 H_2O: 3 TEA was obtained. The mixture was stirred for 2 h, then aged for a further 2 h and transferred to a Teflon-lined autoclave. The reaction was carried out over several cycles at 200°C and then cooled to 45°C. The product was recovered by centrifugation, washed 4–6 times by deionized water, dried at 100°C and calcined at 650°C for 5 h [200].

The synthesis of SAPO-44 is based on two publications [197, 201]. In both cases, the compound was formed by crystallization from a homogeneous mixture silica, pseudobemite, phosphoric acid, deionized water and cyclohexylamine (Et_2NH). The process was carried out in an autoclave with a Teflon pad at 190°C for 48 hours. In the work of Jiesheng Chen's and John M. Thomas's team, a gel was obtained with a molar composition of 0.4 SiO_2:Al_2O_3:P_2O_5:Et_2NH:55H_2O. The resulting product was then calcined at 550°C for 3–5 h to remove the residuals [197]. A more detailed procedure is presented in the work of S. Ashtekar, S.V.V. Chilukuri and D. K. Chakrabarty. The gel was composed of Al_2O_3: 1.0 P_2O_5: 1.0 SiO_2: 1.9 R: 63 H_2O (R = Et_2NH). For this purpose, 90 g of deionized water, 34.59 g of phosphoric acid and 21.86 g of pseudobemite were mixed. A second mixture of 60 g of deionized water, 28.27 g of cyclohexylamine and 9 g of colloidal silica was also prepared. After mixing the two solutions. they were transferred to an autoclave with a Teflon cartridge and crystallized at 190°C for 48 hours. The product was then separated by filtration and dried at 110°C [201].

MOR zeolite

Mordenite was synthesized by mixing 0.34 g $NaAlO_2$, 0.56 g aqueous NaOH and 8.0 g colloidal silica (Ludox AM 30) [202]. A gel with a molar composition of 1.0 SiO_2: 0.052 Al_2O_3: 0.23 Na_2O: 7.95 H_2O was obtained, after which it was thoroughly ground in a mortar for 10 minutes. A white powder was obtained which was placed in a Teflon bottle and aged for a further 50 minutes. After the addition of the silica precursor (Davisil 636, 646 and 645) the pH was measured twice: it was 12.85 after 30 minutes and 12.67 after 60 minutes. The re-obtained gel was put in a steel autoclave with a Teflon lining. The whole was heated at 170°C for 4 days, after which the system was cooled. The precipitated powder was separated, washed four times in 100 ml of hot water (75–80°C), filtered, dried at 600°C for 14 h and then calcined at 550°C for 10 h (temperature increase of 2°C/min).

As a source of silica during synthesis, a commercial water bath (module 4.0) was used in the following work [203]. The silica was obtained from hydrated silica gel (about 60% SiO_2) by repeated treatment of water glass with 1M ammonium chloride and 0.5 M hydrochloric acid so as to obtain a pH of 10. Mordenite was synthesized from a gel with a molar ratio of SiO_2:Al_2O_3:Na_2O:TEAOH:CTAB:CA:H_2O = 1.0:(0.033–0.067):0.58:(0–0.23):(0–0.25):(0–0.06):105–120. 16 g of the obtained silica gel was diluted in 150 g of distilled water to obtain a silica sol (1). Then 0.67 g of $NaAlO_2$ and 4.1 g of NaOH with 150 g of distilled water (2) were mixed and the mixture was prepared by adding the appropriate amounts of organic templates: tetraethylammonium hydroxide (35% TEAOH), cetyltrimethylammonium bromide (98% CTAB) and n-acetylamine (98% CA) in 60 g distilled water (3). All three obtained mixtures were combined with each other under vigorous stirring until a homogeneous gel was obtained. The obtained gel was aged at room temperature overnight (pH = 11.5) and placed in an autoclave with a Teflon pad. The crystallization process was carried out at 140°C for 3h, then at 170°C for 196h. The product was separated during filtration, washed with distilled water and dried at 110°C for 24 h. Templates were removed during calcination, initially at 340°C for 3 hours, and then at 550°C for the next 8 hours. The zeolite was also subjected to ion exchange in 0.1 M ammonium nitrate (the process was repeated three times) and finally calcined at 550°C for 4 h. A form of H-MOR zeolite has been also considered.

In the Lie assembly, a gel with a composition of $6Na_2O$:Al_2O_3:$30SiO_2$:$780H_2O$ and a silicon module of Si/Al=15 was obtained. Zeolite was obtained by mixing $NaAlO_2$ with aqueous NaOH solution; colloidal silica was then added and, when a clear mixture was obtained, it was transferred to a Teflon pad autoclave. Crystallization was carried out at 180°C for 24 h. The product was separated from the mixture by filtration, washed with deionized water, dried at 120°C and calcined at 550°C for 2 hours. The resulting mold was ion exchanged in 1M NH_4NO_3 solution at 80°C for 1h (the procedure was repeated three times) and then calcined at 550°C for 4h to convert it into the H-MOR form [204].

The Li team developed a synthesis of zeolite with the same gel composition as in the above work but using microwave radiation [205]. The gel was obtained by mixing sodium aluminate and aqueous sodium hydroxide solution, after which colloidal silica was added. The mixture was stirred for 1 hour at room temperature to react in an MSD-6 type microwave reactor (Sineo Microwave Chemistry Technology Co., Ltd) with a working frequency of 2.45 GHz and a maximum output power of 1 kW. For this purpose, 50 ml of the obtained gel was placed in a 100 ml pressure vessel and the system was heated to 190°C for 2–12h. The product was filtered, washed in deionized water until pH = 8, and dried at 120°C for 12 hours.

In an article published by the Sharma team, the synthesis of MOR zeolite is described using silica orthosiletraetetra (TEOS) or sodium silicate as a source of silica. The aluminum source was aluminum nitrate [$Al(NO_3)_3$] and sodium hydroxide was used as an alkaline medium [206]. The synthesis was carried out by the hydrothermal method, where in the first stage a gel containing silica and aluminum was obtained. To this end, the appropriate quantities of aluminum source (to which silica had been added previously dissolved in water or in a solution of sodium hydroxide) were combined and stirred for 2 hours. The obtained gel was placed in an autoclave with a Teflon pad and crystallized at 100–175°C for 5–24h. Subsequently, the product was recovered, washed (to a pH of about 9), dried at 100°C and – if a TEOS silica source was used – calcined at 550°C for 8 hours.

ERI zeolite

The following synthesis was developed by Anastasia Kharchenko in 1985 [178]. In a flask 1.95 g NaOH, 0.96 g KOH and 3.7 g H_2O were mixed, to which 0.13 g of 10% TMAOH (tetramethylammonium hydroxide) and 0.08 g of aluminum were added. The mixture was stirred until dissolved and then 10 ml of colloidal silica was added. Crystallization was carried out in an autoclave with a Teflon insert at 100°C for 6 days. The product was separated by filtration, washed several times with hot water and dried at 110°C for 24 h.

EMT zeolite

Mintova's team reinvented the traditional synthesis of EMT-type zeolites with the use of ultrasound, but without an organic matrix. It was found that the controlled nucleation and growth process of zeolite crystals depends on the mixture composition of sodium aluminate, sodium silicate and sodium hydroxide, mixed at an appropriate rate. Mintova's study of zeolite intermediates revealed the formation of gel particles of a defined size (5–10 nm). In turn, the controlled formation of homogeneous precursor molecules largely determines the stages of nucleation and growth, and thus the properties of the final product. Amorphous embryos transform into single-guided EMTs of 6–15 nm in 36 h at 30°C. In addition to the synthesis of EMT zeolite, careful control of gel formulation preparations in

combination with low nucleation kinetics at a low temperature enables the production of various zeolites, eliminating the use of costly organic templates [207].

MTW zeolite

Zeolite ZSM-12 is a zeolite from the MTW group. It has a characteristic, one-dimensional, non-commutative 12-ring with dimensions 5.6 x 6.0 Å. The first synthesis of this material was reported by Rosiński and Rubin in 1974 [208]. Since then, ZSM-12 has attracted a lot of attention due to its good catalytic properties in oil processing.

Traditionally synthesis takes place with tetraalkylammonium cations such as $MTEA^+$ and TEA^+ as organic SDA [209]. The Kamimura team performed the synthesis of MTW zeolite by adding calcined ZSM-12 grains to a gel containing a mixture with defined molar ratios of SiO_2/Al_2O_3, H_2O/SiO_2 and Na_2O/SiO_2. They successfully obtained the material without the use of SDA, instead using sodium silicate gel: SiO_2/Al_2O_3 = 60–120, Na_2O/SiO_2 = 0.1-0.2 and H_2O/SiO_2 = 8.25-13.3. Another method is the introduction of ZSM-12 gel and calcined Beta zeolite grains into the solution [159]. During the reaction, ZSM-12 grains grow, and the BEA grains dissolves. MTW zeolite was obtained after 96 h of synthesis. Individual BEA molecules were not noticed during the analysis, this may be due to the similar topology and shape of the channels of these two materials. In addition, the process may have occurred as a result of the Beta zeolite providing a specific surface for the growth of MTW grains.

TON zeolite

TON Zeolites (we distinguish here, among others, ZSM-22, Theta-1 and KZ-2) have a one-dimensional 10-membered pore system with an average size of approx. 0.47 x 0.55 nm. The channels run along the longest dimension of the crystals (crystallographic direction c). Thanks to their unique structure, these zeolites are widely used as catalysts in petrochemical processes such as isomerization, dewaxing and oligomerization. Typically, TON zeolites can be synthesized under hydrothermal conditions using aluminosilicate gels, SDA and organic compounds containing oxygen or nitrogen in the molecule (amines, polyamides and quaternary ammonium compounds) [210, 211]. Wang and colleagues developed an effective synthesis of zeolite from the TON group (material designated as ZJM-4) without the use of organic templates. The process involved the use of silica with large grain sizes in reaction with ZSM-12 zeolite grains [159].

MTT zeolite

The MTT zeolite group, which includes ZSM-23, KZ-1, ISI-6 and SSZ-32, has a channel system with dimensions of 0.52 x 0.45 nm [159]. The organic templates used in the synthesis of MTT zeolites are mainly pyrrolidine, quaternary ammonium cations, isopropylamine,

dimethylamine and DMF [212–214]. The Wu team synthesized MTT zeolite without the use of SBA with a high aluminum content (Si/Al ratio = 20). They obtained a material referred to as ZJM-6 . The crystallization process of this zeolite was carried out relatively quickly (5 h at 170°C) compared to the conventional time for zeolite ZSM-23 (synthesized with a template) [159].

FER zeolite

FER zeolite consists of a two-dimensional system, straight 10MR channels (0.42 x 0.54 nm) and 8MR (0.35 x 0.48 nm) extending along the direction [010]. Zeolites with a low silicon module are obtained without the participation of organic templates. However, the synthesis of ZSM-35 (included in the FER group with high silicon content) always takes place with the template. Typically, polyamides, 1,4-diaminocyclohexay, choline, piperidine, pyrrolidine, cyclohexylamine [215] and tetrahydrofuran [216] are used.

LEV zeolite

LEV is a typical zeolite with small pore sizes (3.6 x 4.8 Å) [159]. Natural LEV zeolite was discovered in 1825 and has the composition $C_9(Al_{18}Si_{36}O_{108}) \cdot 50\ H_2O$. ZK-20, a synthetic zeolite from the LEV group, was synthesized from an aluminosilicate gel using DABCO (1,4-diazabicyclo [2.2.2] octane) as SDA. It is also possible to obtain LEV zeolite using organic cation templates such as N-methylquinuclidines, diethyldimethylammonium, N,N'-bis-dimethylpentanediylammonium, N, N-diethyldimethylpiperidides of chloride and choline hydroxide. Zhang and collaborators performed LEV syntheses without an organic template. The process was carried out using RUB-50 zeolite grains (from the MOR group) with the addition of a small amount of alcohol. The presence of alcohol (e.g. methanol, ethanol, n-propanol or n-butanol) may delay the nucleation of MOR, thereby reducing the rate of its crystallization. As a result, a very pure LEV zeolite can be obtained.

ZSM-34 zeolite

ZSM-34 aluminosilicate zeolite consists of offretite (OFF), erionite (ERI) and cancrinite (CAN). ZSM-34 zeolite was discovered by Rubin and co-workers during synthesis using an organic template, choline [217, 218]. Subsequently, this material was successfully obtained using various diamines ($NH_2C_nH_{2n}NH_2$, n = 4, 6, 8, 10) [159]. ZSM-34 zeolite was successfully synthesized without the use of an organic matrix for the first time by Xiao's team. The process was carried out at 100°C for 7–17 days with an appropriate molar ratio of SiO_2: Al_2O_3: Na_2O: H_2O substrates in zeolite L starting gel [219]. Another example is the synthesis of ZSM-34 without a template, referred to as ZSM-34-S. This process can be carried out at a temperature of 140–180°C, at which this zeolite is crystallized for 2–6 h from seeds of amorphous ZSM-34 aluminosilicate [220]. Another possibility is to obtain

ZSM-34 zeolite from L-zeolite embryos without the use of a template [221]. During the synthesis, the molar ratio of the SiO_2/Al_2O_3, H_2O/SiO_2 and Na_2O/SiO_2 components in the L zeolite starting gel and the crystallization temperature was taken into account. It is also possible to obtain a similar zeolite ZSM-34 with various substituents, such as B, Ga and Fe [222].

ECR-1zeolite

ECR-1 zeolite has a structure similar to mordenite and mazzite [223]. In 1987 it was synthesized by Vaughan and Strohmaier by means of the organic template, bis-(2-hydroxyethyl) dimethylammonium chloride [224]. The first ECR-1 zeolite was synthesized without the use of an organic template under hydrothermal conditions [225]. The process was carried out at a temperature of 100–160°C for 1–14 days in a suitable mole ratio of Na_2O/SiO_2. Based on XRD analysis and SEM images, it can be concluded that after 7 days the reaction produces Y zeolites with a low degree of crystallinity. The ECR-1 zeolite form appears after 9 days of synthesis and until the end of the process its amount increases in relation to zeolite Y, after which, on the 13th day, the pure ECR-1 phase is observed [226].

3.3. Metals substitution in zeolites

Zeolite catalysts with embedded nanoparticles can be obtained in two ways (see Figure 25). The first step is to convert the sodium form of zeolites to ammonium. The process is carried out in polypropylene beakers on a magnetic stirrer. The appropriate amount of zeolite is introduced into a solution of 0.5 M ammonium nitrate (1 g zeolite in a 30 cm^3 solution). The ionic reaction occurs four times during a maximum period of 24 h, after which the ammonium nitrate solution (V) is replaced with a new one. After the exchange, the samples are centrifuged, dried for 1 h at 80°C, and then calcined for 3.5 h at 550°C. Subsequently, the H-zeolite form is subjected to deposition of nanoparticles in a reactor at a temperature of 80°C for 24 h. A suitable amount of zeolite is introduced into the solution at a specified concentration (0.01 M; 0.1 M; 1M) of cations (1 g zeolite per 100 cm^3 solution). After the reaction, the solution with zeolite is centrifuged and dried for 1 h at 80°C. The next step is calcination at 550°C for 3.5 h.

In the case of zeolites with small pore sizes, after being transformed into the H-zeolite form, a hierarchization process is carried out that consists in treating it with the correct concentration of NaOH for a suitable time (0.1 M NaOH, 1g zeolite per 30 cm^3, temperature 65°C for 0.5 h) [178]. The samples are then centrifuged, dried, calcined and deposited by nanoparticles.

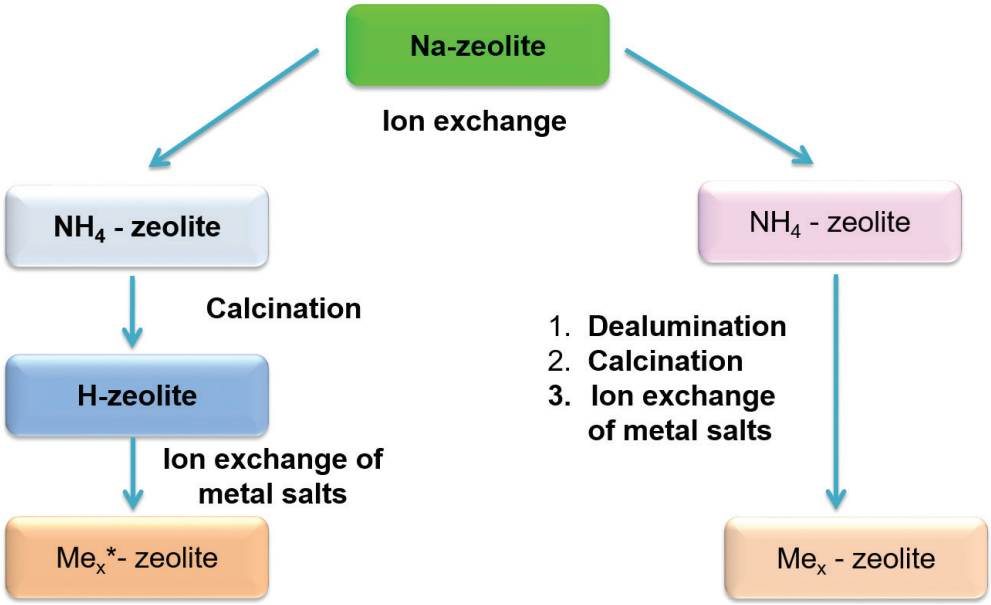

Figure 25. Zeolite modification paths. Me (metals: Sn, Fe, Mn, Cu, V), x (concentration of salt solution, 0.01 M), zeolites: MFI, BEA, CHA, FAU (own work). After the ion exchange hierarchization is also performed (0.1 M NaOH, 65°C , 0.5 h)

Another possible method of designing selective zeolites is the process of exchanging the sodium form for ammonium (described above). The next step is dealumination in a solution of nitric acid for 4 hours at 80°C (1 g zeolite per 100 cm^3 solution). Then, the zeolite is centrifuged, dried and calcined. The mechanism of deposition of nanoparticles takes place in the same way as in the first case.

Various modifications with the use of metal cations are possible in zeolites: (i) isomorphous substitution (where the Si or Al in the framework of zeolite is substituted by metals, Figure 26a and b); (ii) grafting (metals are grafted in the form of monomers, polymers or nanoparticles on the outer surface or in the inner pores of zeolite, Figure 26c–e). In the present study we considered both types of zeolite modifications: substituted metals, and dimeric forms of metals grafted onto the zeolite framework.

To date, most of the theoretical groups have modelled only the substitution of tin inside a zeolite framework [227–233]. However, in the case of our studies, lactic acid was not stabilized above any zeolite frame-centers (neither Si, Al nor Sn in the positions presented in Figure 26 a–b). As the next step, the tin and iron dimers (Figure 26d) were considered in the present study as active sites for lactic acid adsorption, which is a new approach compared to those mentioned previously in the literature [227–233], especially in the case of tin.

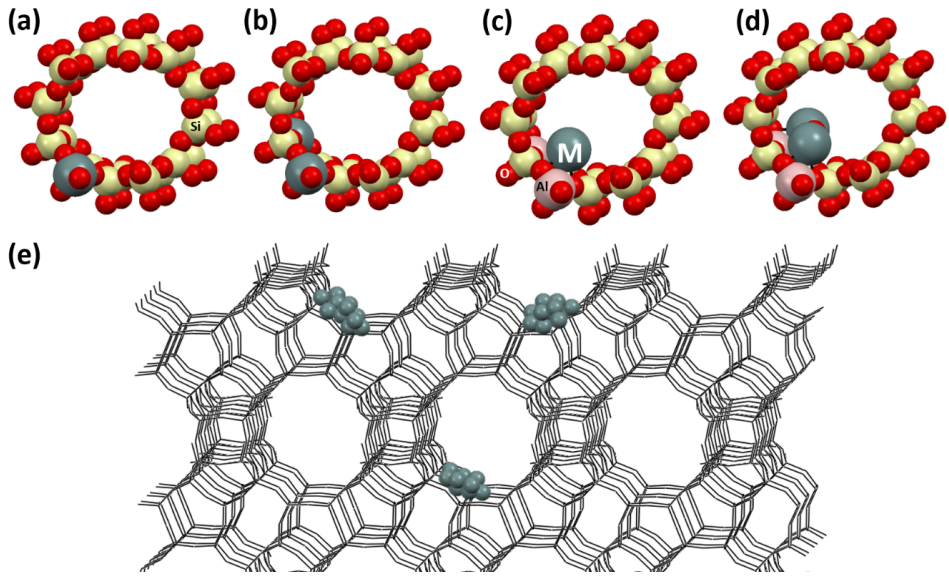

Figure 26. Possible substitution of metal in a BEA-frame. Metal is substituted as (a) single center and (b) two centers. Metal is grafted inside the zeolite pores or surface as (c) M monomers, (d) dimeric complex M-O_b-M in the BEA-pore, (e) nanoparticles inside pores and at the surface (own work)

3.4. Characterization

Assessment of the physico-chemical properties of the catalysts, binders, physical mixtures and shaped bodies resulting from the preparations in the previous section is undertaken in a systematic way using a multi-technique approach (Table 6). Method integration has the ultimate aim of deriving robust relationships between synthesis, properties and catalytic function. Most of these techniques are frequently used for analysis of zeolite powders. The mechanical properties of the shaped bodies are rigorously assessed as this is a major aspect of their practical application.

For the purpose of visualization of pore connectivity in shaped mesoporous zeolites, advanced methods with spatial resolution are required. Several techniques could be applied to the study of intra-crystalline pore connectivity in mesoporous zeolite powders; electron tomography is a powerful tool for three-dimensional structural investigations using transmission electron microscopy (3D-TEM). During catalytic tests, operando infrared spectroscopy permits detection not only of volatile species residing within the catalyst, but also changes in the surface hydroxyl groups during reaction. After treatment, the influence on porosity, composition and structure is confirmed ex situ using X-ray diffraction, physisorption and microscopic methods.

Table 6. Overview of the bulk and surface characterization techniques which can be applied to zeolite catalysts and the insights gained using these methods (own list)

Characterization method	Insights gained
Powder X-ray diffraction	Crystalline phases Phase changes during reaction
Gas adsorption (N_2)	Surface area, pore Vol.
In situ infrared spectroscopy	Adsorbate structure Surface hydroxyl groups, acid strength
Raman spectroscopy	Surface and adsorbate structure
Transmission electron microscopy	Structure, composition, and morphology (shape, size, uniformity)
Temperature programmed reduction/oxidation/ desorption	Reduction and/or oxidation conditions as well as desorption conditions of known adsorbents Amount of acid sites and qualitative strength
X-ray photoelectron spectroscopy	Surface composition and degree of oxidation
Laser diffraction	Particle size distribution
Mechanical stability tests	Crush strength and attrition resistance of the catalysts in shaped and powder form
Mass spectrometry	Product analysis
HPLC, GC	Product analysis
Nuclear magnetic resonance (^{29}Si, ^{27}Al, ^{1}H)	Metal coordination
H_2O adsorption	Mesoporosity and surface reactivity
BET	Surface area, pore Vol.
Mössbauer spectroscopy	Valence and oxidation states of metals in zeolites
Scanning Electron Microscopy	Chemical composition at surface

3.5. Theoretical modeling of zeolites

One of the long-term targets of research in heterogeneous catalysis is to gain an understanding of the investigated processes on a molecular level in order to discover general catalysis principles and/or to develop better catalysts based on rational designs. For a given reaction, both commercial catalysts and model catalysts with identical or at least similar compositions need to be studied by following surface processes and modifications, applying a complementary combination of surface science analytical techniques under

in situ or *quasi in situ* conditions [234]. However, a comprehensive view of the processes occurring on the catalyst surface may only be obtained by combining these experimental results with the modelling of the reaction mechanism using, for example, the *ab initio* density functional theory (DFT) method [235, 236].

DFT method. The principles of the method were devised by Kohn, Hohenberg, Sham and Mermin in the 1960s [237–239]. In the DFT method, the wave function of the N-electron system (defined in 4N-dimensions: spatial coordinates and electrons spin) is replaced by the electron density, $\rho(r)$, defined in 3-dimensional physical space. This method is based on the two main Hohenberg-Kohn theorems: first, the ground state properties of the multi-electron material may be defined as a function of the electron density; second, the theorem defines an energy function for the multi-electron system. Figure 27 shows the definition of multi-electron system total energy as a function of $\rho(r)$. The correct ground state electron density minimizes this energy function.

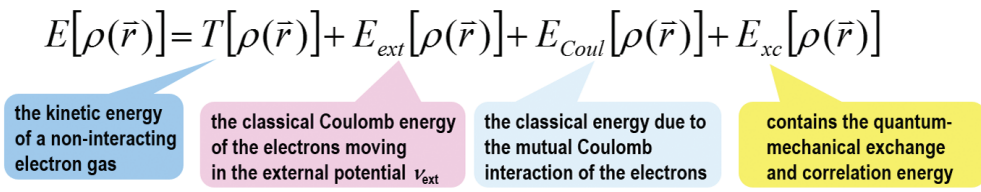

Figure 27. Energy definition in the DFT method [235, 236]

The exact form of the electron exchange and correlation function, E_{xc}, is unknown. In the simplest variants, LDA (*Local Density Approximation*) and LSDA (*Local Spin Density Approximation*), E_{xc} is a function of local electron density [240, 241]. In a more sophisticated definition, GGA (Generalized Gradient Approximation), E_{xc} is extended to include the gradient of electron density [242, 243]. Higher level hybrid functions (e.g. B3LYP) include the mixing of correlative-exchange energy with the exchange of Hartree-Fock energy and gradient corrections [244].

The advantage of the DFT method is the simplicity of calculating the algorithm, which results from the approximate integration of both the exchange and the correlative effects [245]. This allows for the calculation of very large systems, such as catalysts and biological systems, which is not possible using the standard Hartree-Fock method. It is worth emphasizing that DFT produces results comparable to post-HF calculations, Configuration Interaction (CI) or Couple Cluster (CC).

Geometrical model. In DFT studies, two models are used for the geometrical representation of the surface cluster and the periodic model (see Table 7 and Figure 28) [246, 247]. The cluster model neglects long-range interactions and is based on the

assumption of the local nature of interactions between the molecule and the active center located on the surface; the part of the surface with an active center is excluded. The long-range interactions are included by taking into account the influence of the ionic environment (cluster in the electrostatic field [248, 249] or the saturation of broken bonds by hydrogen atoms [246]. The second method is the periodic model [247]; this is a standard solid-state physics model based on the general formalism of band theory and the periodicity of the crystal lattice. A comparison of the advantages (+) and disadvantages (-) of both models is described in Table 7.

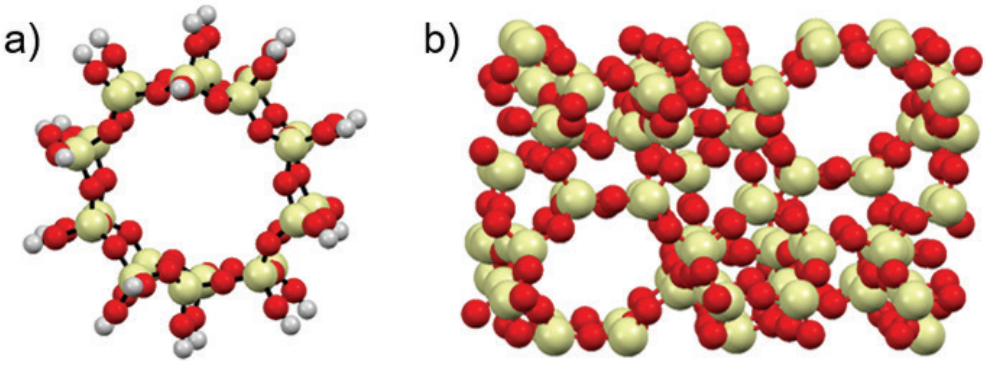

Figure 28. Geometric representation of ZSM-5: a) cluster, b) periodic cell (own work)

Table 7. Comparison of models used for the geometrical representation of the surfaces (own list)

Cluster model	Periodic model
electronic structure of clusters with different sizes & symmetries saturated by H atoms: R(O-H)=0.97Å O-H bonds || broken O-M bonds, all electrons included in calculations	unit cells with different sizes, symmetries & number of layers, large surface-surface separation (e.g. 100Å), different number of K-points, semi-core pseudopotentials
+ localized interaction	+ periodic arrangement of all atoms
+ finite section of surface	+ 3D system
+ detailed geometry & local charge	- catalytic material describing a very large supercell
- problem: embedding	- problem: artificially strong
- limitation: physical/chemical parameters depend on size & geometry of cluster	- coupling adsorbate/molecules, only high coverages, cell size balance needed

Theoretical modeling of the catalytic reaction in zeolites requires several steps (Figure 29) which must succeed in order to find a reaction mechanism at the catalyst surface.

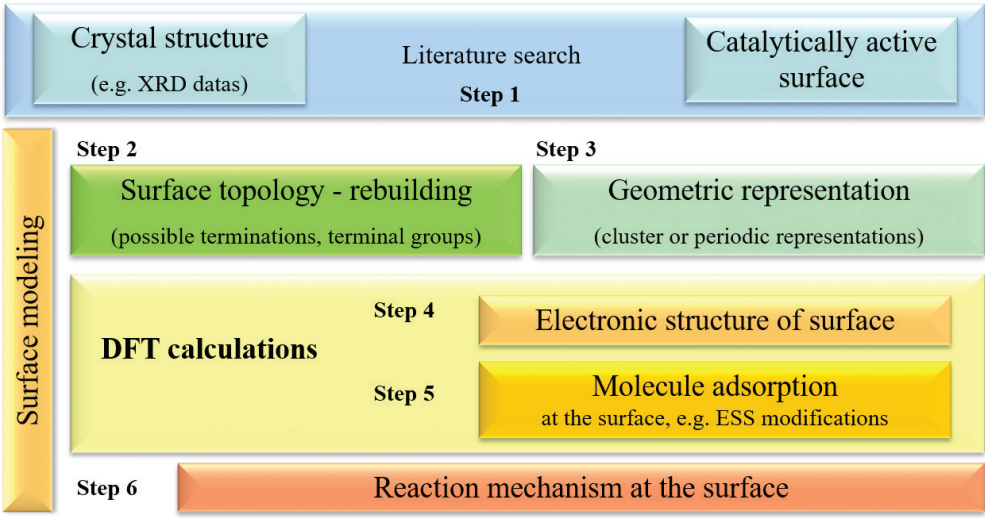

Figure 29. Necessary steps of surface reaction modeling using the DFT method (own work)

After many years of DFT investigations, the level of theoretical insight into electronic structures, geometries, stabilities and adsorption properties of model catalysts is now reaching a level that allows the investigation of more complex catalytically active systems. An important goal for the near future is to build a bridge between the applied industrial catalysts and model systems at an atomic level by using a combination of experimental and theoretical methods. The methodology for the investigation of catalytic systems in such a way requires, in particular, (i) metal-support interface investigations and modeling, (ii) examination of modeling of reaction mechanisms through a comparison of theoretical and experimental spectra, (iii) examination of the mechanism of catalyst deactivation by a combination of experimental and theoretical spectra. Several challenges still remain on the long road to a complete understanding of real-world catalysts: (i) a more detailed explanation of imperfections, e.g. defects, steps, and their effects on the reactivity of catalysts; (ii) a more detailed description of complex systems in which different materials are used for either the support or the supported phase; and (iii) improvement of the models used to obtain the theoretical spectra of complex systems.

During theoretical modelling, the following definitions of electronic parameters are used:

atomic charge distribution – charging of atoms, information concerning ionic binding;
bond order analysis – information concerning the covalent contribution to the total bond;
charge density differences – direct information concerning bond formation; quantification of the charge rearrangement due to bond formation;

electrostatic potential – local charging and binding at the surface; quantification of the electronic and nuclear electrostatic interaction with an external point charge;
energetic distribution of the occupied and empty electron states;
electron densities – description of bonding in ground and transition states;
electrostatic potential maps – information concerning the distribution/delocalization of charge;
total density of states (DOS) and **atom projected density of states** (PDOS) – comparable with the valence energy region ⇒ UPS;
reactivity indices (Fukui functions) – type of attack: nucleophilic, electrophilic, radical;
vibrational frequencies – comparison with IR/Raman frequencies to find adsorbed species
ionization potential of core electrons – to develop theoretical NEXAFS, XAS, XES, RIXS spectra

In an atomic-level scheme, a single, free metal atom has its electrons distributed in known discrete orbitals. When more equivalent atoms are agglomerated to form a small cluster aggregate, the atomic levels split into molecular levels depending on the interatomic interactions. The split levels of one atomic orbital start to overlap energetically with those from another atomic orbital. As long as the aggregate has a molecular character ("metallic molecule"), an energy gap is left between the occupied and unoccupied levels, and the electron motion is still confined and quantized. This situation is typically valid for aggregates up to several hundred atoms. For larger aggregates, metallic bands are formed and there is no longer a gap between the occupied and unoccupied levels (Figure 30) [250].

When single atoms or very small metal particles with up to about 100 atoms (with sizes of a few Å) are deposited onto a surface, they are not only influenced electronically by the atom/molecule-metal transition described above, but their geometrical and/or electronic structures may also be influenced by the support. The origin might be a possible lattice mismatch between the metal and the support, leading to a distortion of the clusters or an electronic interaction between both. However, when larger clusters consisting of several atomic layers are considered, the clusters may relax; this leads to aggregates with electronic and geometrical structures that are relatively similar to the pure solid and thus (almost) independent of the support.

In this sense, a realistic model system that mimics a commercial catalyst must consider several surface scenarios, especially the presence of small clusters and larger agglomerates. Experimentally, both these scenarios can be obtained, e.g. by careful control of the deposition rate and the deposition conditions, leading to only small clusters or only large agglomerates. For theoretical modelling, small particles (with sizes in the range of about 0.1 nm to 1 nm) require studies which include cluster-support interactions, while in the case of larger agglomerates only a (pure) metal model is valid for the description.

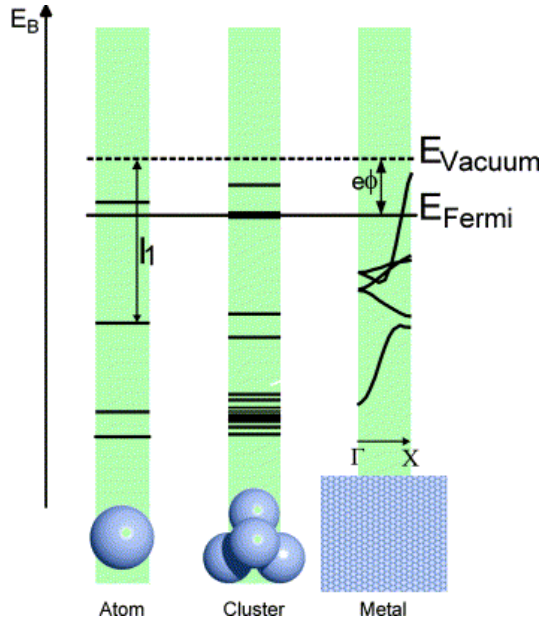

Figure 30. Diagram illustrating the transition from an atom to a metal (E_B, binding energy; I_1, first ionization energy; e: electron charge; ϕ: work function; Γ, X: symmetry points in the Brillouin zone) [250]

So far, knowledge about the molecular structure of complex catalytic systems and the role of their components (nanoparticle shape and size, the support, the role of the interface between the support and the nanoparticles in the activation of catalytic reactions) is still limited. Understanding the effect of the support on the properties of metal nanoparticles is still a challenging subject [235]. The interfacial structure between nanoparticles and their support has always been an important issue in the field of heterogeneous catalysis; however, it is difficult to tackle theoretically due to the very large supercomputing resources that are needed. Information is needed on the nature of the chemical bonding at the surface, the electron transfer at the metal–support interface, how the support influences the adsorption and catalytic properties of the metal nanoparticles, or how it affects the bonding within adsorbed molecules.

3.6. Hierarchization of zeolites

The development of technologies for transforming biomass into various chemical substances is attracting more and more interest for economic and ecological reasons. New solutions and biomass conversion methods which use catalysts are still being sought. The

goal of engineers and scientists is to search for and develop conversion routes that lead to specific products, select the right raw material, and design an effective catalyst, process parameters and technological installation. In the case of catalysts, special attention is paid to zeolites in relation to their promising properties. These microporous aluminosilicates have potential in reactions such as dehydration, isomerization or oxidation. These catalysts have a developed, microporous surface and a three-dimensional channel system. They exhibit high chemical and hydrothermal stability. Thanks to the presence of Brönsted and Lewis centers, they have the ability to transform various raw materials into the desired chemical compounds. Research is still being carried out on a laboratory scale with the use of modified zeolites, but the results obtained so far indicate the success of biorefinery processes in the future [149, 150, 161, 251–254].

The hierarchical structuring of conventional zeolites by post-synthetic modification in alkaline media is one of the most efficient ways of enhancing their performance in diffusion-limited reactions [255]. The extent and distribution of the mesopores introduced has been experimentally observed to depend strongly on the intrinsic properties of the zeolite [256]. Mesoporous materials with 2–25 nm pores have been obtained [257]. Treatment with alkaline solutions brought various results [258], depending on the conditions and template molecules (TPA^+ or TBA^+) [259]. The desilication process was further improved by Groen *et al.* [260, 261], who determined ZSM-5 with a Si/Al ratio of 25–50 at/at. They showed that at lower values the aluminum prevents desilication, thereby limiting mesopore formation, while at higher values complete dissolution occurs. Recently, Sadowska *et al.* [262, 263] studied desilication of ZSM-5 with NaOH using different surface/bulk sensitive experimental methods. They found that desilication depends strongly on the concentration of NaOH in the solution: i) in a diluted NaOH solution, Si is extracted equally from the surface and bulk; ii) in a concentrated NaOH, desilication from the bulk dominates. They also suggested that desilication visibly increased the amount of Si-OH on mesopore walls; also, the stability of Si atoms in the zeolite framework increases in the following order: $(SiO)_3Si–OH<(SiO)_3Si–OSi<(SiO)_3Si–OAl$.

In recent years, extensive research on increasing accessibility and easier diffusion of active substances in microporous zeolite structures has been conducted [264, 265]. A number of tests were carried out in which the receipt of hierarchical structures was confirmed. Two 'top-down' and 'bottom-up' categories were distinguished. In the first case, microporous materials were synthesized, modified, and hierarchical structures were obtained during dealuminations or desilations. However, in the case of the 'bottom up' hierarchization of zeolites, obtaining such structures through synthesis is more complicated and involves the use of so-called hard and soft templates. During synthesis using hard templates, a solid matrix is added to the solution to form limited spaces around the formed zeolite, and then it is removed by calcination. The hard materials used to synthesize hierarchical zeolites are

carbon materials; the advantage is that they can be easily removed from the product as a result of burning. An example of such a template is amorphous carbon, e.g. nano-scale soot particles dispersed in the resulting gel during the zeolite crystallization; this gives rise to a mesoporous structure after removal. This method appears to be universally used for the preparation of mesoporous zeolites, regardless of their chemical composition.

Other examples are carbon nanotubes, $CaCO_3$, metal oxide nanoparticles, polymers, areozels and resins. In a typical preparation, a zeolite synthesis gel is prepared which is mixed with a template to obtain a microporous product. The process is carried out in hydrothermal conditions, during which free space templates are formed; subsequently, they are removed by calcination or treated with acids and bases. This method can be used to synthesize various zeolites and to control the size of the pores obtained [266]. Soft templates are also added to the reaction system and usually interact with the precursor or structure dispersed through covalent hydrogen bonds or by means of van der Waals forces or electrostatic forces, creating a system of voids in the formed zeolite after the removal of templates [267]. Acid properties of zeolites depend on the aluminum content in the crystal lattice. Methods for introducing and modifying aluminum in a zeolite structure are presented below.

Desilication

Due to the unique properties of zeolites, a system of homogeneous pores take part in many catalytic and separation processes [258, 268]. However, their microporous structure (and in some cases the size of micropores) limits the diffusion of molecules to their interior, which has a significant effect on the deterioration of catalytic performance. This performance breakthrough occurred during the synthesis of mesostructural aluminosilicates. Nevertheless, these materials have limited thermal stability and poor acid properties. Research has been carried out on obtaining extra-porous zeolites to obtain materials that are the best catalysts because they have all of the above properties.

One of the most common methods is desilication. This method allows a porous zeolite structure to be obtained. It involves the removal of silicon atoms from zeolite crystals in an alkaline environment (usually NaOH). As a result of this process, hierarchical materials are obtained. Obtaining an additional pore system facilitates diffusion and improves acidic properties. Such an extensive pore system affects the activity, selectivity and lifespan of zeolites in catalytic reactions.

The Si/Al module is strongly influenced by the catalytic properties and the formation of mesoporous material [255, 269]. MFI desilication tests with different modules were carried out and it was found that with a Si/Al ratio in the range of 20–50, the zeolite retains its structure and properties after the hierarchization process. However, zeolites with Si/Al > 50 lose too much silicon during the process, and this process is inhibited (Si/Al <20) when the

prevailing zeolite skeletons are built from a large amount of aluminum. In addition to the silicon module, the hierarchization time and the concentration of the alkaline environment are important factors that affect the process of obtaining mesoporous crystals (Figure 31).

The Groen team carried out a ZSM-5 zeolite desilication process [270]. To this end, 330 mg of material were added to 10 ml of 0.2M NaOH and the process was carried out for 15–120 minutes at a temperature of 35–85°C; the suspension was then cooled in an ice bath. The product was isolated by filtration, washed to pH 7 and dried at 100°C. After the process, the zeolite was converted to the form H-ZSM-5 as a result of a three-fold exchange in 0.1 M NH_4NO_3 solution; it was then calcined for 5 h at 550°C.

Perez-Ramirez's publication presents the BEA zeolite desilication process [271]. The experiment was carried out in a MultiMax reactor (Mettler Toledo). A 0.2 M NaOH solution (5 cm^3) and 166 mg zeolite were introduced. The reactor was sealed. The mixture was stirred at 500 rpm at 65°C for 30 minutes. The zeolite was then cooled, filtered and washed to pH 7, then dried at 100°C and calcined at 550°C for 6h (heating time 3°C / min). The zeolite was converted to the proton form in 0.1 M NH_4NO_3 and re-calcined under the conditions described above.

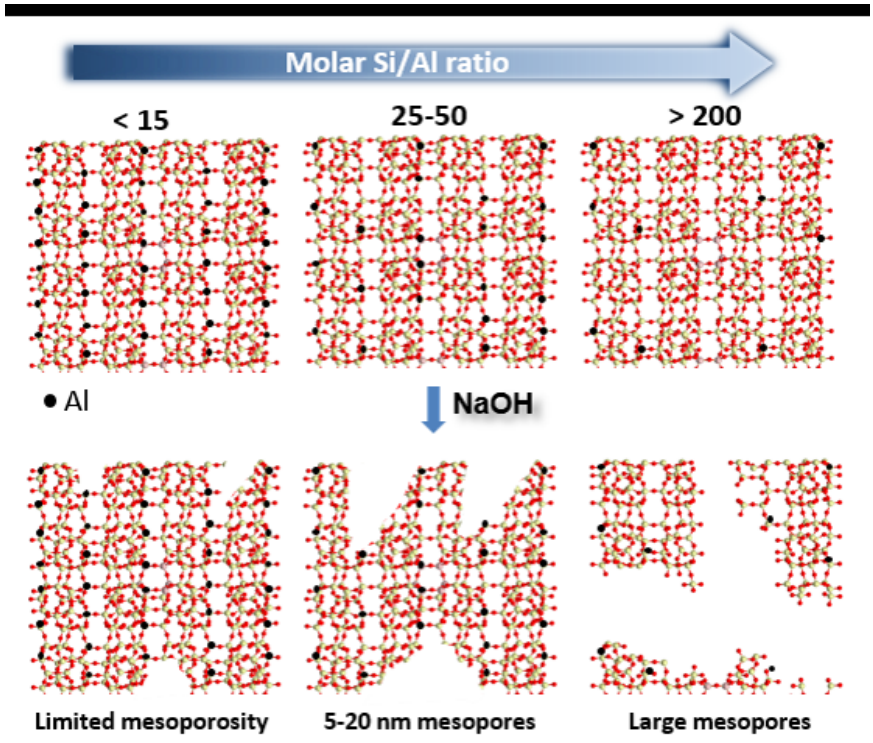

Figure 31. The influence of Si/Al ratio on the desilication treatment of zeolites in NaOH solution [255, 269, 270]

Dealumination

This method involves the removal of aluminum without damaging the zeolite crystal structure. Studies have been carried out and it has been found that zeolites with a higher silicon module show much higher thermal resistance and are more resistant to water vapor. De-ionizing affects the number of acidic centers and determines the activity and selectivity of zeolites used in catalytic processes. The dealumination process is usually carried out in the gas phase as a result of heat treatment and steam, or in solution.

In 1964, Barrer and Makki's team published a work containing the first attempts to remove aluminum from a zeolite skeleton as a result of the action of acid (Figure 32). They performed the dealumination process at 100°C, treating clinoptilolite with 1M HCl [272]. Studies have shown that it is possible to remove 100% of aluminum from the crystal lattice; however, the resulting products have lower thermal stability (> 65%). The process of dealumination with the use of acids is accompanied by the ion exchange of Al-cations present in the crystal lattice by protons from acids, as well as the formation of so-called "hydroxyl socket" defects.

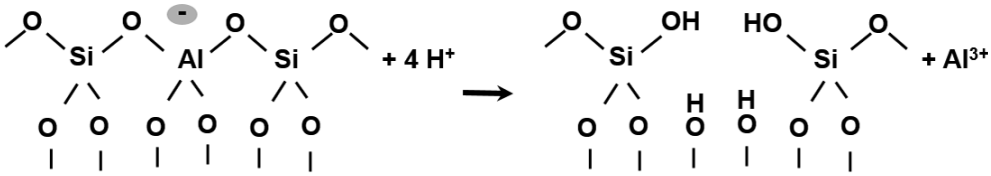

Figure 32. The process of removing aluminum from the crystal structure of zeolite with the use of acids [272]

The process of dealumination was carried out on zeolite USY with the use of nitric acid and sorrel by the Yan team. The zeolite sample was prepared three times by ion exchange in an NH_4NO_3 solution of NaY zeolite (Si/Al = 2.5) at 80°C; it was then washed and dried at 100 °C. After the exchange it was treated with hot air for 4h (600°C) to obtain USY material. The dealuminization process was carried out at room temperature for 8 hours under reflux in a solution of nitric acid (varying in concentration from 0.25 M to 1 M) and oxalic acid (from 0.1 M to 1 M). A ratio of 1 g zeolite per 20 ml solution was used. The sample was then filtered, washed several times with deionized water and dried at 120°C overnight.

On the basis of the XRD analysis and the obtained diffractograms, it was found that the treatment of zeolite with acids of increasing molar concentrations has a negative effect on the crystal structure [273]. Amorphous products are created as a result of destruction of the skeleton of a given material (we observe weaker diffraction peaks). On the other hand, in comparison to nitric acid, oxalic acid is more effective in dealuminations. It acts as a hydrolyzate and chelating agent, forming a trioxalato aluminum complex.

The hydrothermal dealuminization process

In 1971, researchers McDaniel and Maher carried out research to improve the thermal stability of zeolite Y. The process involved two stages: (1) ion exchange to substitute sodium ions with ammonium ions; (2) heat treatment at a temperature of 800°C or higher, or up to 1000°C for faujasite zeolite [274–276]. The samples were then heated under the influence of steam at a pressure of 1 bar. This method has remained unchanged for many years. Kerr suggested a three-step mechanism to remove aluminum from the crystal skeleton. The first stage involves the hydrolytic cleavage of -O-Al-O- bonds by self-steaming. It involves contact with water vapor, which is formed as a reaction product. The next stage is the removal of hydroxyaluminum compounds from the zeolite network (when vacancies are formed); the final stage is the occupying of free places by silicon or aluminum cations. Additionally, thermally stable Y zeolites were obtained as a result of the direct action of water vapor from external sources at a pressure of 1 bar on the H-USY form.

Guisnet *et al.* removed aluminum from the crystal structure of EMT zeolite (Figure 33) [277]. For this purpose, the sodium form of EMT (Si/Al 3.8) was ion-exchanged by

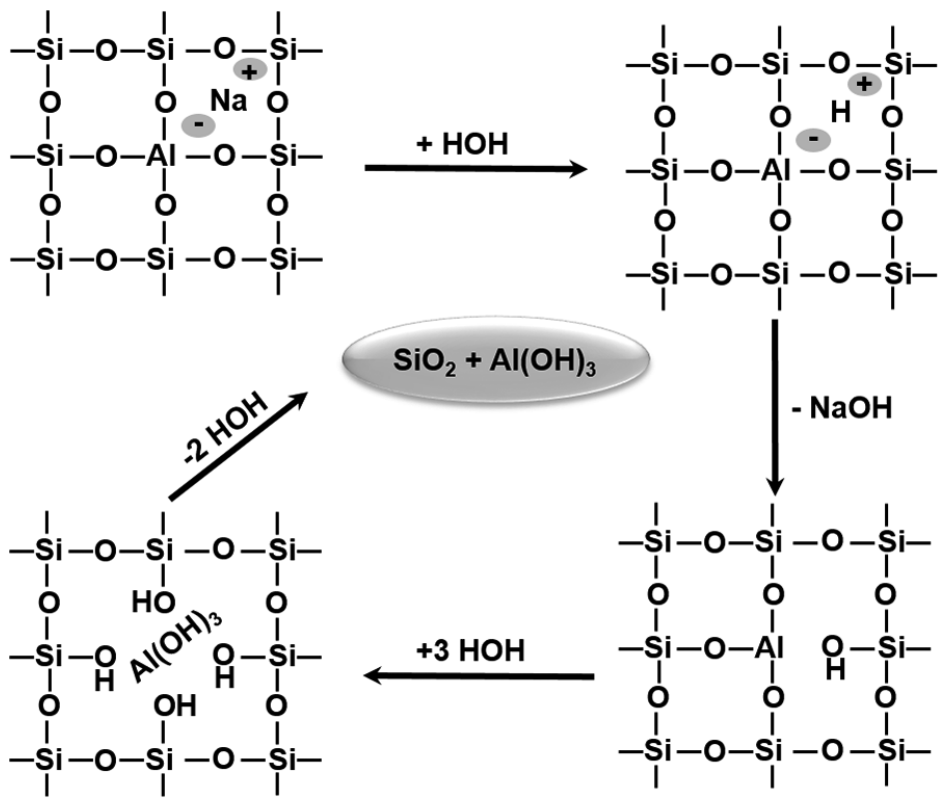

Figure 33. Diagram of aluminum removal from the crystal lattice under the influence of water [277]

a six-fold operation of a 2 M solution of NH_4NO_3 at 80°C: the solution was exchanged four times each hour, then once after 5h and again after another 12h. The samples (with Si/A module = 5.5, 7.6, 13; 31; 52) marked as HEMT X were obtained as a result of hydrothermal treatment at 450–650°C over a period of 0.5–3 h.

Dealumination with other compounds

A method was developed by several groups [278–280] for removing aluminum from the zeolite skeleton with the use of $SiCl_4$ (in the gas phase), $(NH_4)_2SiF_6$ (in solution), CCl_4, $COCl_2$, SO_2Cl_2 and the compound H_4EDTA. EDTA was used and the results were published by the Datka team [281]. The dealuminization process was carried out at 100°C for 1h using 0.4% H_4EDTA solution added to the suspension (water: zeolite = 15: 1). Y zeolite with an Si/Al silicon module = 2.67 was used. The sample was then washed with hot water and dried at 160°C. The use of H_2Na_2EDTA as the aluminum releasing agent from the zeolite network did not trigger a dealuminization process.

Ammonium hexafluorosilicate ($(NH_4)_2SiF_6$) is another dealumination agent. Its application causes a gentle process in which isomorphic substitution of aluminum with silicon takes place. Thanks to this method, it is possible to obtain materials that are practically free of aluminum embedded in the crystal lattice. The first tests and results were presented in 1994 [282, 283]: instead of an aqueous solution $(NH_4)_2SiF_6$, a method was used for removing aluminum in a solid form, which was then washed with water. The Dias team performed dealumination of three zeolites (ZSM-5, MOR, FER) using the solid form of $(NH_4)_2SiF_6$ to remove 5, 10, 15 and 20 mol% of aluminum from each sample, resulting in 12 samples in total. To this end, the sodium versions of zeolites were substituted with ammonium cations as a result of the three-fold ion exchange in 1M NH_4NO_3 solution. 12 g samples of each ammonium version of the zeolite were treated with solid ammonium hexafluorosilicate at a temperature of 80°C for 2 h in a vacuum oven. Subsequently, all samples were washed with 800 ml of hot water (80°C); they were then dried and calcined at 550°C for 8 h to remove ammonia and protonated forms of the above zeolites. The following are the reactions that are possible during this process:

$$\{AlO_{4/2}\}^-(NH_4)^+_{(s)} + (NH_4)_2[SiF_6]_{(s)} \rightarrow \{SiO_{4/2}\}_{(s)} + (NH_4)_3[AlF_6]_{(s)} \quad (1)$$

$$2(NH_4)_3 + [AlF_6]_{(s)} + 4H_2O_{(l)} \rightarrow 2(NH_4)_3 + [AlF_4(OH)_2]_{(s)} + HF_{(l)} \quad (2)$$

$$(NH_4)_3[AlF_6]_{(s)} \rightarrow NH_4[AlF_4]_{(s)} + NH_4HF_{2(s)} + NH_{3(g)} \quad (3)$$

$$\{AlO_{4/2}\}^-(NH_4)^+_{(s)} + 4HF_{(l)} \rightarrow \{H_4O_{4/2}\}_{(s)} + (NH_4)_4[AlF_4]_{(s)} \quad (4)$$

As a result of this process, ammonium hexafluorosilicate is removed from the structure of the aluminum crystal and substituted into the formed silicon vacancy. Reaction (1) occurs in a solid state. However, it is possible to obtain the products presented in equation (2). Therefore, it is very important to control the temperature during the process. It is not possible to obtain a zeolite structure completely devoid of aluminum because the produced ammonium tetrafluoroaluminate acts as an inhibitor. If the dealumination reaction occurs in water (3), the products are $NH_4[AlF_4]$ complex, ammonia and ammonium hydrofluoric acid, which additionally affects the removal of aluminum from the zeolite. The ammonium hydrofluoric acid complex reacts with aluminum (4) and results in the formation of hydroxyl sockets.

Alumination and realumination of zeolites

In addition to removing aluminum from the crystalline structure, it is also possible to incorporate it through alumination (increasing the amount of aluminum with tetrahedral coordination), i.e. substitution of aluminum in zeolite from an external source. The substances used in the alumination process are aluminum chloride ($AlCl_3$) and a solution of aluminate ($NaAlO_2$) [284].

The alumination process was performed in the Y zeolite using a KOH solution with various molar concentrations [285]. The ammonium form of Y-zeolite was introduced into the alkaline solution at concentrations of 0.1, 0.25, 0.5, 1, 2 M KOH (1 g zeolite per 50 ml solution). The experiment was carried out at 30, 60, 80 and 100°C and the effect of the process time was checked. Based on the results, it can be concluded that the longer the zeolite resides in the alkaline solution, the more the degree of realumination increases; 24 hours after the test, realumination reaches 86% (for 0.25 M KOH). Temperature also plays an important role. The optimum for this process at 0.25 M is 80°C. The higher the concentration of the KOH solution, the smaller the Si/Al module; this means that more aluminum is present in the crystal lattice [286].

Silanization

Silanization is the deposition of silicon compounds on the surface of zeolites or porous materials, thanks to which it is possible to modify the catalytic and sorption properties. The use of organosilanes makes it possible to obtain secondary mesoporous structures which show strong affinity with silicate and aluminosilicates; after calcination, hierarchical forms of zeolites are obtained [287].

Silanization can be divided into so-called silanization of seeds (seed silanization), silanization of polymers (polymer silanization) and silanization with amphiphile silanization substances. In the case of seed silanization, the following steps are distinguished: a) pre-crystallization of the zeolite gel, b) functionalization of crystal seeds in reaction with organosilanes, c) seed crystallization and crystal growth under hydrothermal conditions,

d) calcination of zeolite to remove the silanizing agent and the template. Due to the use of silanizing agents during the synthesis of zeolite, the pore size of the zeolite can be affected; in the case of MFI zeolite, the obtained macropores have a size of 2–5 nm when phenylaminopropyltrimethoxysilane (PHAPTMS) is used [287].

The Han team carried out silanization on MFI zeolite (Figure 34) [288]. The samples were dried at various temperatures (25°C, 200°C, 400°C and 600°C) for 5 hours. Subsequently, 5 g of zeolite was placed in 25 g of toluene and the mixture was stirred at room temperature for 1 h. Then 4 g chlorosilane (SiH_3Cl) was added to the mixture and heated under reflux at 70°C for 12h. The samples were filtered, washed several times with toluene, and dried at 110°C for 5 h to remove the solvent.

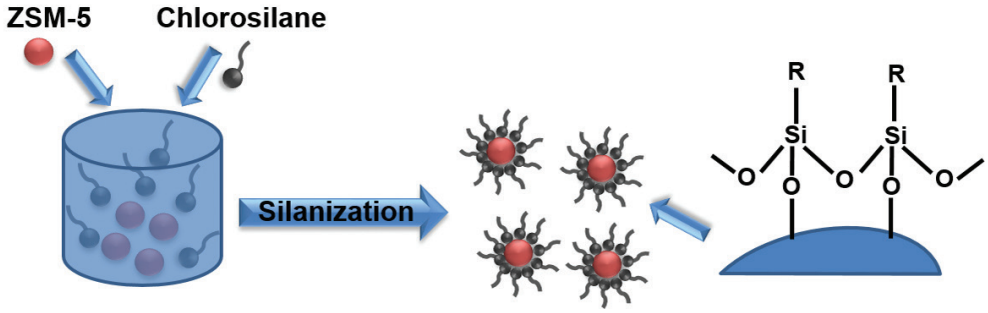

Figure 34. Scheme of ZSM-5 zeolite modification as a result of silanization [288]

In the work of Mitchell *et al.*, reactions of MFI zeolite in a hexane solution were carried out with aminopropyltriethoxysilane and mercaptopropyltrimethoxysilane [289]. For this purpose, the proton zeolite form was dried at 350°C for 4h. The dried material (0.25 g) was introduced into n-hexane and then one of the silanizing agents (0.001 mol) was added dropwise. The process was carried out at 25°C for 24 h. The product was then filtered, washed with n-hexane and distilled water, and dried at 80°C.

Another example of silanization is the action on H-ZSM-5 and H-FER zeolites of a TEOS solution in acetone, acidified with a solution of maleic acid [290]. The suspension was refluxed for 1 hour. The samples were then filtered and calcined at 550°C.

3.7. Modeling of hierarchical zeolites

Besides very interesting experimental findings, until now the atomistic-level knowledge of the global desilication process mechanism in alkaline media has been very limited. One major obstacle to an improved understanding is the difficulty in modeling the complex and

non-periodic structure of mesopores in hierarchical zeolites. Several groups have tackled ZSM-5 crystal structure and model adsorption processes using both cluster and periodic DFT calculations [291–297]

The starting point for the hierarchization of zeolite is understanding the structure of micropores. One example is ZSM-5 with characteristic channels. A model of ZSM-5 with around 50,000 atoms is presented in Figure 35. We used this model to present various scenarios of mesopore formation in ZSM-5 zeolite, as will be shown in detail in the next pages.

The desilication and dealumination process has recently been studied theoretically on the example of SSZ-13 and SAPO-34 [298,299]. Researchers simulated the sequential addition of water molecules from steam to form a silanol nest as well as $Al(OH)_3H_2O$ and $Si(OH)_4$. However, due to the high energy barriers of dealumination, a more preferred mechanism of Al-O breaking still needs to be found. Additionally, the desilication process occurs in alkaline aqueous solution and would require much more complex consideration.

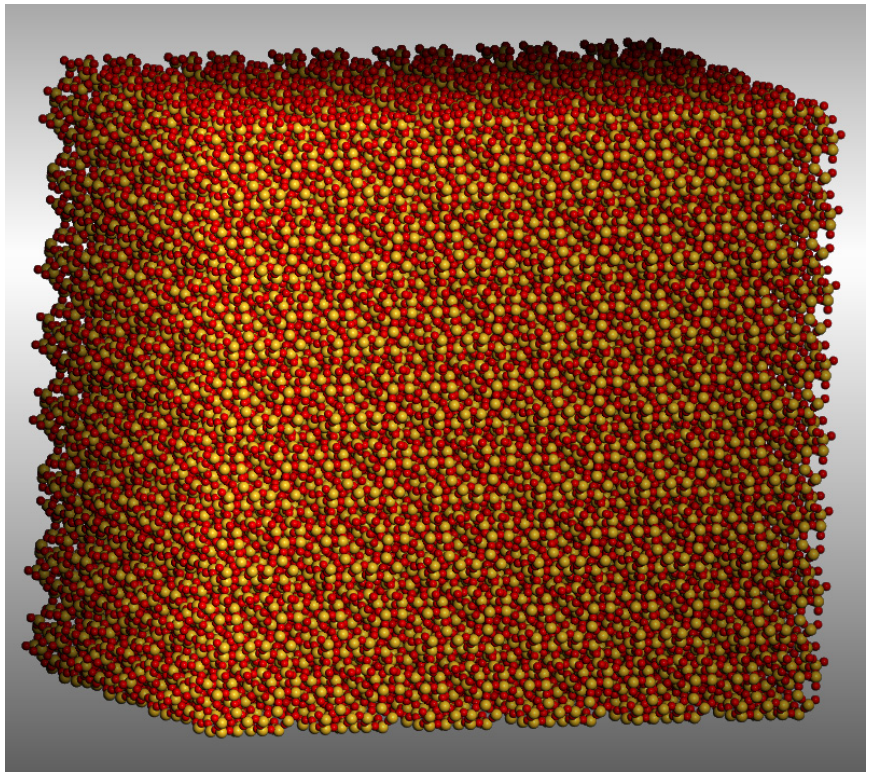

Figure 35. Micropore structure in ideal ZSM-5 zeolites [256]: size 11x11x11 nm, realistic model for modelling mesopores up to 6–7 nm

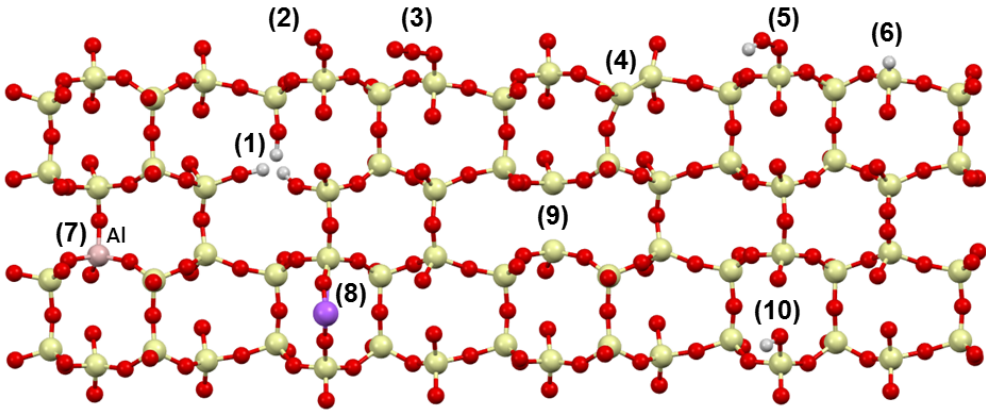

Figure 36. Elemental structural defects in silica [300–302]: (1) hydroxyl nest, (2) peroxy group, (3) peroxide group, (4) Si-Si bridge, (5) silicon hyperoxide group, (6) Si-H group, (7) aluminum framework, (8) exchangeable Na^+ countercation, (9) oxygen vacancy, and (10) terminal silanol group

The framework defects are expected to play an essential role in the hierarchization process and offer good prospects to understand demetalation. Various types of structural detects can be observed in silicate materials [300–303]: i) intrinsic structural defects (Si-Si bridge, silicon hydrate, oxygen vacancies); ii) impurities (anion and cation substitutions); iii) coordination defects (hydroxyl nest, peroxide, hyperoxide, sikanol hydroxide, silicon hydroperoxide) (see Figure 36).

In the case of hierarchical zeolites, coordination defects are the most crucial, especially hydroxyl nests and various types of silanols due to their important role in desilication [304]. Hydroxyl nest formation has been extensively studied by Bordiga *et al.* [305, 306]. Pascale *et al.* [307] calculated the formation energy of a silanol nest with respect to orthosilicic acid (H_4SiO_4) and reported the structure of nests using different computational approaches. Using cluster models, Lisboa *et al.* [297] studied a number of reaction intermediates for dealumination of a zeolite.

Very recently Silaghi *et al.* [308] showed the challenges of the molecular aspects of dealumination and desilication of zeolites. They also strongly emphasized that the mechanism of mesopore formation during desilication and dealumination is still a scientific challenge and is beyond the scope of current state-of-the-art periodic DFT. Therefore, one possibility is local consideration using state-of-the-art cluster DFT and understanding the defect formation mechanism and the demetalation phenomena.

The hypothetical 3D structure of open and constructed mesopores is illustrated in Figures 37 and 38 below. In the pure alkaline solution, open mesopores are observed, while in the case of zeolite pre-treated by template molecules, constricted mesopores have been found with an entrance neck of 2 nm diameter [256].

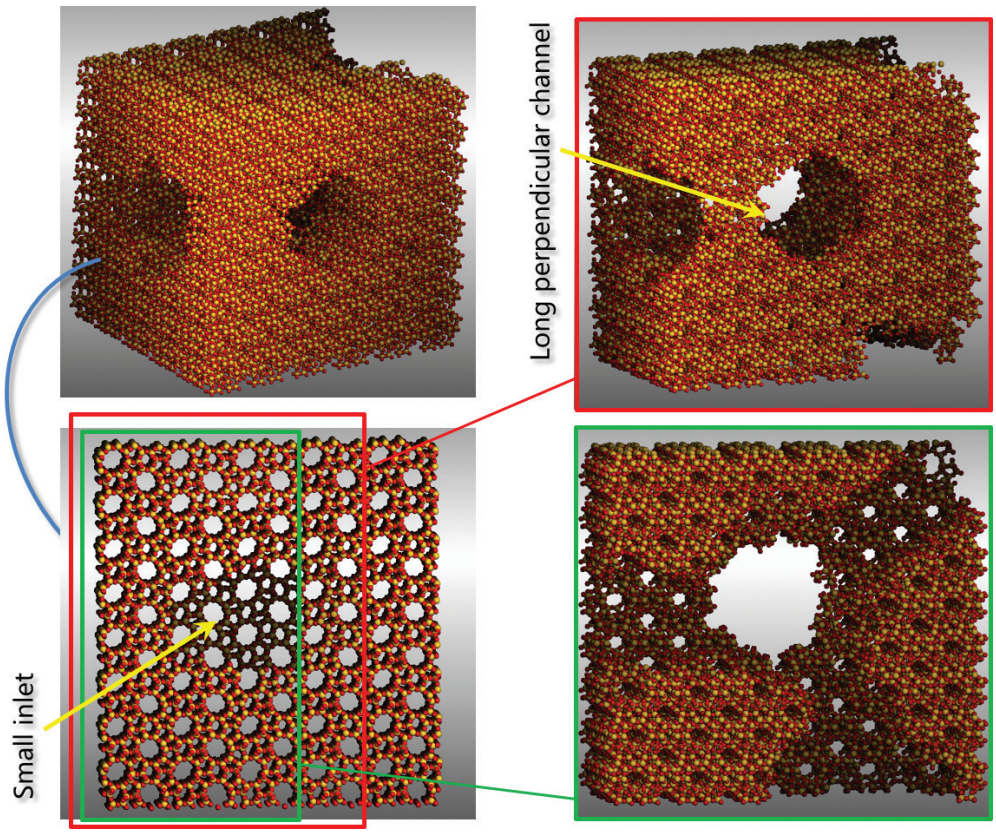

Figure 37. Mesopore structure in alkaline-treated ZSM-5 zeolites [256]: open and interconnected mesopores, 6 nm

As is shown in Figure 39, mesopore formation in ZSM-5 starts from the 6-Si ring between the channels and (001) the surface; this successfully forms the hydroxyl nest. As an effect of the hydroxyl nest, the process of hierarchization proceeds and large mesopores are formed, as is shown in Figure 40.

We identified a different mechanism of mesopore formation in hierarchical zeolites: the mesopores in ZSM-5 are formed in three dimensions, while the ZSM-22 needle is corroded only at the edges and walls (see Figure 41).

Studies of TPA adsorption at (001) surface offers a chance to understand the formation of constricted mesopores. The TPA stabilizes at the (001) surface and prevents its desilication (Figure 42). Therefore, desilication occurs at ring 6 and leads to the formation of a neck into the bulk of the zeolite, where alkaline media penetrate the crystal and form occluded mesopores.

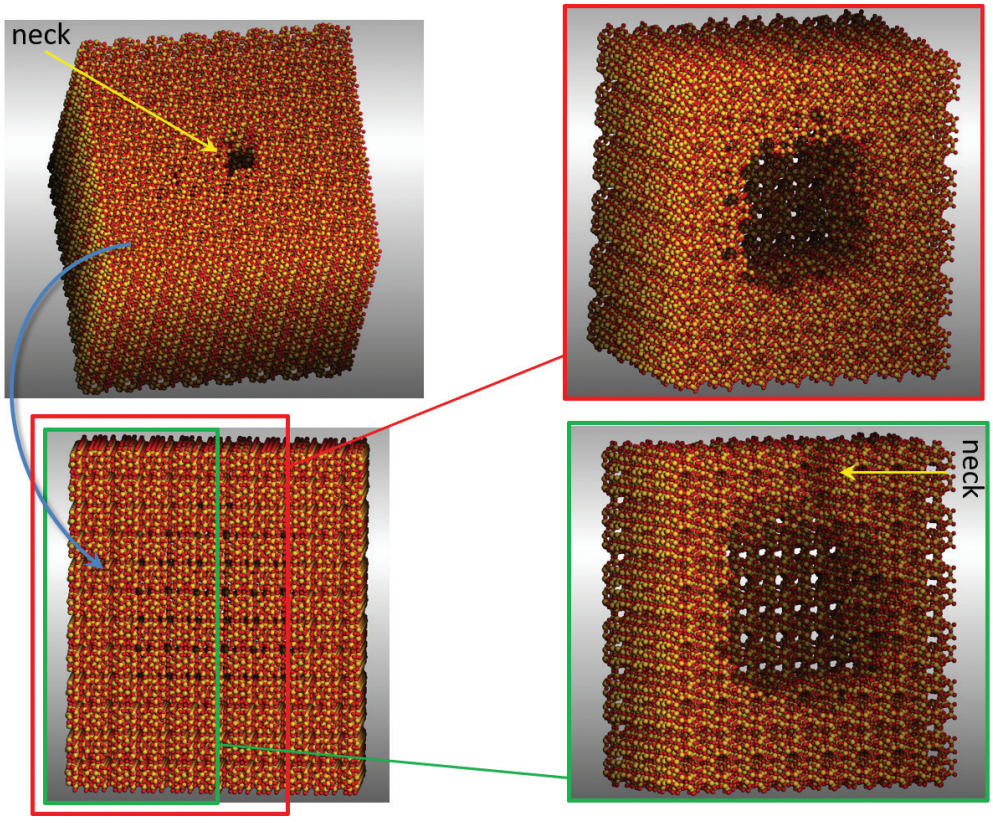

Figure 38. Mesopore structure in alkaline-treated ZSM-5 zeolites [256]: constricted mesopore (6 nm) with neck

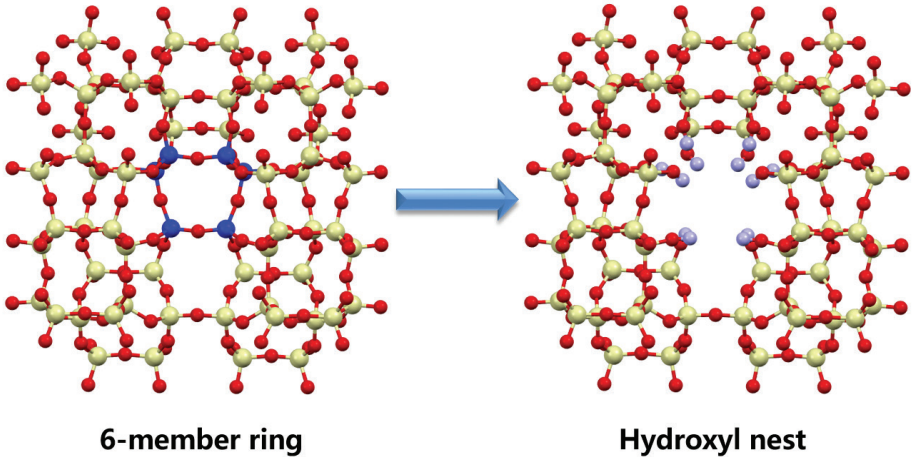

Figure 39. Hierarchization of ZSM-5 starting from a 6-member ring (own work)

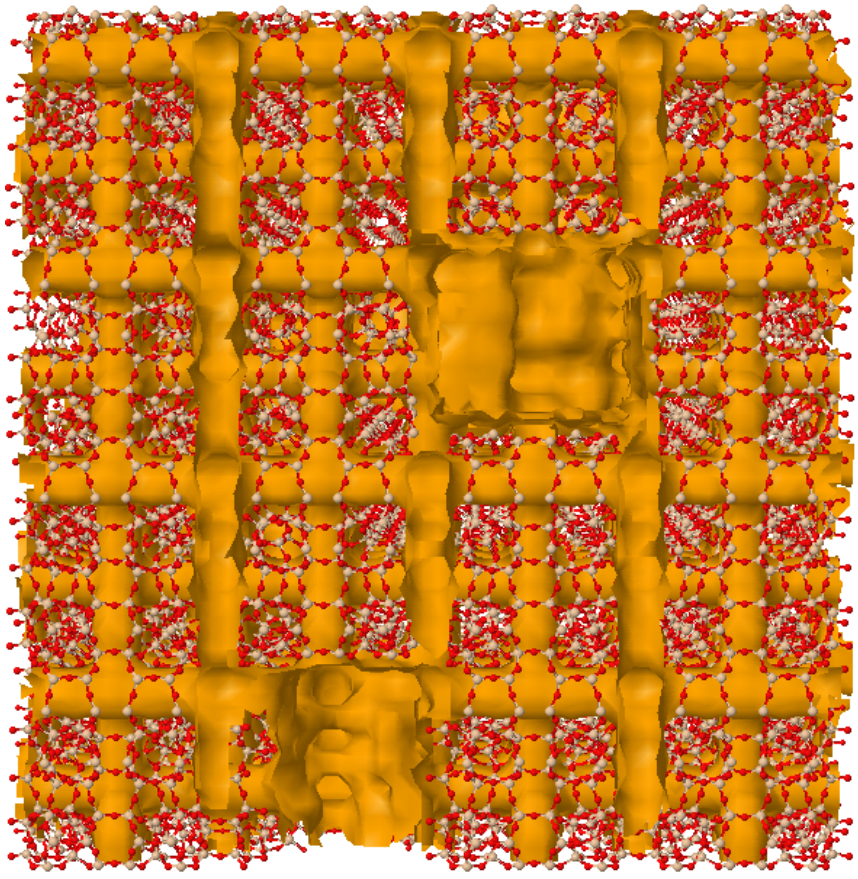

Figure 40. Hierarchization of ZSM-5 (own work)

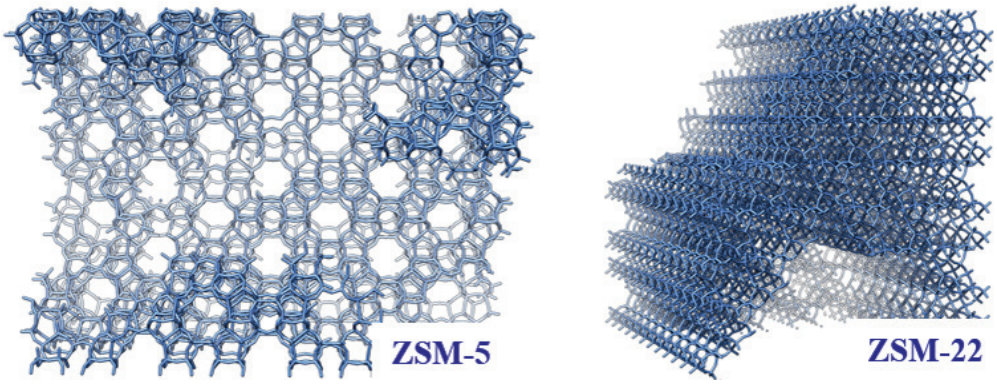

Figure 41. Hierarchical zeolites: ZSM-5 and ZSM-22 representations (own work)

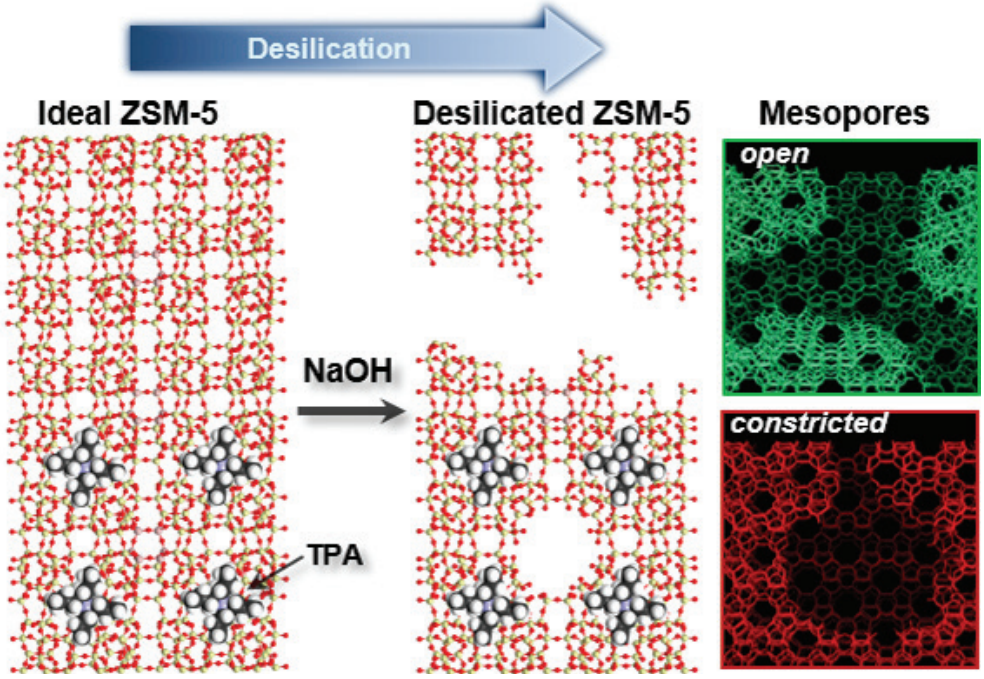

Figure 42. Suggested desilication of ZSM-5 zeolite in alkaline solution with and without a template molecule (TPA) (own work)

3.8. 3D printing of zeolites models

The structure of zeolites is very complicated; therefore, a 3D model of their crystallographic structure is extremely helpful. The printing of 3D models of zeolites is a complicated, time-consuming and multistage process; however, the effects are very helpful in understanding how channel systems are distributed in certain zeolites as well as how the possible hierarchization and reaction mechanisms occur inside the pores of zeolites.

There are various types of 3D printers and printing technologies [309]:

- **Fused deposition modeling (FDM):** objects are built layer-by-layer from the bottom up by heating and extruding thermoplastic filament.
- **Laminated object manufacturing (LOM):** layers of adhesive-coated paper, plastic or metal laminates are fused together using heat and pressure and then cut to shape with a computer-controlled laser or knife.
- **Digital Light Processing (DLP):** the material used for printing is liquid plastic/photopolymer resin. The resin hardens quickly under the intense light produced by

an arc lamp. A layer of hardened material is created and when a layer is finished, it is then moved up and the next layer is started.

- **Stereolithography (SLA):** this printing process uses 3D CAD data and involves a uniquely designed 3D printing machine called a stereolithograph. The liquid plastic/photopolymer is converted into solid 3D objects.
- **Selective Laser Sintering (SLS):** similar to the SLA, but it uses powdered material in the printing process.
- **Selective laser melting (SLM):** 3D CAD data are used in process; fine metal powder is evenly distributed onto a plate, then each slice of a 2D layer image is intensively fused by applying high laser energy to the powdered plate. Metals that can be used for SLM include stainless steel, titanium, cobalt chrome and aluminum.
- **Electronic Beam Melting (EBM):** similar to the SLM technique but uses an electron beam as its power source.

The best in our opinion for the purpose of printing molecular models of zeolites is Stereolithography (SLA). Figure 44 shows the effect of 3D printing of three types of zeolites with different pore sizes using the SLA technique.

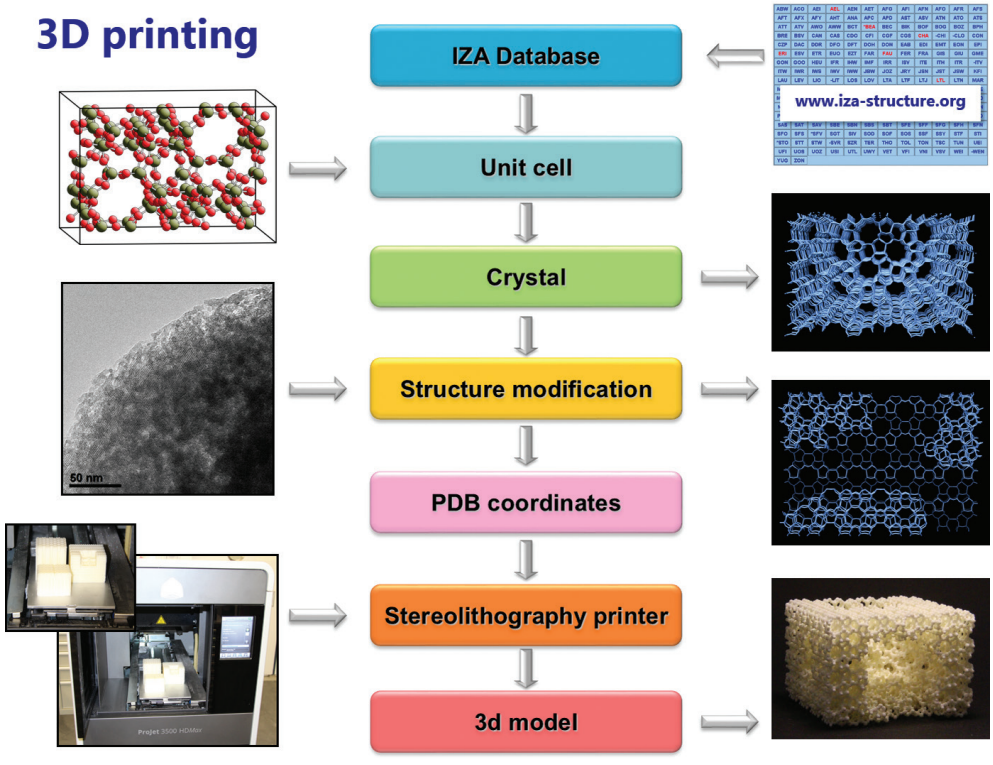

Figure 43. Multistage path of printing 3D models of crystal structures of zeolites (own work)

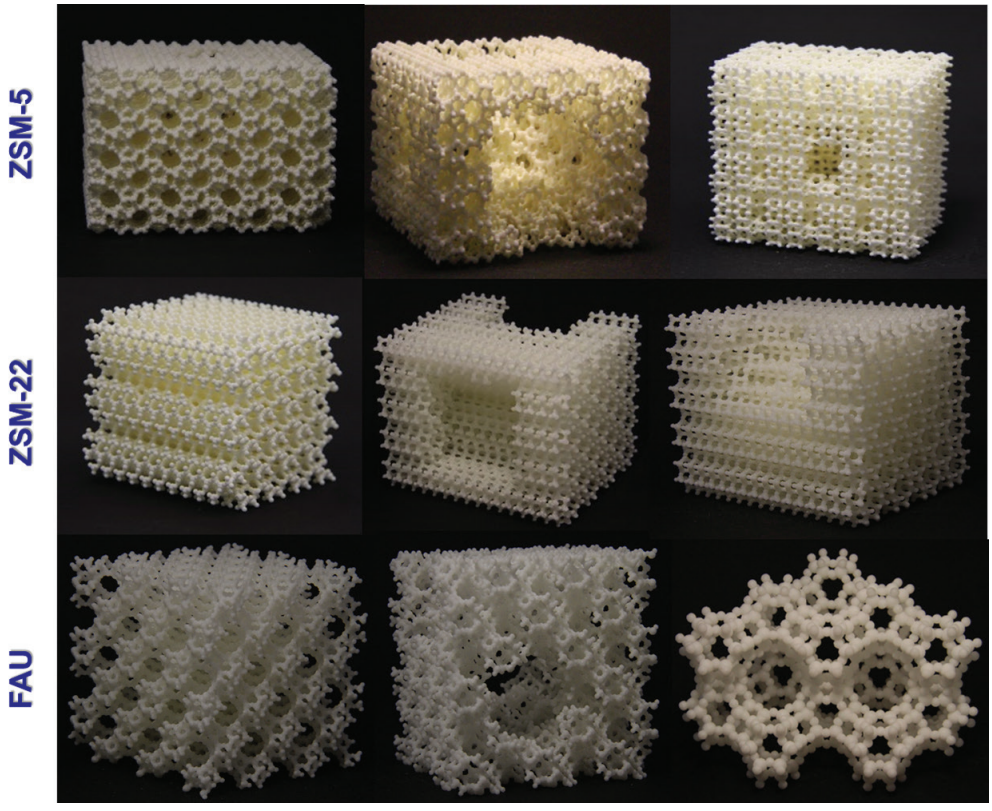

Figure 44. Photography of 3D models of zeolites (own work)

4. ZEOLITES FOR BIOMASS CONVERSION

4.1. Experiments

Catalytic testing of structured zeolites is essential to verify their performance in powder form. Comparison of the performance (activity, selectivity, and stability) of the powdered zeolites (and physical mixtures of the zeolites and forming agent) and shaped catalysts enables determination of the influence of the mesoporosity and binding system on the catalytic properties of the investigated zeolites. The catalysts can be tested in following conditions: (i) in gaseous phase using a fixed bed, continuous flow tubular reactor (Figure 45); (ii) in liquid phase using periodic reactors (Figure 46).

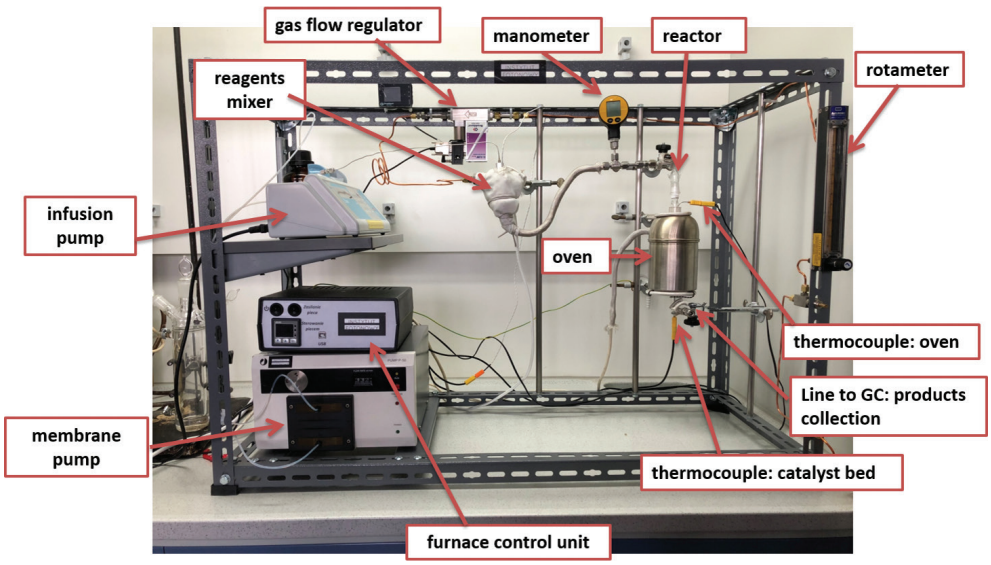

Figure 45. Unit for catalytic tests in gaseous phase (own work)

In both cases, the samples are collected during the process and analyzed using gas chromatography as well as mass spectrometry. Each process is unique and requires separate consideration according the process parameters. One example reaction is the dehydration reaction of lactic acid into acrylic acid.

Figure 46. Periodic reaction with heating coat for catalytic tests in liquid phase (own work)

We carried out the dehydration reaction of lactic acid in gaseous phase in a vertical fixed-bed quartz reactor, under atmospheric pressure at a temperature of 370°C. The reaction feed, which was an aqueous solution containing 40 wt% lactic acid with 2 cm^3/h flow rates, was pumped into the reactor and driven by inert gas (50 mL/min, inert gas: He).

In liquid phase using periodic reactors, the process is taken in relatively low temperature, mostly below 100°C. Due to the good performance of zeolite catalysts, different non-aqueous solvents such as methanol, ethanol or isopropanol are used to avoid blocking of active sites by water molecules. This type of reaction is very interesting from the industrial point of view.

In both cases besides acrylic acid, other products can be detected: propionic acid, 1,2-propanediol, 2,3-pentanedione, acetaldehyde and lactide. Another problem is the existence of water and organic phases, which makes the process very difficult. Additionally, the products have a tendency to be polymerized. Therefore, the development of this process requires a lot of multidisciplinary research before it can finally applied in industrial practice. However, it is worth consideration.

4.2. Theoretical modeling

Metal-substituted BEA and MFI are the most studied zeolites, especially for reactions where Lewis acidity is required [227–230]. Many groups of researchers have already investigated zeolites substituted with tin and other metals. The activity of Sn-BEA in conversions of glucose to fructose has been observed, while the same reaction was not noticed over Sn–MFI [231]. Other groups have correlated the adsorption of probe molecules, such as

ammonia, acetonitrile, water or pyridine, with the Lewis acidity of M–BEA (M = Ti, Zr, Sn), [232] and specifically Sn–BEA [233].

Iron-exchanged zeolite is an active catalyst for a large number of reactions, of which the most important are selective catalytic reduction (SCR) of nitrogen oxides with ammonia or hydrocarbons [310–314], the N_2O decomposition reaction [315, 316] and oxidation processes [317–320]. The stabilization of dimeric Fe-O-Fe iron complexes in the ZSM-5 framework has been already investigated using a DFT approach with a cluster model [292]. Fe-BEA zeolite has been also studied theoretically for nitrous oxide decomposition [321, 322] in similar way; however, these authors consider monomeric Fe.

Several clusters which represent BEA zeolite have been analyzed and finally $M_2Si_{22}O_{64}H_{32}$ (ideal) and $M_2Si_{12}O_{39}H_{22}$ (hierarchical) clusters (M=Al, Si, Sn, Fe) have been used in an LA dehydration reaction (Figure 47).

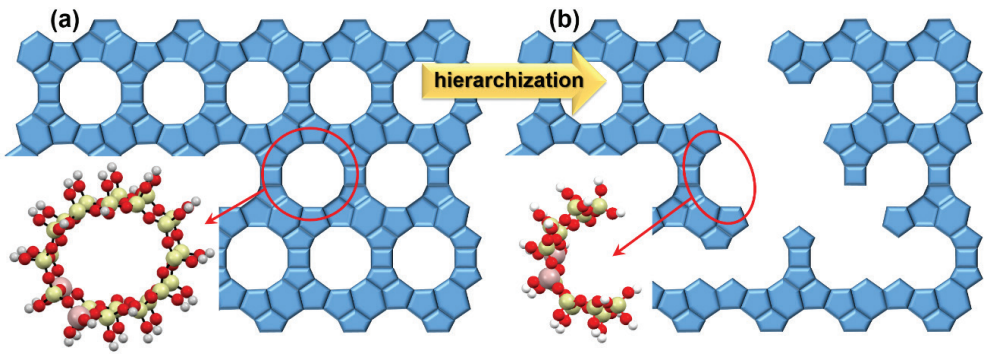

Figure 47. Clusters representing a BEA structure: (a) $M_2Si_{22}O_{64}H_{32}$ (ideal) and (b) $M_2Si_{12}O_{39}H_{22}$ (hierarchical) clusters (M=Al, Si, Sn). Blue structures represent Si-Si bonds in BEA before and after hierarchization (own work)

The location of aluminum cations was chosen according to previous findings [292], which showed that the distance between Al-Al centers was around 5 Å. The distance between aluminum cations at the chosen positions (Figure 48) in a BEA frame is 4.98 Å.

We considered the ideal hierarchical structure of BEA zeolite: the 'ideal' model means the ideal structure, while the 'hierarchical' model indicates the zeolite structure after hierarchization. Metal M-O_b-M dimers have been found to be stable above oxygen bound with aluminum centers of BEA zeolite. The structure and exact role of the active iron sites in these catalytic reactions are still the subject of discussion. For the SCR of NO_x, various active iron sites, such as small oxygen-bridged clusters $[HO\text{-}Fe\text{-}O\text{-}Fe\text{-}OH]^{2+}$ [323,324], isolated Fe^{2+} and Fe^{3+} ions [325, 326], or extra-framework Fe-O-Al and grafted Fe-O-Si species [327, 328], have been suggested. Previous studies suggest that all these iron species

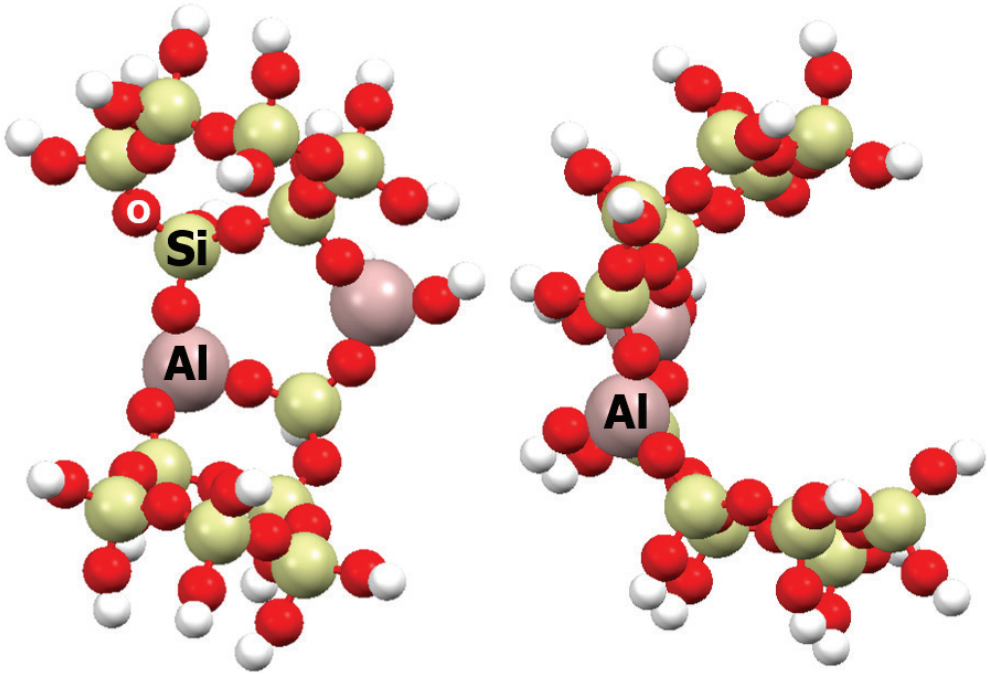

Figure 48. Location of Al cations in a BEA frame (own work)

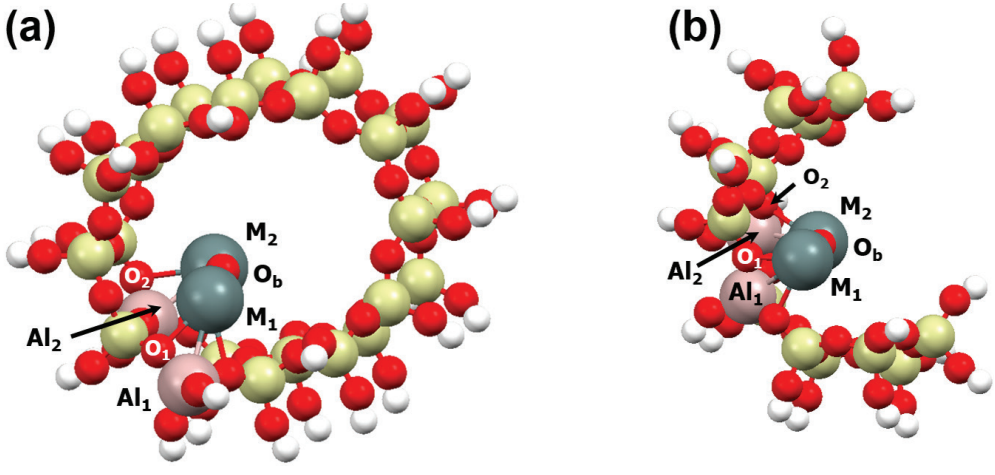

Figure 49. Dimeric complex M-O_b-M (where M= Sn or Fe) in BEA: (a) ideal inside pore, (b) after hierarchization (own work)

usually coexist in the pores of the ZSM-5 framework; binuclear iron and isolated iron species have been suggested to be active sites for the SCR reaction [329, 330].

Tin and iron dimers are considered in the present study as active sites for lactic acid adsorption; compared with the previously mentioned literature [227–230], this is a new approach, especially in case of tin. Previously, most theoretical researchers substituted tin inside a zeolite frame. However, in our studies lactic acid was not stabilized above any zeolite frame-centers; therefore, we tried the dimeric models used previously in studies of isocyanic acid adsorption [292]. We investigated the stabilization of dimeric M-O_b-M complexes (where M= Sn or Fe) in the BEA pore and at the BEA surface (observed after hierarchization of BEA zeolite in alkaline media) (Figure 49).

The structure of the M-O_b-M dimer does not depend on the cluster: dimers of each metal (Sn or Fe) have a similar structure in 'ideal' ($Al_2Si_{22}O_{64}H_{32}$) and 'hierarchical' ($Al_2Si_{12}O_{39}H_{22}$) clusters. However, we observed differences in the geometry of the dimers for the metals Sn and Fe.

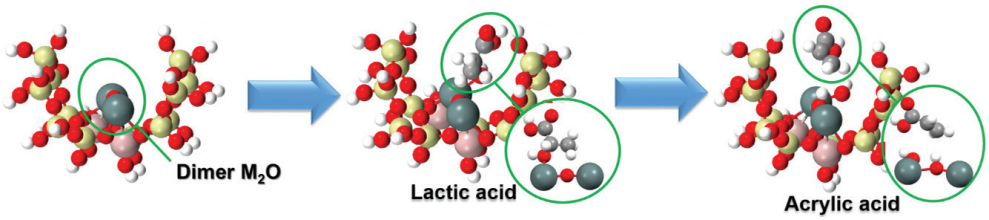

Figure 50. Dimer M_2O, lactic and acrylic acid structures at the surface model of BEA zeolite (own work)

We found the mechanism of direct lactic acid dehydration in Sn- and Fe-BEA zeolite, both ideal and after hierarchization,. The geometric compatibility of the metallic dimers and lactic acid allows the proposed direct dehydration mechanism, in which the oxygen center of the hydroxyl group of LA-α-carbon interacts with the metal center of the dimer and hydrogen is subtracted from LA-β-carbon and bound with the bridge oxygen of the metal dimer (Figure 50). The adsorption of lactic acid is endothermic in the case of Sn-BEA, slightly endothermic in ideal Fe-BEA, and exothermic in the case of hierarchical Fe-BEA catalyst.

5. CONCLUSIONS AND FUTURE

The urgent need for more sustainable production of chemicals from renewable feedstock (e.g. biomass) has led to intense research efforts in the search for novel porous nano-materials such as zeolites. Catalysts are still discovered through a combination of trial-and-error and serendipity d ue to limited understanding of the molecular structure and complexity of active centers. The main goal of research should be the design of zeolites at the nano-scale with improved catalytic performance that is optimized for biomass transformation to dedicated chemicals. The research should focus on zeolites with different pore sizes. Zeolites that are commercially available in purely microporous form could also be prepared in mesoporous form and with the addition of selected metal nanoparticles. New insights from both molecular modelling and experimental methods is essential to obtain knowledge about zeolite topology and catalytic properties. The integration of experimental and theoretical paths is a novel approach and guarantees rapid progress in the development of new catalysts and processes, as well as exceptional training for students in the subject of nano-design of zeolite-based catalysts for selective conversion of biomass into chemicals. We designed realistic three-dimensional models of zeolites with added internal metal nanoparticles. A variety of unresolved problems and uncertainties remain in relation to biomass transformation into valuable chemicals; solving these problems would have a significant impact on the development of the science and economy of zeolite catalysts as well as on the environmentally friendly production of important chemicals. The development of catalytic routes for the conversion of bio-renewable feedstocks to selected key petrochemicals is an important issue, both for the EU and globally. Active sites and the electronic structure of zeolite catalysts during reactions are important for the development of a new class of catalysts with a declared molecular structure.

The problem with using zeolites in biomass conversion is the production of a large number of by-products. Another problem is the existence of many phases during these processes, e.g. water and organic phases, which makes the process very difficult at an industrial scale. Additionally, the products have a tendency to be polymerized. Therefore, the development of a process will require a lot of multidisciplinary research before it can be finally applied in industrial practice. However, it is worthy of consideration, especially using zeolites with designed structures and properties.

REFERENCES

[1] Pacala S., Socolow R., *Science* 305, 2004, 968.

[2] Werpy T., Petersen G., Top Value Added Chemicals from Biomass, Vol. I: *Results of Screening for Potential Candidates from Sugars and Synthesis Gas*, Report No. NREL/TP-510-35523, National Renewable Energy Laboratory, Golden, CO, 2004.

[3] The roadmap for biomass technologies in the U.S., Biomass R&D Technical Advisory Committee, US Department of Energy, Accession No. ADA 436527, 2002.

[4] Grala A., Zieliński M., Dudek M., Dębowski M., Ostrowska K., Technologie kondycjonowania biomasy lignocelulozowej przed procesem fermentacji metanowej, Interdyscyplinarne zagadnienia w Inżynierii i Ochronie Środowiska, Oficyna Wydawnicza Politechniki Wrocławskiej 4, Wrocław 2014, 261–272.

[5] Demirbas A., Demirbas I., *Energy Conversion and Managment* 48, 2007, 2386–2398.

[6] Chandra R., Takeuchi H., Hasegawa T., *Renewable and Sustainable Energy Reviews* 16, 2012, 1462–1476.

[7] Clark J., Deswarte F., Introduction to Chemicals from Biomass, Second Edition, John Wiley & Sons, Ltd. Published 2015.

[8] Lalak J., Kasprzycka A., Murat A., Paprota E.M., Tys J., *Acta Agrophysica* 21, 2014, 51–62.

[9] Burczyk B., *Wiadomości chemiczne* 63, 2009, 9–10.

[10] Tan K.T., Lee K.T., Mohamed A.R., *Energy Policy* 36(9), 2008, 3360–3365.

[11] Balat M., Balat H., Oz C., *Progress in Energy and Combustion Science* 34, 2008, 551–573.

[12] http://www.oze.edu.pl/biomasa-i-biopaliwa/biomasa-i-biopaliwa/definicja-biomasy [access: 16.02.2017].

[13] Lalak J., Kasprzycka A., Murat A., Paprota E.M., Tys J., Obróbka wstępna biomasy bogatej w lignocelulozę w celu zwiększenia wydajności fermentacyjnej metanowej, *Acta Agrophysica* 21, 2014, 51–62.

[14] Fernando S., Adhikari S., Chandrapal C., and Murali N., *Energy & Fuels* 20, 2006, 1727–1737.

[15] http://www.consilium.europa.eu/pl/policies/climate-change/2030-climate-and-energy-framework/ [access: 10.08.2018].

[16] Tan K.T., Lee K.T., Mohamed A.R., *Energy Policy* 36, 2008, 3360–3365.

[17] Clark J., Deswarte F., Introduction to Chemicals from Biomass, Second Edition, John Wiley & Sons, 2015.

[18] Balat M., Balat H., Oz C., *Progress in Energy and Combustion Science* 34, 2008, 551–573.
[19] Lin Y.-C., Huber G.W., The critical role of heterogeneous catalysis in lignocellulosic biomass conversion, *Energy Environmental Science* 2, 2009, 68–80.
[20] Lin Y.-C., Huber G.W., *Energy Environ. Sci.* 2, 2009, 68.
[21] Corma A., Iborra S., Velty A., *Chem. Rev.* 107, 2007, 2411.
[22] Gandini A., *Green Chem.* 13, 2011, 1061.
[23] Corma A., *Chem. Rev.* 95, 1995, 559.
[24] Rinaldi R., Schüth F., *Energy Environ. Sci.* 2, 2009, 610.
[25] Stöcker M., *Angew. Chem. Int. Ed.* 47, 2008, 9200.
[26] Pérez-Ramírez J., Christensen C.H., Egeblad K., Christensen C.H., Groen J.C., *Chem. Soc. Rev.* 37, 2008, 2530.
[27] Verboekend D. , Pérez-Ramírez J., *Catal. Sci. Technol.* 1, 2011, 879.
[28] Milina M., Mitchell S., Crivelli P., Cooke D., Pérez-Ramírez J., *Nature Commun.* 5, 2014, 4922.
[29] Zhang X.Q., Trinh T.T., van Santen R.A., Jansen A.P.J., *J. Am. Chem.Soc.* 133, 2011, 6613.
[30] Szyja B.M., Hensen E.J.M., van Santen R.A., *Catal. Today* 169, 2011, 156.
[31] Li G., Pidko E.A., van Santen R.A., Li C., Hensen E.J.M., *J. Phys. Chem. C* 117, 2013, 413.
[32] Lisboa O., Sanchez M., Ruette F., *J. Molec. Catal. A: Chem.* 294, 2008, 93.
[33] Malola S., Svelle S., Bleken F.L., Swang O., *Angew. Chem. Int. Ed.* 51, 2012, 652.
[34] Kumar P., Barrett D.M., Delwiche M.J., Stroeve P., *Industrial and engineering Chemistry Research* 48, 2009, 3713–3729.
[35] Mood S.H., Golfeshan A.H., Tabatabaei M., Jouzani G.S., Najafi G.H., Gholam M., Ardjmand M., *Renewable and Sustainable Energy Reviewes* 27, 2013, 77–93.
[36] Swatloski R.P., Spear S.K., Holbrey J.D., Rogers R.D., *J. Am. Chem. Soc.* 124, 2002, 4974.
[37] Fort D.A., Remsing R.C., Swatloski R.P., Moyna P., Moyna G., Rogers R.D. *et al., Green Chem.* 9, 2007, 63.
[38] Weingarth D., Czekaj I., Zhaofu Fei, Foelske A., Dyson P., Wokaun A., Kötz R., *The Electrochemical Society Journals* 159, 2012, H611.
[39] Zakrzewska M.E., Bogel-Lukasik E., Bogel-Lukasik R., *Energy Fuels* 24, 2010, 737.
[40] Hayaki S., Kido K., Sato H., Sakaki S., *Phys. Chem. Chem. Phys.* 12, 2010, 1822.
[41] Krekeler C., Dommert F., Schmidt J., Zhao Y.Y., Holm C., Berger R., Della L.S., *Phys. Chem. Chem. Phys.* 2010, **12**, 1817.
[42] Doherty T.V., Mora-Pale M., Foley R.J., Linhardt S.E., Dordick J.S., *Green Chem.* 2010, **12**, 1967.
[43] Bals B., Wedding C.H., Balan V., Sendich E., Dale B., *Bioresource Technology* 102, 2011, 1277–1283.

[44] Kurabi A., Berlin A., Gilkes N., Kilburn D., Bura R., Robinson J. *et al., Applied Biochemistry and Biotechnology* 121, 2005, 219–230.
[45] Menon V., Rao M., *Progress in Energy and Combustion Science* 38, 2012, 522–550.
[46] Alonso D.M., Bond J.Q., Dumesic J.A., *Green Chem.* 12, 2010, 1493–1513.
[47] Hamelinck C.N., Faaij A.P.C., Uil H.D., Boerrigter H., *Energy* 29, 2004, 1743–1771.
[48] Dry M.E., *Applied Catalysis A:General*, 189, 1999, 185–190.
[49] Rosowski F., Hinrichsen O., Muhler M., Ertl G., *Catal. Lett.* 36, 1996, 229.
[50] Abrevaya H., Cohn M.J., Targos W.M., Robota H.J., *Catal. Lett.* 7, 1990, 183.
[51] Heinen A.W., Peters J.A., van Bekkum H., *Carbohydr. Res.* 328, 2000, 449.
[52] Herrera V.A.S., Oladele O., Kordás K., Eränen K., Mikkola J.-P., Murzina D.Y., Salmia T., *J. Chem. Technol. Biotechnol.* 86, 2011, 658.
[53] Wang W., Liu H., Wu T., Zhang P., Ding G., Liang S., Jiang T., Han B., *J. Mol. Catal. A: Chem.*, 355, 2012, 174.
[54] Dalla'Betta R.A., Shelef M., *J. Catal.* 48, 1977, 111.
[55] Kowalczyk Z., Stołecki K., Rarog-Pilecka W., Miskiewicz E., Wilczkowska E., Karpinski Z., *Appl. Catal. A: General* 342, 2008, 35.
[56] Vogel F., Catalytic Conversion of High-Moisture Biomass to Synthetic Natural Gas in Supercritical Water, in: Handbook of Green Chemistry, Vol. 2: Heterogeneous Catalysis, Editor: R.H. Crabtree; WILEY-VCH, Weinheim, 2009.
[57] Waldner M.H., Krumeich F., Vogel F., *J. Supercritical Fluids* 43, 2007, 91.
[58] Tennison S.R., in: Catalytic Ammonia Synthesis, Editor: J.R. Jennings, Plenum Press, New York, 1991, 303.
[59] Kowalczyk Z., Sentek J., Jodzis S., Mizera E., Gòralski J., Paryjczak T., Diduzko R., *Catal. Lett.* 45, 1997, 65.
[60] Forni L., Molinari D., Rossetti I., Pernicone N., *Appl. Catal. A: General* 185, 1999, 269.
[61] Jacobsen C.J.H., Dahl S., Hansen P.L., Törnqvist E., Jensen L., Topsøe H., Prip D.V., Møenshaugb P.B., Chorkendorff I., Structure sensitivity of supported ruthenium catalysts for ammonia synthesis, *J. Mol. Catal. A: Chem.* 163,2000, 19.
[62] García-García F.R., Guerrero-Ruiz A., Rodríguez-Ramos I., *Top. Catal.* 52, 2009, 758.
[63] Song Z., Cai T., Hanson J.C., Rodriguez J.A., Hrbek J., *J. Am. Chem. Soc.* 126, 2004, 8576.
[64] Raróg-Pilecka W., Miskiewicz E., Szmigiel D., Kowalczyk Z., *J. Catal.* 231, 2005, 11.
[65] Hansen T.W., Hansen P.L., Dahl S., Jacobsen C.J.H., *Catal. Lett.* 84, 2002, 7.
[66] Bielawa H., Hinrichsen O., Birkner A., Muhler M., The Ammonia-Synthesis Catalyst of the Next Generation: Barium-Promoted Oxide-Supported Ruthenium, *Angew. Chem. Int. Ed.* 40, 2001, 1061.
[67] Van Hardeveld R., Van Montfoort A., *Surf. Sci.* 4, 1966, 396.

[68] Nielsen R.M., Murphy S., Strebel C., Johansson M., Nielsen J.H., Chorkendorff I., *Surf. Sci.* 603, 2009, 3420.
[69] Lizzit S., Baraldi A., Groso A., Reuter K., Ganduglia-Pirovano M.V., Stampfl C., Scheffler M., Stichler M., Keller C., Wurth W., Menzel D., *Physical Review B* 63, 2001, 205419.
[70] Lu Y., Sun Q., Jia Y., He P., *Surface Science* 602, 2008, 2502–2507.
[71] Hofmann J.P., Rohrlack S.F., Heß F., Goritzka J.C., Krause P.P.T., Seitsonen A.P., Moritz W., Over H., *Surface Science* 606, 2012, 297–304.
[72] Sinha N.K., Neurock M., *Journal of Catalysis* 295, 2012, 31–44.
[73] Peterson A.A., Dreher M., Wambach J., Nachtegaal M., Dahl S., Nørskov J.K., Vogel F., *ChemCatChem*. 4, 2012, 1185-1189.
[74] Czekaj I., Pin S., Wambach J., *J. Phys. Chem. C*. 117, 2013, 26588–26597.
[75] Czekaj I., Loviat F., Raimondi F., Wambach J., Biollaz S., Wokaun A., *Appl. Catalysis A: General* 329, 2007, 68–78.
[76] Ertl G., Knözinger H., Weitkamp J., Handbook of Heterogeneous Catalysis, Wiley Company, Weinheim, 1997.
[77] Nazimek D., Machocki A., Borowiecki T., Adsorption, *Science & Technology* 16, 1998, 747.
[78] Jacobs J.P., Lindfors L.P., Reintjes J.G.H., Jylhä O., Brongersma H.H., *Catal. Lett.* 25,1994, 315.
[79] Sarapatka T.J., *Chem. Phys. Letters* 212, 1993, 37.
[80] Shern C.S., J.S. Tsay, T. Fu, *Appl. Surf. Sci.* 92, 1996, 74.
[81] Tanner R.E., Goldfarb I., Castell M.R., Briggs G.A.D., *Surf. Sci.* 486, 2001, 167.
[82] Carey J.D., Ong L.L., Silva S.R.P, *Nanotechnology* 14, 2003, 1223.
[83] Seemann M.C., Schildhauer T.J., Biollaz S.M.A., Stucki S., Wokaun A., *Appl. Catalysis A: General*, 313, 2006, 14.
[84] Lamber R., Schulz-Ekloff G., *Surf. Sci.* 258, 1991, 107.
[85] Shih K., Leckie J.O., *J. Euro. Ceramic Soc.* 27, 2007, 91.
[86] Lamber R., Schulz-Ekloff G., *Surf. Sci.* 258, 1991, A595.
[87] Sehested J., Gelten J.A.P., Remediakis I.N., Bengaard H., Nørskov J.K., *J. Catal.* 223, 2004, 432.
[88] Czekaj I., Loviat F., Wambach J., Wokaun A., *Chimia Vol.* 4/09, 2009, 193–196.
[89] Loviat F., Czekaj I., Wambach J., Wokaun A., *Surf. Sci.* 603, 2009, 2210–2217.
[90] Bridgwater A.V., *Biomass and Bioenergy* 38, 2012, 68–94.
[91] Qi Z., Jie C., Tiejun W., Ying X., *Energy Conversion and Management* 48, 2007, 87–92.
[92] Chiaramonti D., Oasmaa A., Solantausta Y., *Renewable and Sustainable Energy Reviews* 11, 2007, 1056–1086.
[93] Demirbas A., Me*Energy Conversion and Management* 41, 2000, 633–646.

[94] Demirbas A., *Energy Conversion and Management* 42, 2001, 1357–1378.
[95] McKendry P., *Bioresource Technology* 83, 2002, 47–54.
[96] Lim J.S., Manan Z.A., Alwi S.R.W., Hashim H., *Renewable and Suitable Energy Reviews* 16, 2012, 3084–3094.
[97] Zhang L., Xu C., Champagne P., *Energy Conservation and Management* 51, 2010, 969–982.
[98] Menon V., Rao M., *Progress in Energy and Combustion Science* 38, 2012, 522–550.
[99] Hendriks A.T., Zeeman G., *Bioresour. Technol.* 100, 2009, 10–18.
[100] Sun Y., Cheng J., *Bioresour. Technol.* 83, 2002, 1–11.
[101] Van Dyk J.S., Pletschke B.I., *Biotechnology Advances* 30, 2012, 1458–1480.
[102] Maitan-Alfenas G.P., Visser E.M., Guimara V.M., *Current Opinion in Food Science* 1, 2015, 44–49.
[103] Gallezot P., *ChemSusChem* 1, 2008, 734–737.
[104] Himmel M.E., Ding S.Y., Johnson D.K., Adney W.S., Nimlos M.R., Brady J.W., Foust T.D., *Science* 315, 2007, 804–807.
[105] Xian M., Sustainable Production of Bulk Chemicals. Integration of Bio-, Chemo- Resources and Processes, Springer 2016.
[106] Anbarasan P., Baer Z.C., Sreekumar S., Gross E., Binder J.B., Blanch H.W., Clark D.S., Toste F.D., *Nature* 491, 2012, 235.
[107] Leja K., Lewandowicz G., Grajek W., *Biotechnologia* 4 (87), 2009, 88–101.
[108] Biernat K., *Czysta Energia* 11, 2010, 33–36.
[109] Besson M., Gallezot P., Pinel C., *Chem. Rev.* 114, 2014, 1827–1870.
[110] Wang A., Zhang T., *Acc. Chem. Res.* 46, 2013, 1377–1386.
[111] Wang X.C, Meng L.Q, Wu F., Jiang Y.J, Wang L., Mu X.D., *Green Chem.* 14, 2012, 758–765.
[112] Scholz D., Aellig Ch., Mondelli C., Perez-Ramirez J., *ChemCatChem* 7, 2015, 1551–1558.
[113] Amada Y., Watanabe H., Hirai Y., Kajikawa Y., Nakagawa Y., Tomishige K., *ChemSusChem* 5, 2012, 1991.
[114] Sulewski M., Urbaniak W., *Czysta Energia* 6, 2011, 27–28.
[115] Feng J., Fu H., Wang J., Li R., Chen H., Li X., *Catalysis Communications* 9, 2008, 1458–1464.
[116] Cai C.M., Zhang T., Kumara R., Wymana C.E., *J. Chem. Technol. Biotechnol.* 89, 2014, 2–10.
[117] Eseyin A.E., Steele P.H., *International Journal of Advanced Chemistry* 3 (2), 2015, 42–47.
[118] Saha B., Abu-Omar M.M., *Green Chem.* **16,** 2014, 24–38.
[119] Dijkman W.P., Fraaije M.W., *Appl. Environ. Microbiol.* 80, 2014, 1082–1090.

[120] Nicholas K.M., Selective Catalysis for Renewable Feedstocks and Chemicals, Springer 2014.
[121] Zhang J., Lin L., Liu S., *Energy Fuels* 26, 2012, 4560.
[122] Anbarasan P., Baer Z.C., Sreekumar S., Gross E., Binder J.B., Blanch H.W., Clark D.S., Toste F.D., *Nature* 491, 2012, 235.
[123] Song H., Lee S.Y., *Enzyme and Microbial Technology* 39, 2006, 352–361.
[124] Wang S., Dorcet V., Roisnel T., Bruneau C., Fischmeister C., *Organometallics* 36, 2017, 708–713.
[125] Girisuta B., Janssen L.P.B.M., Heeres H.J., A Kinetic *Chemical Engineering Research and Design* 84(A5), 2006, 339–349.
[126] Mustafin K., Cárdenas-Lizana F., Keane M.A., J. Chem. Techn. Biotechn. 92, 2017, doi: 10.1002/jctb.5258 .
[127] Ahmed El-Imam A., Du Ch., *J. Biodivers Biopros. Dev.* 1,2014,2.
[128] Le Nôtre J., Witte-van Dijk S.C., van Haveren J., Scott E.L.,Sanders J.P., *ChemSusChem*. 7(9), 2014 2712–20.
[129] Nampoothiri K.M., Nair N.R., John R.P., *Bioresource Technology* 101, 2010, 8493–8501.
[130] Lasprilla A.J.R., Martinez G.A.R., Lunelli B.H., Jardini A.L., Filho R.M., *Biotechnology Advances* 30, 2012, 321–328.
[131] Martinez F.A.C., Balciunas E.M., Salgado J.M., González J.M.D., Converti A., Pinheiro de Souza Oliveira R., *Trends in Food Science & Technology* 30, 2013, 70–83.
[132] Scholz D., Aellig Ch., Mondelli C., Perez-Ramirez J., *ChemCatChem* 7, 2015, 1551–1558.
[133] Garlotta D., *Journal of Polymers and the Environment* 9, 2001, 63–84.
[134] Hong J.H., Lee J.M., Kim H.R.,. Hwang Y.K, Chang J.S., Halligudi S.B., Han Y.H., *Applied Catalysis A: General* 3962011, 194–200.
[135] Zhang J., Zhao Y., Pan M., Feng X., Ji W., Au C-T., *ACS Catal* 1, 2011, 32–41.
[136] Suo X., Zhang H., Ye Q., Dai X., Yu H., Li R., *Chemical Engineering Research and Design* 104, 2015, 346–356.
[137] Baran E., *Rynek Chemiczny* 12, 2007, 8-11.
[138] Grzywa E., Molenda J., Technologia podstawowych syntez organicznych, Tom 2, Wyd. 3, WNT, Warszawa 2000.
[139] Kijeński J., Migdał A., Rejewski P., Kędziora A., *POLIMERY 61,* 2016, 702-709.
[140] Zhang J., Lin J., Peilin C., *The Canadian Journal of Chemical Engineering* 86(6), 2006, 1047-1053..
[141] Yan B., Tao L-Z., Liang Y., Xu B-Q., *ACS Catal*. 4, 2014, 1931–1943.
[142] Ghantani V.C., Dongare M.K., Umbarkar S.B., *RSC Adv*. 4, 2014, 33319.
[143] Matsuura Y., Onda A., Yanagisawa K., *Catalysis Communications* 48, 2014, 5–10.
[144] C. Tang, J. Peng, G. Fan, X. Li, X. Pu,W. Bai *Catalysis Communications* 43, 2014, 231–234.

[145] Hammaecher C., Paul J.-F., *Journal of Catalysis* 300, 2013, 174–182.
[146] Blanco E., Lorentz C., Delichere P., Burel L., Vrinat M., Millet J.M.M., Loridant S., *Applied Catalysis B: Environmental* 180, 2016, 596–606.
[147] Guo Z., Theng D.S., Tang K.Y., Zhang L., Huang L., Borgna A., Wang C., *Phys. Chem. Chem. Phys*., 18, 2016, 23746.
[148] a) R. Beerthuis, G. Rothenberg, N. R. Shiju *Green Chem.* 17, 2015, 1341.
[149] Dapsens P.Y., Mondelli C., Perez-Ramírez J.r, *ACS Catal*. 2, 2012, 1487–1499.
[150] Dapsens P.Y., Mondelli C., Perez-Ramirez J., *Chem. Soc. Rev*. 44, 2015, 7025.
[151] Martinez C., Corma A., Reference Module in Chemistry, Molecular Sciences and Chemical Engineering Comprehensive Inorganic Chemistry II (Second Edition), From Elements to Applications 2013, 103–131, Vol. 5: Porous Materials and Nanomaterials.
[152] International Zeolite Asociation: http://www.iza-online.org/ [21.03.2017].
[153] http://biodrain.pl/produkty/zeolity/ [21.03.2017].
[154] Fruijtier-Pölloth C., *Arch. Toxicol*. 83, 2009, 23–35.
[155] Chałupnik S., Franus W., Wysocka M. *et al*., *Sci. Pollut. Res.* 20, 2013, 7900.
[156] Handke M., Krystalochemia krzemianów, Wydawnictwo AGH, Kraków 2005.
[157] Grzybowska-Świerkosz B., Elementy Katalizy Heterogenicznej, Wydawnictwo Naukowe PWN, Warszawa 1993.
[158] Meng X., Wang L., Xiao F.S. Sustainable Routes for Zeolite Synthesis, *Zeolites in Sustainable Chemistry Synthesis, Characterization and Catalytic Applications*, Springer 2016.
[159] Meng X., Xiao F.S. , Chem Rev 14, 2014, 1521–1543.
[160] Davis M.E., *Chem. Mater*. 26, 2014, 239–245.
[161] Cejka J., Corma A., Zones S., Zeolites and Catalysis: Synthesis, Reactions and Applications, Vol. 1, 2010 Wiley-VCH.
[162] Sels B., Kustov L., Zeolites and Zeolite-like Materials, Elsevier 2016.
[163] Suib S.L., New and Future Developments in Catalysis: Chapter 12. Environmental Synthesis Concerns of Zeolites, Elsevier 2013.
[164] Wu Q., Wang X., Qi G., Guo Q., Pan S., Meng X., Xu J., Deng F., Fan F., Feng Z., Li C., Maurer S., Müller U., Xiao F.S., *J. Am. Chem. Soc.* 136 (10), 2014, 4019–4025.
[165] Cheng Y., Wang L.J., Li J.S., Yang Y.C., Sun X.Y., *Materials Letters* 59, 2005, 3427–3430.
[166] Tang Z., Kim S.J., Gu X., Dong J., *Microporous and Mesoporous Materials* 118, 2009, 224–231.
[167] Diaz I., Kokkoli E., Terasaki O., Tsapatsis M., *Chem. Mater.* 16, 2004, 5226–5232.
[168] Bonilla G., Diaz I., Tsapatsis M., Jeong H.-K., Lee Y., Vlachos D.G., *Chem. Mater.* 16, 2004, 5697–5705.

[169] Szostak R., Pan J.M., Lillerud K.P., *J. Phys.Chem*. 99, 1995, 2104.
[170] First E.L., Gounaris C.E., Wei J., Floudas C.A., *Physical Chemistry Chemical Physics,* 13, 2011, 17339.
[171] Ernst S., Weitkamp J., Martens J.A., Jacobs P.A., *Appl. Catal*. 48, 1989, 137.
[172] Hayasaka K., Liang D., Huybrechts W., de Waele B.R., Houthoofd K.J., Eloy P., Gaigneaux E.M., van Tendeloo G., Thybaut J.W., Marin G.B., Denayer J.F.M., Baron G.V., Jacobs P.A., Kirschhock C.E.A., Martens J.A., *Chem.–Eur. J*. 13, 2007, 10070.
[173] Wu Q., Liu X., Zhu L., Ding L., Gao P., Wang X., Pan S., Bian C., Meng X., Xu J., Deng F., Maurer S., Müller U., Xiao F.S., *J. Am. Chem. Soc.* 137 (3), 2015, 1052–1055.
[174] Zhang P., Wang L. *et al., J. Mater. Chem.* 21, 2011, 12026–12033.
[175] Jin Y., Qi G., Yang C., Xu J., Chen F., Meng X., Deng F., Xiao F.S., *Angew. Chem. Int. Ed*., 52, 2013, 9172–9175.
[176] Zhou Ming, Rownaghi A.A., Hedlund J., Electronic Supplementary Material (ESI) for RSC Advances, This journal is © The Royal Society of Chemistry 2013.
[177] Kleinwort R., PhD Thesis: Kristallisationskinetische Untersuchungen zur Synthese von Zeolithen, University of Hamburg, 1994.
[178] Mintova S., Barrier N., Verified Syntheses of Zeolitic Materials. Third Revised Editon, Published on behalf of the Synthesis Commission of the International Zeolite Association, 2016, ISBN: 978-0-692-68539-6.
[179] Chheda J.N., Huber G.W., Dumesic J.A., *Angew. Chem. Int. Ed*. 46, 2007, 7164-7183.
[180] Lassinantti Gualtieri M., *Microporous and Mesoporous Materials* 117, 2009, 508–510.
[181] Miyake K., Hirota Y., Uchida Y., Nishiyama N., *J. Porous. Mater*. 23, 2016, 1395–1399.
[182] Dutta P.K., Puri M., *The Journal of Physical Chemistry* 91, 1987, 4329–4333.
[183] Srivastava R., Iwasa N., Fujita S., Arai M., *Chem. Eur. J.* 14, 2008, 9507–9511.
[184] Choi M., Na K., Ryoo R., *Chem. Commun*. 20, 2009, 2845–2847.
[185] Zhu J., Zhu Y., Zhu L., Rigutto M., van der Made A., Yang Ch., Pan S., Wang L., Zhu L., Jin Y., Sun Q., Wu Q., Meng Xiangju, Zhang D., Han Y., Li J., Chu Yueying, Zheng A., Qiu S., Zheng X., Xiao F.S., *J. Am. Chem. Soc.* 136, 2014, 2503–2510.
[186] Majano G., Delmotte L., Valtchev V., Mintova S., *Chem. Mater.* 21 (18), 2009, 4184–4191.
[187] Xie B., Song J., Ren L., Ji Y., Li J., Xiao F.S., *Chem. Mater.,* 20 (14), 2008, 4533–4535.
[188] Julius C., Octane-Enhancing, *Catalysis Reviews*. 31, 1989, 215.
[189] Lechert H., Kacirek H., *Zeolites* 13, 1992, 192.
[190] Inayat A., Knoke I., Spiecker E., Schwieger W., *Angew.Chem. Int. Ed*. 2012, 51, 1962–1965.
[191] Ginter D.M., Bell A.T., Radke C.J., Synthesis of Microporous Materials, Vol. 1, Molecular Sieves, M.L Occelli, H.E Robson (eds.), Van Nostrand Reinhold, New York, 1992, p. 6.

[192] Christidis G.E. and Papantoni H., *The Open Mineralogy Journal* 2, 2008, 1–5.
[193] Bourgogne M. *et al.*, United States Patent 4, 503, 024, March 5, 1985.
[194] Ji Y., Deimund M.A., Bhawe Y., Davis M.E., *ACS Catal.* 5, 2015, 4456–446.
[195] Jang E. *et al., Journal of Membrane Science* 549, 2018, 46–59.
[196] Marchese L. *et al., Microporous and Mesoporous Materials* 30, 1999, 145–153.
[197] Gao F. *et al., Applied Catalysis B: Environmental* 162, 2015, 501–514.
[198] Gao F., Walter E.D., Washton N.M., Szanyi J., Peden Ch.HF, *ACS Catal.* 3, 2013, 2083–2093.
[199] Zhou R. *et al., Journal of Membrane Science* 444, 2013, 384–393.
[200] Guo Z., Miao P., Zhu W., Guo L., Li F., Xue Y., Yin Q., Yuan R., Xu L., *Catalysts* 7, 2017, 150.
[201] Ashtekar S., Chilukuri S.V.V., Chakrabarty D.K., *J. Phys. Chem.* 98, 1994, 4878–4883.
[202] Zhang L. *et al., Microporous and Mesoporous Materials* 126, 2009, 115–124.
[203] Jin Y. *et al., Microporous and Mesoporous Materials* 147, 2012, 259–266.
[204] Li X.F. *et al., Journal of Catalysis* 262, 2009, 257–265.
[205] Li G. *et al., Solid State Sciences* 13, 2011, 662-664.
[206] Sharma *et al.* P., *Journal of Colloid and Interface Science* 325, 2008, 547–557.
[207] Ng E.P., Goupil J.M., Vicente A., Fernandez C., Retoux R., Valtchev V., Mintova S., *Chem. Mater.* 24 (24), 2012, 4758–4765.
[208] Rosinski E.J, Rubin M.K., Patent: US 4391785 "A reparation of ZSM-12 type zeolites".
[209] Ernst S., *Zeolites* 7, 1987, 458–462.
[210] Ernst S., *Applied Catalysis*, 48, 1989, 137–148**.**
[211] Marler B., *Zeolites*, 7, 1987, 393–397.
[212] Valyicsik E.W., Patent: US 4076842 A „Synthesis of ZSM-23 zeolite".
[213] Valyicsik E.W., Patent: US 4531012 A „Organic template for synthesis of ZSM-23 zeolite".
[214] Wang B., Gao Q., Gao J., Ji D., Wang X., Suo J., *Applied Catalysis A: General*, 2004, 167–172.
[215] Xu W.Q., Yin Y.G., Suib S.L., Edwards J.C., O'Young C.L., *J. Phys. Chem*. 99, 1995, 9443–9451.
[216] Guo G., Sun Y., Long Y., *Chem. Commun***.** 2000, 1893–1894.
[217] Rubin M.K., Rosinski E.J., Plank C.J., Patent: US 4086186 A „Crystalline zeolite ZSM-34 and method of preparing the same".
[218] Yang S., Evmiridis N.P., *Microporous Materials* 6, 1996, 19–26.
[219] Wu Z., Song J., Ji Y., Ren L., Xiao F.S., *Chem. Mater.* 20 (2), 2008, 357–359.
[220] Yang, C. Ren L., Zhang H., Zhu L., Wang L., Meng X., Xiao F.S., *J. Mater. Chem*., 22, 2012, 12238–12245.

[221] Wu Z., Song J., Ji Y., Ren L., Xiao F.S., *Chem. Mater.* 20 (2), 2008, 357–359.
[222] Zhang L., Yang C., *Chem. Mater.*, 22, 2010, 3099–3107.
[223] Leonowicz M.E., Vaughan D.E.W., *Nature* 329, 1987, 819–821.
[224] Vaughan D.E., Strohmaier K.G., Patent: US 4657748 A „Crystalline zeolite (ECR-1) and process for preparing it".
[225] Csia Chen C.S., Schlenker J.L., Wentzek S.E., *Zeolites* 4, 1996, 393–400.
[226] Song J., Dai L., Ji Y., Xiao F.S., *Chem. Mater.* 18 (12), 2006, 2775–2777.
[227] Montejo-Valencia B.D., Salcedo-Pe´ rez J.L., Curet-Arana M.C., *J. Phys. Chem*. C 120, 2016, 2176–2186.
[228] Osmundsen C.M., Holm M.S., Dahl S., Taarning E., *Proc. R. Soc. London, Ser*. A 468, 2012, 2000–2016.
[229] Wolf P., Valla M., Rossini A.J., Comas-Vives A., Núñez-Zarur F., Malaman B., Lesage A., Emsley L., Copéret, C., Hermans I., *Angew. Chem. Int. Ed. Engl.* 53, 2014, 10179–83.
[230] Corma A., Domine M.E., Nemeth L., Valencia S.*J. Am. Chem. Soc*. 124, 2002, 3194–3195.
[231] Lew C.M., Rajabbeigi N., Tsapatsis M., *Microporous and Mesoporous Materials* 153, 2012, 55–58.
[232] Yang G., Pidko E., Hensen E.J.M., *J. Phys. Chem.* C 117, 2013, 3976–3986.
[233] Boronat M., Concepcion P., Corma A., Renz M., Valencia S., *J. Catal.* 234, 2005, 111–118.
[234] Czekaj I., Loviat F., Raimondi F., Wambach J., Biollaz S., Wokaun A., *Appl. Catalysis A: General* 329, 2007, 68.
[235] Czekaj I., Loviat F., Wambach J., Wokaun A., *Chimia* 4, 2009, 193.
[236] Loviat F., Czekaj I., Wambach J., Wokaun A., A. Model studies of nickel deposition at γ-Al_2O_3 surface: combination of experimental and theoretical results, *Surf. Sci.* 603, 2009, 2210.
[237] Hohenberg P., Kohn W., *Phys. Rev. B* 136, 1964, 864.
[238] Parr R.G., Yang W., Density Functional Theory of Atoms and Molecules, Oxford University Press, New York 1989.
[239] Kohn W., Sham L.J., *Phys. Rev. A,* 140, 1965, 1133.
[240] Dahl J.P., Avery J. (ed.), Local Density Approximations in Quantum Chemistry and Solid-State Physics, Plenum, New York 1984.
[241] Vosko S.H., Wilk L., Nusair M., *Can. J. Phys*., 58, 1980, 1200.
[242] Perdew J.P., Burke K., Ernzerhof M., *Phys. Rev. Lett*., 77, 1996, 3865; *Erratum: Phys. Rev. Lett*., 78, 1997, 1386.
[243] Hammer B., Hansen L.B., Nørskov J.K., *Phys. Rev. B*, 59, 1999, 7413.
[244] Adamo C., Barone V., *J. Chem. Phys*., 110, 1999, 6158.
[245] Chojnacki H., *Wiadomości Chemiczne*, 48, 1994, 11.

[246] Hermann K., Witko M., [in:] *The Chemical Physics of Solids Surfaces*, Vol. 9, Oxide Surfaces, D. P. Woodruff (ed.), Elsevier Science, Amsterdam 2001, 136–198.
[247] Geneste G., Morillo J., Finocchi F., *Surf. Sci.*, 2003, 508, 532–535.
[248] Bredow T., Pacchioni G., *Chem. Phys. Lett.*, 355, 2002, 417.
[249] Jug K., Geudtner G., Bredow T., *Mol. Catal.*, 82, 1993, 171.
[250] Freund H.J., Bäumer M., Kuhlenbeck H., *Adv. in Catalysis*, 45, 2000, 333–384.
[251] Taarning E., Osmundsen C.M., Yang X., Voss B., Andersen S.I., Christensen C.H., *Energy & Environmental Science*, 4(3), 2011, 793–804.
[252] Garcia-Martinez J., Kunhao L., Mesoporous Zeolites. Preparation, Characterization and Applications, Wiley-VCH 2015.
[253] Jae J., Tompsett G.A., Foster A.J., Hammond K.D., Auerbach S.M., Lobo R.F., Huber G.W., *Journal of Catalysis* 279, 2011, 257–268.
[254] Ennaert T., Van Aelst J., Dijkmans J., De Clercq R., Schutyser W., Dusselier M.L, Verboekend D., Sels B.F., *Chem. Soc. Rev.*, 45, 2016, 584.
[255] Verboekend, D., Pérez Ramírez J., Catal. Sci. Technol. 1, 2011, 879–890.
[256] Milina M., Mitchell S., Crivelli P., Cooke D., Pérez-Ramírez J. *Nature Commun.* 5, 2014, 3922, doi: 10.1038/ncomms4922.
[257] Gil B., Mokrzycki Ł., Sulikowski B., Olejniczak Z., Walasa S., *Catal. Today* 152, 2010, 24–32.
[258] Pérez-Ramírez J., Abelló S., Bonilla A., Groen J.C., *Adv. Funct. Mater.* 19, 2009, 164–172.
[259] Pérez-Ramírez J., Verboekend D., Bonilla A., Abelló S., *Adv. Funct. Mater.* 19, 2009, 3972–3979.
[260] Groen J.C., Jansen J.C., Moulijn J.A., Pérez-Ramirez J., *J. Phys. Chem. B* 108, 2004, 13062–13065.
[261] Groen J.C., Peffer L.A.A., Moulijn J.A., Pérez-Ramírez J., *Chem. Eur. J.* 11, 2005, 4983–4994.
[262] Sadowska K., Wach A., Olejniczak Z., Kuśtrowski P., Datka J., *Microporous and Mesoporous Materials* 167, 2013, 82–88.
[263] Sadowska K., Góra-Marek K., Drozdek M., Kuśtrowski P., Datka J., Martinez Triguero J., Rey F., *Microporous and Mesoporous Materials* 168, 2013, 195–205.
[264] Liu Z., Yingjie H., Jianjian Wang, Dong X., Tian Q., Han Y., *Mater. Chem. Front.* 1, 2017, 2195–2212.
[265] Perez-Ramırez J., Christensen C.H., Egeblad K., Christensend C.H., Groen J.C., *Chem. Soc. Rev*. 37, 2008, 2530–2542.
[266] Hartmann M., GOnche Machoke A., Schwieger W., *Chem. Soc. Rev.* 45, 2016, 3313–3330.
[267] Li K., Valla J., Garcia-Martinez J., *ChemCatChem* 6, 2014, 46–66.

[268] Groen J.C., Peffer L.A.A., Moulijn J.A., Perez-Ramirez J., *Microporous and Mesoporous Materials* 69, 2004, 29–34.
[269] Verboekend D., Pérez-Ramirez J., *Chem. Eur. J.* 17, 2011, 1137–1147.
[270] Groen J.C. *et al., Physicochem. Eng. Aspects* 241, 2004, 53–58.
[271] Perez-Ramirez J., Abello S., Bonilla A., Groen J.C., *Adv. Funct. Mater.* 19, 2009, 164–172.
[272] Karge H.G., Weitkamp J., Molecurar Sieves. Science and Technology Vol. 3. Post-Synthesis Modification I, Springer-Verlag Berlin Heidelberg NewYork, 2002, ISBN 3-540-64334-6.
[273] Yan Z., Ma D., Zhuang J., Liu X., Han X., Bao X., Chang F., Xu L., Liu Z., *Journal of Molecular Catalysis A: Chemical* 194, 2003, 153–167.
[274] Dutartre R., de Menorval L.C., Di Renzo F., McQueen D., Fajula F., Schultz P., *Miropor. Mater*. 6, 1996, 311.
[275] Lutz W., *Advances in Materials Science and Engineering* 2014, Article ID 724248, 1-20.
[276] Karge H.G., Weitkamp J., Molecurar Sieves. Science and Technology, Vol. 3. Post-Synthesis Modification I, Springer-Verlag Berlin Heidelberg NewYork, 2002, ISBN 3-540-64334-6.
[277] Morin S., Berreghis A., Ayrault P., Gnep N.S., Guisnet M., *Faraday Trans.* 93, 1997, 3269–3275.
[278] van Donk S., Janssen A.H., Bitter J.H., de Jong K.P., *Catal. Rev*. 45, 2003, 297–319.
[279] Hannus *et al.*, Colloids Surfaces A: *Physicochem. Eng. Aspects* 101, 1995, 199–206.
[280] Cheng H., Reinhard M., *Environ. Sci. Technol.* 40, 2006, 7694–7701.
[281] Datka J., Kolidziejski W., Klinowski J., Sulikowski B., *Catalysis Letters* 19, 1993, 159–165.
[282] Müller J.M., Mesquita G.C., Franco S.M., Borges L.D., de Macedo J.L., Dias J.A., Dias S.C.L., *Microporous and Mesoporous Materials* 204, 2015, 50–57.
[283] Karge H.G., Weitkamp J., Molecurar Sieves. Science and Technology Vol. 3. Post-Synthesis Modification I, Springer-Verlag Berlin Heidelberg NewYork, 2002, ISBN 3-540-64334-6.
[284] Yang C., Xu Q., *J. Chem. Soc., Faraday Trans*. 93(8), 1997, 1675–1680.
[285] Engelhardt G., Lohse U., *Journal Of Catalysis* 88, 1984, 513–515.
[286] Klinowski J., *Studies in Surface Science and Catalysis* 52, 1989, 39–71.
[287] Serrano D.P., Aguado J., Escola J.M., Peral A., Morales G., Abella E., *Catalysis TodayVol*. 168,2011, 86–95.
[288] Han X. *et al., Applied Surface Science* 257, 2011, 9525–9531.
[289] Mitchell S. *et al., Materials Chemistry and Physics* 127, 2011, 278–284.
[290] Bauer F. *et al., Journal of Catalysis* 251, 2007, 258–270.
[291] Chen L., Curtiss L.A., Assary R.S., Greeley J., Kerber T., Sauer J., *J. Phys. Chem. C*, 115, 2011, 21785–21790.
[292] Czekaj I., Branderberger S., Kröcher O., *Micro. Mesop. Materials* 169, 2013, 97–102.

[293] Zhang X.Q., Trinh T.T., van Santen R.A., Jansen A.P.J., *J. Phys. Chem. C* 115, 2011, 9561–9567.
[294] Zhang X.Q., Trinh,T.T., van Santen R.A., Jansen A.P.J., *J. Am. Chem.Soc.* 133, 2011, 6613–6625.
[295] Szyja B.M., Hensen E.J.M., van Santen R.A., *Catal. Today* 169, 2011, 156–166.
[296] Li G., Pidko E.A., van Santen R.A., Li C., Hensen E.J.M., *J. Phys. Chem. C* 117, 2013, 413–426.
[297] Lisboa O., Sanchez,M., Ruette F., *J. Molec. Catal. A: Chem.* 294, 2008, 93–101.
[298] Malola S., Svelle S., Bleken F.L., Swang O., *Angew. Chem. Int. Ed.* 51, 2012, 652–655.
[299] Fjermestad T., Svelle S., Swang O., *J. Phys. Chem. C* 117, 2013, 13442–13451.
[300] Sokol A.A., Catlow C.R.A., Garces,J.M. , Kuperman A., *J. Phys. Chem B* 106, 2002, 6163–6177.
[301] Sokol A.A., Catlow C.R.A., Garces,J.M. , Kuperman A., *Advanced Materials* 12, 2000, 1801–1805.
[302] Sokol A.A., Catlow C.R.A., Garces,J.M. , Kuperman A., *J. Phys.: Condens. Matter* 16, 2004, 2781–2794.
[303] Svelle S., Sommer L., Barbera K., Vennestrom P.N.R., Olsbye U., Lillerud K.P., Bordiga S., Pan Y.H., Beato P., *Catal. Today* 168, 2011, 38–47.
[304] Barbera K., Bonino F., Bordiga S., Janssens T.V.W., Beato P., *J. Catal.* 280, 2011, 196–2053.
[305] Bordiga S., Roggero I., Ugliengo P., Zecchina A., Bolis V., Artioli G., Buzzoni R., Marra G., Rivetti, F., Spano G., Lamberti C., *J. Chem. Soc. Dalton Trans.* 21, 2000, 3921–3929.
[306] Bordiga S., Ugliengo P., Damin A., Lamberti C., Spoto G., Zecchina A., Spano G., Buzzoni R., Dalloro L., Rivetti F., *Topics in Catalysis* 15,2001, 43–52.
[307] Pascale F., Ugliego P., Civalleri B., Orlando R., D'Arco P., Dovesi R., *J. Chem. Phys.* 117, 2002, 5337–5346.
[308] Silaghi M.C. , Chizallet C. , Raybaud P., *Micro. Mesop. Materials* 191, 2014, 82–96.
[309] http://3dprintingfromscratch.com/common/types-of-3d-printers-or-3d-printing-technologies-overview/ [access: 05.11.2018].
[310] Sun Q., Gao Z.X., Chen H.Y., Sachtler W., *Journal of Catalysis* 201, 2001, 89.
[311] Heindrich F., Schmidt C., Loeffler E., Menzel M., Gruenert W., *Journal of Catalysis* 212, 2002, 157.
[312] Kröcher O., Devadas M., Elsener M., Wokaun A., Soger N., Pfeifer M., Demel Y., Mussmann L., *Appl. Catal. B* 66, 2006, 208.
[313] Ma A.Z., Grünert W., *Chem. Commun*. 1999, 71.
[314] Schwidder M., Grünert W., Bentrup U., Brückner A., *J. Catal*. 239, 2006, 173.
[315] Rivallan M., Ricchiardi G., Bordiga S., Zecchina A., *J. Catal*. 264, 2009, 104.

[316] Pirutko L.V., Chernyavsky V.S., Starokon E.V., Ivanov A.A., Kharitonov A.S., Panov G.I., *Appl. Catal. B* 91, 2009, 174.
[317] Fellah M.F., van Santen R.A., Onal I., *J. Phys. Chem.* C 113, 2009, 15307.
[318] Yuranov I., Bulushev D.A., Renken A., Kiwi-Minsker L., *Appl. Catal.* A 319, 2007, 128.
[319] Ivanov D.P., Piryutko L.V., Sobolev V.I., *Petro. Chem*. 44, 2004, 322.
[320] Ehrich H., Schwieger W., Jahnisch K., *Appl. Catal. A-Gen*. 272, 2004, 311.
[321] Chen B., Liu N., Liu X., Zhang R., Li Y., Li Y., Sun X., *Catalysis Today* 175, 2011, 245.
[322] Dai C., Lei Z., Wang Y., Zhang R., Chen B., *Microporous and Mesoporous Materials* 167, 2013, 254.
[323] Battiston A.A., Bitter J.H., Koningsberger D.C., *J. Catal.* 218, 2003, 163.
[324] Chen H.Y., Sachtler W.M.H., *Catal. Today* 42, 1998, 73.
[325] Schwidder M., Kumar M.S., Klementiev K., Pohl M.M., Brückner A., Grünert W., *J. Catal*. 231, 2005, 314.
[326] Krishna K., Makkee M., *Catal. Today* 114, 2006, 23.
[327] Hensen E.J.M., Zhu Q., van Santen R.A., *J. Catal.* 220, 2003, 260.
[328] Zecchina A., Rivallan M., Berlier G., Lamberti C., Ricchiardi G., *Phys. Chem. Chem. Phys.* 9, 2007, 3483.
[329] Sun K., Xia H., Feng Z., van Santen R., Hensen E., Li C., *J. Catal.* 254, 2008, 383.
[330] Panov G.I., Uriarte A.K., Rodkin M.A., Sobolev V.I., *Catal. Today* 41, 1998, 365.